CHANNEL SPIN MIXING RATIOS

IN

HIGH RESOLUTION PROTON INELASTIC SCATTERING ON ^{46}Ti

by

JOHN R. CHANDLER

A thesis submitted to the Graduate Faculty of
North Carolina State University at Raleigh
in partial fulfillment of the
requirements for the Degree of
Doctor of Philosophy

DEPARTMENT OF PHYSICS

RALEIGH

1 9 7 8

APPROVED BY

---------- ----------
Chairman of Advisory Committee

---------- ----------

ABSTRACT

CHANDLER, JOHN R. Channel Spin Mixing Ratios in High Resolution Proton Inelastic Scattering on ^{46}Ti. (Under the direction of Gary E. Mitchell).

The $^{46}Ti(p,p'\gamma)^{46}Ti$ reaction was investigated between the proton bombarding energies 2.25 and 3.10 MeV using the high resolution system of the Triangle Universities Nuclear Laboratory 3 MV Van de Graaff accelerator. Both the proton and the de-excitation gamma-ray angular distributions were measured for thirty-four p-wave and f-wave resonances. Expressions for the angular distributions are given for the inelastically scattered protons and for the de-excitation gamma-rays in two angular momentum coupling schemes for p-wave and f-wave resonances. Simple expressions are also derived for transformations between the two representations. The results of the two singles measurements unambiguously determine the spin of the compound state for each resonance, and the magnitudes and the relative sign between the inelastic amplitudes are obtained. In general the experimental results in the analogue state regions are nonstatistical. The off-analogue data also

suggest possible nonstatistical effects. In addition, properties of the observed analogue states are obtained with emphasis on the fine structure of the analogue at E_p = 2.87 MeV.

BIOGRAPHY

John Russell Chandler

Personal:	Born August 10, 1951, Aiken, South Carolina
Education:	B.S. in Physics, N. C. State University, 1973
Positions:	Teaching Assistant, N.C.S.U., 1973 to 1975
	Research Assistant, N.C.S.U., 1975 to present
Membership:	Phi Kappa Phi
	Sigma Pi Sigma
	Pi Mu Epsilon

ACKNOWLEDGEMENTS

I would like to express my appreciation to my advisor, Dr. G. E. Mitchell, for his support during all phases of this research project, and for his guidance during my last seven years at N. C. State. Sincere appreciation is also extended to Dr. E. G. Bilpuch for his advice and help during the course of this experiment. The support of the other members of my committee, Drs. D. R. Tilley, C. P. Gould, and J. E. Huneycutt, Jr. is greatly appreciated.

Special thanks should go to K. B. Sales, C. R. Westerfeldt, B. H. Chou, and W. A. Watson for taking portions of this data. I also appreciate the help of W. K. Wells and Dr. T. R. Dittrich in developing the analysis of the experiment.

I owe special thanks to Mr. S. E. Edwards and Dr. M. R. Roberson for their assistance in understanding the computer interface and their suggestions while writing the computer software. The assistance of Mr. R. Rummel and Mr. A. G. Lovette in maintaining the equipment used in this experiment is particularly appreciated. Also, I would like to thank Mrs. Joseph Bailey for her careful preparation of the figures in this dissertation.

I owe a warm thanks to my parents and family for their moral support throughout my life, and to my brother for his interest in my work. Most of all, I would like to

thank my wife, Debbie, for her unending support and encouragement during the past several years.

This work was supported in part by the United States Department of Energy. Some of the analysis was performed at Triangle Universities Computation Center, which is supported in part by the National Science Foundation.

TABLE OF CONTENTS

LIST OF FIGURES

Page

Page

LIST OF TABLES

Page

Chapter 1

INTRODUCTION

For the past several years, high resolution proton elastic scattering experiments have been performed at the Triangle Universities Nuclear Laboratory. The study of fragmented analogue states has been the major emphasis of these experiments. During the last three years, proton inelastic scattering experiments have also been conducted on some of the same nuclei. The purpose of the inelastic scattering experiments is to establish definite spin assignments for the compound states and to obtain information about the channel spin mixing of the inelastic proton decay. The present work is a continuation of the inelastic studies and consists of a measurement of the angular distributions of both the inelastically scattered proton and the subsequent de-excitation gamma-ray.

In the present experiment measurements were performed for the reaction $^{46}Ti(p,p')^{46}Ti^*$ at the angles 90°, 120°, 135°, and 160°, and for the $^{46}Ti(p,p'\gamma)^{46}Ti$ reaction at the angles 30°, 45°, 60°, and 90°. In the earlier experiments, only p-wave resonances (those formed by incident proton orbital angular momentum equal to 1) were studied.

The present work emphasizes p-wave resonances, but also extends the method to f-wave resonances (those formed by incident proton orbital angular momentum equal to 3). The method used in the inelastic studies has been reviewed by Dittrich (1976). First one measures the angular distribution of the protons decaying from the compound state to an excited state of the the residual nucleus. This aligned excited state subsequently decays by gamma-ray emission. Additional information is obtained from the measurement of the gamma-ray angular distribution. Consider $1/2^-$ and $3/2^-$ compound states. A compound state with spin and parity of $1/2^-$ is unaligned and will produce both an isotropic particle distribution and an isotropic de-excitation gamma-ray distribution. A $3/2^-$ compound state will be aligned and at least one and sometimes both the particle and gamma-ray angular distributions will be anisotropic. Therefore, measurement of the two angular distributions will uniquely determine the spin J of the compound nucleus.

More importantly the measurement of the angular distributions yields additional information. There are two inelastic decay channels from a $3/2^-$ compound state; in general, the ratio of the amplitudes in these two channels may have any value. Two solutions are normally obtained from both the particle angular distribution and from the de-excitation gamma-ray angular distribution. The combi-

nation of the results of the two measurements yields one common solution. The magnitudes of the partial reduced width amplitudes and the relative sign between these amplitudes can be obtained for the $3/2^-$ resonances.

The measurement of such mixing ratios is quite recent; the theoretical implications are only now being investigated in detail. The distribution of these ratios is generally expected to be random except near analogue states. Experiments on ^{50}Cr and ^{44}Ca have provided nonstatistical results near analogue states, but also suggest that nonstatistical results may occur in regions without analogues.

The current experiment is the first to use the new Prime 300 computer and CAMAC interface at T. U. N. L. The new system was developed to provide a dependable and efficient means for performing the experiments, and required building electronics for the interface and writing software to handle data acquisition. CAMAC has become a standard throughout the world, and the present system provides a flexible interface for future experiments. A detailed description of the interface is contained in the Appendix.

Chapter 2 presents the general angular distribution equations for both inelastically scattered protons and de-excitation gamma-rays. The formalism used is that of the statistical and efficiency tensor description of nu-

clear scattering. The equations are presented in two different angular momentum coupling schemes: total angular momentum and channel spin. Specific equations applicable to the current experiment are given for both coupling schemes and for both p-wave and f-wave resonances. A mixing ratio is defined and equations relating this ratio to coefficients of the angular distribution are listed. In order to connect the two angular momentum representations, transformations for the mixing ratios are given.

The experimental equipment and procedures are described in Chapter 3. The 3 MV Van de Graaff accelerator-homogenizer system is discussed, and proton and gamma-ray detection methods are explained. In addition the method used in preparing the targets is described.

In Chapter 4 the data, data analysis, and results are presented. All p-wave and f-wave resonances previously observed between E_p = 2.25 and 3.10 MeV were studied. From the angular distribution measurements, mixing ratios were calculated. A discussion of the errors in the mixing ratio values is also included. Reduced widths, magnitudes of reduced width amplitudes, and the relative phases of the reduced width amplitudes were determined for each $3/2^-$ and $5/2^-$ resonance. Calculations to consider the statistical nature of the data are presented. Properties of the observed analogue states are obtained, with emphasis on the fine structure of the analogue at E_p = 2.87 MeV.

Chapter 2

ANGULAR CORRELATION THEORY

2.1 General Angular Correlation Theory

Angular correlations in nuclear reactions are treated by Blatt and Biedenharn (1952), Biedenharn and Rose (1953), Kraus et al. (1956), and many others. The procedure followed consists of choosing a general wave function made up of a superposition of incident plane waves and outgoing spherical waves. For the angular distribution of a given reaction product, an average is performed over all possible angular momenta and initial state spin values, and a summation is made over all resulting final states. This averaging and summation procedure is very tedious for the general case of arbitrary spins and angular momenta.

An alternate method assumes mixed states which can be described by density matrices. The application of this approach to angular correlations is reviewed by Dittrich (1976). By definition the density matrix method includes averaging over unobserved parameters of the system and includes corrections for detection efficiency.

The reaction to be described is the formation of a state B from a state A and an angular momentum j, and the breakup of B into state C and angular momentum j'. The probability that an event from this reaction will be detected is given in the total angular momentum representation by

$$W = \Sigma\ (k_C n_C k_j, n_j | k_B n_B)\ (k_A n_A k_j n_j | k_B n_B)\ \hat{k}_C \hat{k}_j, \hat{k}_A \hat{k}_j$$

$$\cdot \begin{Vmatrix} C_1 & j'_1 & B_1 \\ C_2 & j'_2 & B_2 \\ k_C & k_j, & k_B \end{Vmatrix} \begin{Vmatrix} A_1 & j_1 & B_1 \\ A_2 & j_2 & B_2 \\ k_A & k_j & k_B \end{Vmatrix} (\hat{B}_1 \hat{B}_2)^2\ \varepsilon^*_{k_C n_C}(C_1 C_2)$$

$$\cdot \varepsilon^*_{k_j, n_j, (j'_1 j'_2)}\ \rho_{k_A n_A}(A_1 A_2)\ \rho_{k_j n_j}(j_1 j_2)$$

$$\cdot \langle B_1 C_1 j'_1 | O_C | B_1 \rangle \langle B_2 C_2 j'_2 | O_C | B_2 \rangle^* \qquad 2.1.1$$

where: the number subscripts represent different magnitudes of the angular momenta; the form (k n k' n' | k" n") is a Clebsch-Gordon coefficient; the circumflex over a number represents $(2k+1)^{1/2}$; the quantity in brackets is a Wigner 9-j coefficient; ρ is a statistical tensor describing the mixed states; ε is an efficiency tensor specifying the efficiency of the detection of outgoing radiation; O is a general interaction operator describing the scatter-

ing process; and the sum is over all possible k, n, and angular momenta. If in addition the state C decays into state D and angular momentum L,

$$W = \Sigma\ (k_A n_A k_j n_j | k_B n_B)(k_C n_C k_j' n_j' | k_B n_B)(k_D n_D k_L n_L | k_C n_C)$$

$$\cdot \begin{vmatrix} A_1 & j_1 & B_1 \\ A_2 & j_2 & B_2 \\ k_A & k_j & k_B \end{vmatrix} \begin{vmatrix} C_1 & j_1' & B_1 \\ C_2 & j_2' & B_2 \\ k_C & k_j' & k_B \end{vmatrix} \begin{vmatrix} D_1 & L_1 & C_1 \\ D_2 & L_2 & C_2 \\ k_D & k_L & k_C \end{vmatrix} \hat{k}_A \hat{k}_C \hat{k}_D \hat{k}_j \hat{k}_j' \hat{k}_L$$

$$\cdot (\hat{B}_1 \hat{B}_2)^2 \hat{C}_1 \hat{C}_2 \rho_{k_A n_A}(A_1 A_2)\ \rho_{k_j n_j}(j_1 j_2)\ \varepsilon^*_{k_j', n_j'}(j_1' j_2')$$

$$\cdot \varepsilon^*_{k_D n_D}(D_1 D_2)\ \varepsilon^*_{k_L n_L}(L_1 L_2)\ \langle B_1 C_1 j_1' | O_C | B_1 \rangle$$

$$\cdot \langle B_2 C_2 j_2' | O_C | B_2 \rangle^*\ \langle C_1 | O_D | C_1 D_1 L_1 \rangle\ \langle C_2 | O_D | C_2 D_2 L_2 \rangle^* \qquad 2.1.2$$

An alternative scheme which is very useful is the channel spin representation. In channel spin formalism, the channel spin s of the reaction is the vector sum of the spin of the particle and the spin of the nucleus. The total angular momentum is then the sum of the channel spin and the proton orbital angular momentum. Fig. 2.1 gives the general angular momentum coupling equations in both representations and illustrates the reaction schematically. In channel spin, Eq. 2.1.1 becomes

$$W = \Sigma\ (k_s n_s k_\ell n_\ell | k_B n_B)(k_s, n_s, k_\ell, n_\ell, | k_B n_B)\ \hat{k}_s, \hat{k}_s \hat{k}_\ell, \hat{k}_\ell$$

$$\cdot \begin{vmatrix} s_1 & \ell_1 & B_1 \\ s_2 & \ell_2 & B_2 \\ k_s & k_\ell & k_B \end{vmatrix} \begin{vmatrix} s_1' & \ell_1' & B_1 \\ s_2' & \ell_2' & B_2 \\ k_s, & k_\ell, & k_B \end{vmatrix} (\hat{B}_1 \hat{B}_2)^2\ \rho_{k_s n_s}(s_1 s_2)$$

$$\cdot \rho_{k_\ell n_\ell}(\ell_1 \ell_2)\ \varepsilon^*_{k_s, n_s,}(s_1' s_2')\ \varepsilon^*_{k_\ell, n_\ell,}(\ell_1' \ell_2')$$

$$\cdot \langle B_1 s_1' \ell_1' | O_C | B_1 \rangle \langle B_2 s_2' \ell_2' | O_C | B_2 \rangle^* \qquad 2.1.3$$

Eq. 2.1.2 in channel spin formalism becomes

$$W = \Sigma\ (k_s n_s k_\ell n_\ell | k_B n_B)(k_s, n_s, k_\ell, n_\ell, | k_B n_B)$$

$$\cdot (k_C n_C k_{i_p}, n_{i_p}, | k_s, n_s,)(k_D n_D k_L n_L | k_C n_C)\ \hat{k}_s \hat{k}_s, \hat{k}_\ell \hat{k}_\ell, \hat{k}_C$$

$$\cdot \hat{k}_{i_p}, \hat{k}_D \hat{k}_L (\hat{B}_1 \hat{B}_2)^2\ \hat{s}_1' \hat{s}_2' \hat{C}_1 \hat{C}_2$$

$$\cdot \begin{vmatrix} s_1 & \ell_1 & B_1 \\ s_2 & \ell_2 & B_2 \\ k_s & k_\ell & k_B \end{vmatrix} \begin{vmatrix} s_1' & \ell_1' & B_1 \\ s_2' & \ell_2' & B_2 \\ k_s, & k_\ell, & k_B \end{vmatrix} \begin{vmatrix} s_1' & C_1 & i_{p_1}' \\ s_2' & C_2 & i_{p_2}' \\ k_s, & k_C & k_{i_p}, \end{vmatrix} \begin{vmatrix} D_1 & L_1 & C_1 \\ D_2 & L_2 & C_2 \\ k_D & k_L & k_C \end{vmatrix}$$

$$\cdot \rho_{k_s n_s}(s_1 s_2)\ \rho_{k_\ell n_\ell}(\ell_1 \ell_2)\ \varepsilon^*_{k_{i_p}, n_{i_p}, }(i_{p_1}, i_{p_2},)$$

$$\cdot \varepsilon^*_{k_\ell, n_{\ell'}}(\ell_1'\ell_2')\ \varepsilon^*_{k_D n_D}(D_1 D_2)\ \varepsilon^*_{k_L n_L}(L_1 L_2)$$

$$\cdot \langle B_1 s_1'\ell_1' | O_C | B_1\rangle \langle B_2 s_2'\ell_2' | O_C | B_2\rangle^* \langle C_1 | O_D | C_1 D_1 L_1\rangle^*$$

$$\cdot \langle C_2 | O_D | C_2 D_2 L_2\rangle \qquad 2.1.4$$

This equation describes the coupling of s and ℓ to form state B; state B then breaks up into s' and ℓ', giving state C; and state C splits into L and state D.

2.2 Simplified Angular Distribution Formulas

To describe the angular distributions of $^{46}Ti(p,p')^{46}Ti^*$ and $^{46}Ti(p,p'\gamma)^{46}Ti$, Eqs. 2.1.1, 2.1.2, 2.1.3, 2.1.4 can be used along with a few assumptions. Assume that the target nuclei are unpolarized and that the incident particles can be described by a plane wave with the z-axis along the beam direction. The particle angular distribution in the total angular momentum representation is then

$$W(\theta_{p'}) = \Sigma(-1)^{A-2B_2+C-2j_1-2j_1'+i_p+i_{p'}+3k+\frac{1}{2}(\ell_1-\ell_2+\ell_1'-\ell_2')}$$

$$\cdot (\hat{B}_1\hat{B}_2)^2\ (\hat{A}\hat{i}_p\hat{i}_{p'}4\pi)^{-2}\ Z(\ell_1 j_1 \ell_2 j_2; i_p k)$$

$$\cdot W(j_2 B_2 j_1 B_1; Ak)\ Z(\ell_1' j_1' \ell_2' j_2'; i_p, k)\ W(j_2' B_2 j_1' B_1; Ck)$$

$$\cdot P_k(\theta_p,)\ \langle B_1 C_1 j_1' | O_C | B_1 \rangle\ \langle B_2 C_2 j_2' | O_C | B_2 \rangle^*$$

2.2.1

The total angular momentum representation of the gamma-ray angular distribution is

$$W(\theta_\gamma) = \Sigma (-1)^{A-B_1-B_2-2C_2+D+i_p-2j_1+j'-L_1+L_2+(\frac{1}{2})k+\frac{1}{2}(\ell_1-\ell_2)}$$

$$\cdot \frac{\hat{C}_1 \hat{C}_2 \hat{L}_1 \hat{L}_2 (\hat{B}_1 \hat{B}_2)^2}{8\pi (\hat{A} \hat{i}_p \hat{i}_{p'})^2}\ Z(\ell_1 j_1 \ell_2 j_2; i_p k)\ W(j_2 B_2 j_1 B_1; Ak)$$

$$\cdot W(B_2 C_2 B_1 C_1; j'k)\ W(L_2 C_2 L_1 C_1; Dk)\ (L_1 1 L_2 -1 | k0)$$

$$\cdot P_k(\theta_\gamma)\ J_k\ \langle B_1 C_1 j' | O_C | B_1 \rangle\ \langle B_2 C_2 j' | O_C | B_2 \rangle^*$$

$$\cdot \langle C_1 | O_D | C_1 D L_1 \rangle^*\ \langle C_2 | O_D | C_2 D L_2 \rangle \qquad 2.2.2$$

where J_k is the cylindrical attenuation coefficient defined by Ferguson (1965) and Thompson et al. (1968).

In the channel spin representation, the particle angular distribution is

$$W(\theta_{p'}) = \Sigma(-1)^{s+s'-2B_2+\frac{1}{2}(\ell_2-\ell_1+\ell_2'-\ell_1')} (4\pi\hat{A}\hat{i}_p)^{-2}$$

$$\cdot Z(\ell_1 B_1 \ell_2 B_2; sk)\ Z(\ell_1' B_1 \ell_2' B_2; s'k)\ P_k(\theta_{p'})$$

$$\cdot \langle B_1 s' \ell_1' | O_C | B_1 \rangle\ \langle B_2 s' \ell_2' | O_C | B_2 \rangle^* \qquad 2.2.3$$

The gamma-ray angular distribution is

$$W(\theta_\gamma) = \Sigma(-1)^{s-B_2-B_1-s_1'-s_2'-2C_2+D+\ell'+i_p,+L_2-L_1-1+\frac{1}{2}(\ell_2-\ell_1+7k)}$$

$$\cdot \frac{\hat{B}_1\hat{B}_2\hat{s}_1'\hat{s}_2'\hat{C}_1\hat{C}_2\hat{L}_1\hat{L}_2}{8\pi(\hat{i}_p\hat{i}_p,\hat{A})^2}\ Z(\ell_1 B_1 \ell_2 B_2; sk)\ W(B_2 s_2' B_1 s_1'; \ell' k)$$

$$\cdot W(s_2' C_2 s_1' C_1; i_p, k)\ W(L_2 C_2 L_1 C_1; Dk)\ (L_1 1 L_2 -1 | k0)$$

$$\cdot P_k(\theta_\gamma)\ J_k\ \langle B_1 s_1' \ell' | O_C | B_1 \rangle\ \langle B_2 s_2' \ell' | O_C | B_2 \rangle^*$$

$$\cdot \langle C_1 | O_D | C_1 D L_1 \rangle^*\ \langle C_2 | O_D | C_2 D L_2 \rangle \qquad 2.2.4$$

Figure 2.1 Energy Level Scheme and Angular Momentum Coupling Equations.

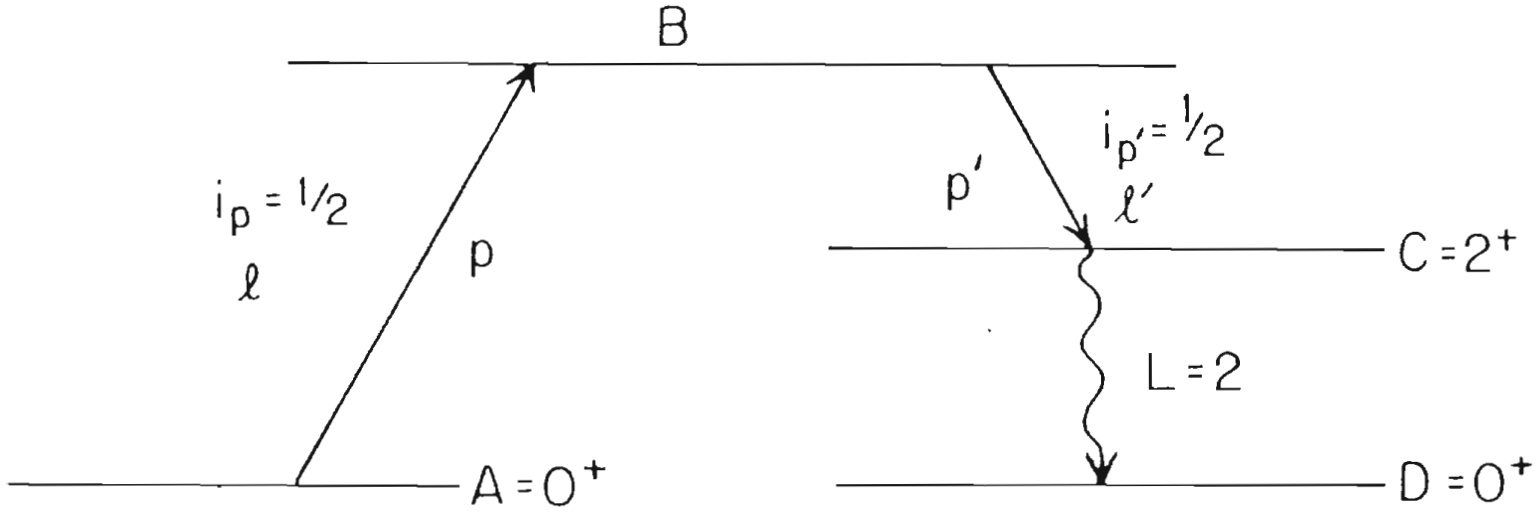

	ENTRANCE CHANNEL	EXIT CHANNEL
CHANNEL SPIN REPRESENTATION	$\vec{s} = \vec{A} + \vec{i}_p$ $\vec{B} = \vec{s} + \vec{\ell}$	$\vec{s}' = \vec{C} + \vec{i}_{p'}$ $\vec{B} = \vec{s}' + \vec{\ell}'$
TOTAL ANGULAR MOMENTUM REPRESENTATION	$\vec{j} = \vec{\ell} + \vec{i}_p$ $\vec{B} = \vec{A} + \vec{j}$	$\vec{j}' = \vec{\ell}' + \vec{i}_{p'}$ $\vec{B} = \vec{C} + \vec{j}'$

2.3 Distributions for P and F-Wave Resonances

The reaction $^{46}Ti(p,p'\gamma)^{46}Ti$ can be explicitly described by the equations of the previous section. Specifically, the ground state spin is 0+, the first excited state C has spin 2+, the final state D has spin 0+, and the protons have spin 1/2. The resonances studied had incoming orbital angular momentum of either 1 or 3, and the outgoing orbital angular momentum $\ell'=3$ was neglected due to low penetrability.

The explicit results for p-wave resonances were given by Dittrich (1976). In that case the compound state has spin either 3/2 or 1/2. For the $1/2^-$ state the angular momentum values are $j=1/2$; $j'=3/2$; $s=1/2$; and $s'=3/2,5/2$; while the values for the $3/2^-$ state are $j=3/2$; $j'=1/2,3/2$; $s=1/2$; and $s'=3/2,5/2$. In the total angular momentum representation, the general equations become:

$$W(\theta_{p'}) = 1 - \frac{2/5(\langle j_1'\rangle\langle j_3'\rangle^* + \langle j_3'\rangle\langle j_1'\rangle^*) + 3/5|\langle j_3'\rangle|^2}{|\langle j_1'\rangle|^2 + |\langle j_3'\rangle|^2} P_2(\theta_{p'}) \qquad 2.3.1$$

$$W(\theta_\gamma) = 1 + \frac{1/2|\langle j_1'\rangle|^2}{|\langle j_1'\rangle|^2 + |\langle j_3'\rangle|^2} Q_2 P_2(\theta_\gamma) \qquad 2.3.2$$

where Q_2 is the attenuation factor defined as the ratio J_2/J_0 and tabulated for 3"X3" NaI(Tl) detectors by Ferguson (1965). The value for Q_2 was taken to be 0.98. For $5/2^-$ resonances a Q_4 term, defined as the ratio J_4/J_0, was needed in addition to Q_2; Q_4 was set equal to 0.95. The matrix element $\langle j' \rangle$ represents the transition between two states through the j' channel. The subscripts used with j' represent twice the j' value for that particular channel. In the channel spin representation, the general equations reduce to

$$W(\theta_{p'}) = 1 + \frac{1/5|\langle s'_5 \rangle|^2 - 4/5|\langle s'_3 \rangle|^2}{|\langle s'_3 \rangle|^2 + |\langle s'_5 \rangle|^2} P_2(\theta_{p'}) \qquad 2.3.3$$

$$W(\theta_\gamma) = 1 +$$

$$1/10 \frac{|\langle s'_3 \rangle|^2 - 2(\langle s'_3 \rangle\langle s'_5 \rangle^* + \langle s'_5 \rangle\langle s'_3 \rangle^*) + 4|\langle s'_5 \rangle|^2}{|\langle s'_3 \rangle|^2 + |\langle s'_5 \rangle|^2} Q_2 P_2(\theta_\gamma)$$

2.3.4

The s' subscripts are used in the same manner as the j' subscripts.

For the f-wave case, the compound state has a spin of either 5/2 or 7/2. The $5/2^-$ state has s=1/2; s'=3/2,5/2; j=5/2; and j'=1/2,3/2; while the $7/2^-$ state has s=1/2; s'=3/2,5/2; j=7/2; and j'=3/2. Using Eqs. 2.2.1 and 2.2.2 the angular distributions in the total angular momentum representation for the $5/2^-$ state reduce to:

$$W(\theta_{p'}) = 1 + 4/5 \frac{2\sqrt{2/7}\,(\langle j_1'\rangle\langle j_3'\rangle^* + \langle j_3'\rangle\langle j_1'\rangle^*) - 1/7|\langle j_3'\rangle|^2}{|\langle j_1'\rangle|^2 + |\langle j_3'\rangle|^2} P_2(\theta_{p'}) \qquad 2.3.5$$

$$W(\theta_\gamma) = 1 + \frac{4/7|\langle j_1'\rangle|^2 + 10/49|\langle j_3'\rangle|^2}{|\langle j_1'\rangle|^2 + |\langle j_3'\rangle|^2} Q_2 P_2(\theta_\gamma) + \frac{32/49|\langle j_3'\rangle|^2 - 4/7|\langle j_1'\rangle|^2}{|\langle j_1'\rangle|^2 + |\langle j_3'\rangle|^2} Q_4 P_4(\theta_\gamma) \qquad 2.3.6$$

Using Eqs. 2.2.3 and 2.2.4, the angular distributions in the channel spin representation for the $5/2^-$ state become:

$$W(\theta_{p'}) = 1 + \frac{4/5|\langle s_3'\rangle|^2 - 32/35|\langle s_5'\rangle|^2}{|\langle s_3'\rangle|^2 + |\langle s_5'\rangle|^2} P_2(\theta_{p'}) \qquad 2.3.7$$

$$W(\theta_\gamma) = 1 + 2/5 \frac{|\langle s_3' \rangle|^2 + 46/49 |\langle s_5' \rangle|^2}{|\langle s_3' \rangle|^2 + |\langle s_5' \rangle|^2} Q_2 P_2(\theta_\gamma)$$

$$- 2/5 \frac{6\sqrt{14}\ /49 (\langle s_3' \rangle \langle s_5' \rangle^* + \langle s_5' \rangle \langle s_3' \rangle^*)}{|\langle s_3' \rangle|^2 + |\langle s_5' \rangle|^2} Q_2 P_2(\theta_\gamma)$$

$$+ 4/49 \frac{|\langle s_5' \rangle|^2 + 2\sqrt{14}\ (\langle s_3' \rangle \langle s_5' \rangle^* + \langle s_5' \rangle \langle s_3' \rangle^*)}{|\langle s_3' \rangle|^2 + |\langle s_5' \rangle|^2} Q_4 P_4(\theta_\gamma) \qquad 2.3.8$$

The distributions for the $7/2^-$ states, in the total angular momentum representation, are

$$W(\theta_{p'}) = 1 + 5/7\ P_2(\theta_{p'}) \qquad 2.3.9$$

$$W(\theta_\gamma) = 1 + 25/49\ Q_2 P_2(\theta_\gamma) - 18/49\ Q_4 P_4(\theta_\gamma) \qquad 2.3.10$$

In the channel spin representation, the distributions for the $7/2^-$ resonances are the same:

$$W(\theta_{p'}) = 1 + 5/7\ P_2(\theta_{p'}) \qquad 2.3.11$$

$$W(\theta_\gamma) = 1 + 25/49\ Q_2 P_2(\theta_\gamma) - 18/49\ Q_4 P_4(\theta_\gamma) \qquad 2.3.12$$

Since only the relative cross section is normally of interest, the coefficient of the zeroth order term of the Legendre polynomial expansion has been normalized to one. All of the distributions then have the form

$$W(\theta) = 1 + a_2 P_2(\theta) + a_4 P_4(\theta) \qquad 2.3.13$$

It should be noted that there is no ϕ dependence; the angular correlation is a function only of the angle between the detector and the beam direction. Only even order Legendre polynomial terms contribute and the order of the highest nonzero Legendre polynomial is less than or equal to 2ℓ (Yang 1948). The angular distributions for $1/2^-$ resonances are therefore isotropic. The highest order polynomial is two for p-wave resonances, and four for f-wave resonances. It is also noteworthy that the particle angular distributions from the f-wave resonances have no P_4 terms, and that both the a_2 and a_4 coefficients are constants for the $7/2^-$ case.

Since these equations have been specified in two representations, a transformation between the two formalisms must exist. The general transformation is

$$\langle C|s'|B\rangle = \sum_{j'} \langle C|j'|B\rangle \, (-1)^{\ell'+i_{p'}-j'} \, \hat{s}'\hat{j}' \cdot W(Ci_p, B\ell'; s'j') \qquad 2.3.14$$

For the $3/2^-$ case this becomes

$$\langle C|s'_3|B\rangle = 1/\sqrt{5}\ (\langle C|j'_1|B\rangle + 2\langle C|j'_3|B\rangle) \qquad 2.3.15$$

$$\langle C|s'_5|B\rangle = 1/\sqrt{5}\ (-2\langle C|j'_1|B\rangle + \langle C|j'_3|B\rangle) \qquad 2.3.16$$

The last two equations can be solved for the inverse transformation

$$\langle C|j'_1|B\rangle = 1/\sqrt{5}\ (\langle C|s'_3|B\rangle - 2\langle C|s'_5|B\rangle) \qquad 2.3.17$$

$$\langle C|j'_3|B\rangle = 1/\sqrt{5}\ (2\langle C|s'_3|B\rangle + \langle C|s'_5|B\rangle) \qquad 2.3.18$$

For the $5/2^-$ compound state, Eq.2.3.14 yields

$$\langle C|s'_3|B\rangle = 1/\sqrt{15}\ (2\sqrt{2}\ \langle C|j'_1|B\rangle + \sqrt{7}\ \langle C|j'_3|B\rangle) \qquad 2.3.19$$

$$\langle C|s'_5|B\rangle = 1/\sqrt{15}\ (-\sqrt{7}\ \langle C|j'_1|B\rangle + 2\sqrt{2}\ \langle C|j'_3|B\rangle) \qquad 2.3.20$$

The inverse transformation is

$$\langle C|j'_1|B\rangle = 1/\sqrt{15}\ (2\sqrt{2}\ \langle C|s'_3|B\rangle - \sqrt{7}\ \langle C|s'_5|B\rangle) \qquad 2.3.21$$

$$\langle C|j'_3|B\rangle = 1/\sqrt{15}\ (\sqrt{7}\ \langle C|s'_3|B\rangle + 2\sqrt{2}\ \langle C|s'_5|B\rangle) \qquad 2.3.22$$

The $1/2^-$ and $7/2^-$ cases need no transformation since all coefficients are constants.

2.4 Mixing Ratios

In the previous section two possible values for the exit channel spin and the exit total angular momentum have been given for the $3/2^-$ and $5/2^-$ compound states. In general there will be a mixture of the two decay amplitudes. The mixing ratios are defined

$$\delta_{s'} = \frac{\langle s'_5 \rangle}{\langle s'_3 \rangle} \qquad 2.4.1$$

$$\delta_{j'} = \frac{\langle j'_3 \rangle}{\langle j'_1 \rangle} \qquad 2.4.2$$

Using the angular distribution expressions, the mixing ratios can be expressed in terms of a_2 and a_4. Eqs. 2.3.1 and 2.3.3 give for the particle distributions

$$\delta_{p'_{j'}} = \frac{-2 \pm \sqrt{4-25a_2^2-15a_2}}{5a_2+3} \qquad 2.4.3$$

$$\delta_{p_s'} = \pm\sqrt{\frac{4+5a_2}{1-5a_2}} \qquad 2.4.4$$

Eq. 2.4.3 gives the mixing ratio for $3/2^-$ compound states in the total angular momentum representation, while Eq. 2.4.4 gives the result in the channel spin representation. From Eqs. 2.3.2 and 2.3.4 the mixing ratios for the gamma-ray distributions are obtained.

$$\delta_{\gamma_j'} = \pm\sqrt{\frac{1-2a_2}{2a_2}} \qquad 2.4.5$$

$$\delta_{\gamma_s'} = \frac{2 \pm 5\sqrt{2a_2-4a_2^2}}{4-10a_2} \qquad 2.4.6$$

Similar results may be obtained for the $5/2^-$ compound state. Using Eqs. 2.3.5 and 2.3.7, the results for the particle distributions are

$$\delta_{p_j'} = \frac{8\sqrt{14}\ /35 \pm \sqrt{128/175 - 4a_2/35 - a_2^2}}{a_2 + 4/35} \qquad 2.4.7$$

$$\delta_{p_s'} = \pm\sqrt{\frac{4/5 - a_2}{32/35 + a_2}} \qquad 2.4.8$$

For the gamma-ray distributions, Eqs. 2.3.6 and 2.3.8

yield

$$\delta_{\gamma_{j'}} = \pm\sqrt{\frac{4/7 - a_2}{a_2 - 10/49}} \qquad 2.4.9$$

$$\delta_{\gamma_{s'}} = \frac{-12\sqrt{14}\ /245 \pm \sqrt{-40/343 + 38a_2/49 - a_2^2}}{a_2 - 92/245} \qquad 2.4.10$$

In addition to Eqs. 2.4.9 and 2.4.10, the mixing ratios from the gamma-ray distributions can be solved in terms of a_4. Using distribution Eqs. 2.3.6 and 2.3.8 yields

$$\delta_{\gamma_{j'}} = \pm\sqrt{\frac{a_4 + 4/7}{32/49 - a_4}} \qquad 2.4.11$$

$$\delta_{\gamma_{s'}} = \frac{8\sqrt{14}\ /49 \pm \sqrt{128/343 + 4a_4/49 - a_4^2}}{a_4 - 4/49} \qquad 2.4.12$$

It should be noted that Eqs. 2.4.3 through 2.4.12 all have two solutions.

Eqs. 2.3.15, 2.3.16, 2.3.17, and 2.3.18 may be combined to obtain the transformation equations.

$$\delta_{j'} = \frac{2 + \delta_{s'}}{1 - 2\delta_{s'}} \qquad 2.4.13$$

$$\delta_{s'} = \frac{-2 + \delta_{j'}}{1 + 2\delta_{j'}} \qquad 2.4.14$$

for the $3/2^-$ compound state. Eq. 2.4.13 transforms the mixing ratio from channel spin to total angular momentum representation, while Eq. 2.4.14 makes the opposite transformation. Eqs. 2.3.19, 2.3.20, 2.3.21, and 2.3.22 give the following transformations for the $5/2^-$ compound state:

$$\delta_{j'} = \frac{\sqrt{7} + 2\sqrt{2}\,\delta_{s'}}{2\sqrt{2} - \sqrt{7}\,\delta_{s'}} \qquad 2.4.15$$

$$\delta_{s'} = \frac{-\sqrt{7} + 2\sqrt{2}\,\delta_{j'}}{2\sqrt{2} + \sqrt{7}\,\delta_{j'}} \qquad 2.4.16$$

A convenient parameter Φ is defined by

$$\Phi \equiv \tan^{-1}\delta \qquad 2.4.17$$

with the angle ϕ between $-90°$ and $+90°$. Using Eq. 2.4.1 gives

$$\Phi_{s'} = \tan^{-1}\left(\frac{\langle s'_5\rangle}{\langle s'_3\rangle}\right) \qquad 2.4.18$$

for the channel spin representation. A value of $\Phi=\pm 90^{\circ}$ corresponds to pure $s'=5/2$, while $\Phi=0^{\circ}$ corresponds to pure $s'=3/2$. Other values correspond to channel spin mixing.

In the total angular momentum representation

$$\Phi_{j'} = \tan^{-1}\left[\frac{<j_3'>}{<j_1'>}\right] \qquad 2.4.19$$

The variation of a_2 and a_4 with Φ is shown in Figs. 2.2, 2.3, 2.4, and 2.5.

From an examination of Figs. 2.2, 2.3, 2.4, and 2.5, it is apparent that a linear relationship exists between the angles in the two representations. Using Eq. 2.4.17, Eq. 2.4.13 can be written as

$$\tan \Phi_{j'} = \frac{2 + \tan \Phi_{s'}}{1 - 2 \tan \Phi_{s'}} \qquad 2.4.20$$

This can be rewritten as

$$\tan \Phi_{j'} = \frac{\tan \{ \tan^{-1} (2)\} + \tan \Phi_{s'}}{1 - \tan \{ \tan^{-1} (2)\} \tan \Phi_{s'}} \qquad 2.4.21$$

The equation for the tangent of a sum of two angles is

$$\tan (X + Y) = \frac{\tan X + \tan Y}{1 - \tan X \tan Y} \qquad 2.4.22$$

Eq. 2.4.21 can now be written as

$$\tan \Phi_{j'} = \tan \{ \tan^{-1} (2) + \Phi_{s'} \} \qquad 2.4.23$$

Or

$$\Phi_{j'} = \Phi_{s'} + \tan^{-1}(2) \qquad 2.4.24$$

Obviously it also holds that

$$\Phi_{s'} = \Phi_{j'} - \tan^{-1}(2) \qquad 2.4.25$$

This is just the relation illustrated in Figs. 2.2 and 2.3 for the $3/2^-$ compound state, since $\tan^{-1}(2)$ is 63.4°.

The $5/2^-$ compound state can be treated similarly. The results are

$$\Phi_{j'} = \Phi_{s'} + \tan^{-1}(1/2\ \sqrt{7/2}) \qquad 2.4.26$$

$$\Phi_{s'} = \Phi_{j'} - \tan^{-1}(1/2\ \sqrt{7/2}) \qquad 2.4.27$$

and $\tan^{-1}(1/2\ \sqrt{7/2})$ is 43.1°. The fact that the a_2 and a_4 curves shift identically is shown in Eqs. 2.4.26 and 2.4.27.

Figure 2.2 Graph of the a_2 Coefficient Versus Arctangent of Mixing Ratio for Gamma-Ray and Proton Angular Distributions of the $3/2^-$ Compound State in the Total Angular Momentum Representation.

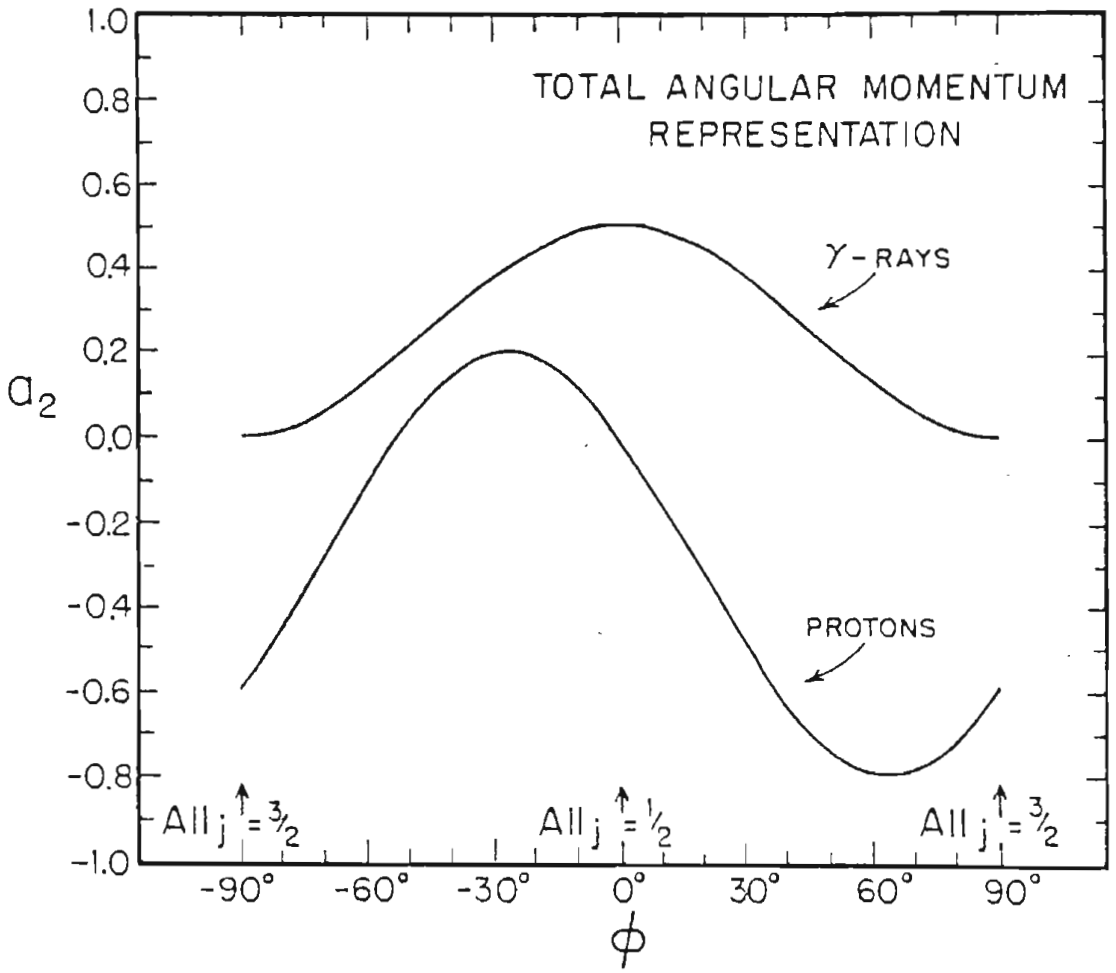
TOTAL ANGULAR MOMENTUM
REPRESENTATION
γ-RAYS
PROTONS
a_2
1.0
0.8
0.6
0.4
0.2
0.0
-0.2
-0.4
-0.6
-0.8
-1.0
All $j = 3/2$
All $j = 1/2$
All $j = 3/2$
-90°
-60°
-30°
0°
30°
60°
90°
ϕ

Figure 2.3 Graph of the a_2 Coefficient Versus Arctangent of Mixing Ratio for Gamma-Ray and Proton Angular Distributions of the 3/2$^-$ Compound State in the Channel Spin Representation.

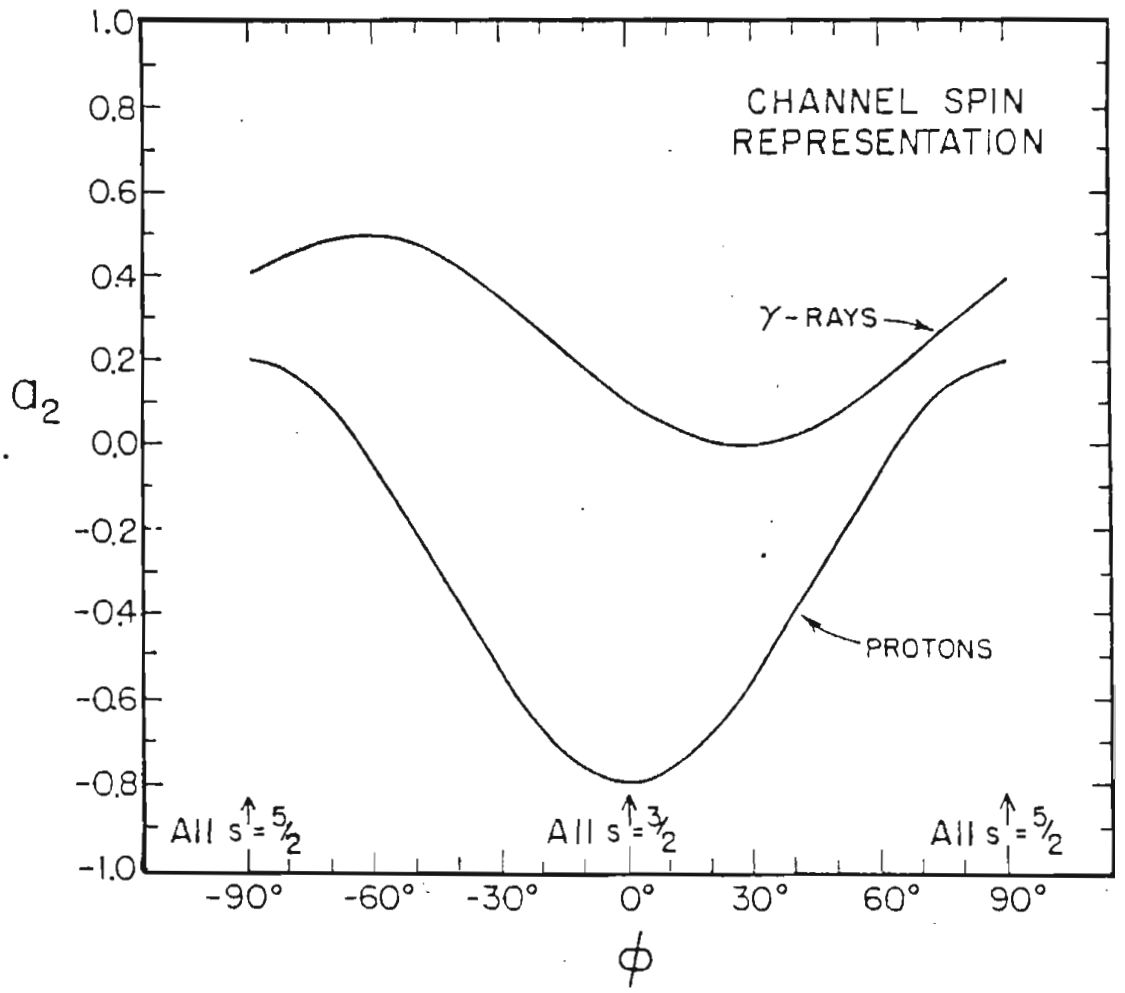
CHANNEL SPIN
REPRESENTATION
γ-RAYS
PROTONS
All s↑=5/2
All s↑=3/2
All s↑=5/2
a2
φ
1.0
0.8
0.6
0.4
0.2
0.0
-0.2
-0.4
-0.6
-0.8
-1.0
-90°
-60°
-30°
0°
30°
60°
90°

Figure 2.4 Graph of the a_2 and a_4 Coefficients Versus Arctangent of Mixing Ratio for Gamma-Ray and Proton Angular Distributions of the 5/2- Compound State in the Total Angular Momentum Representation.

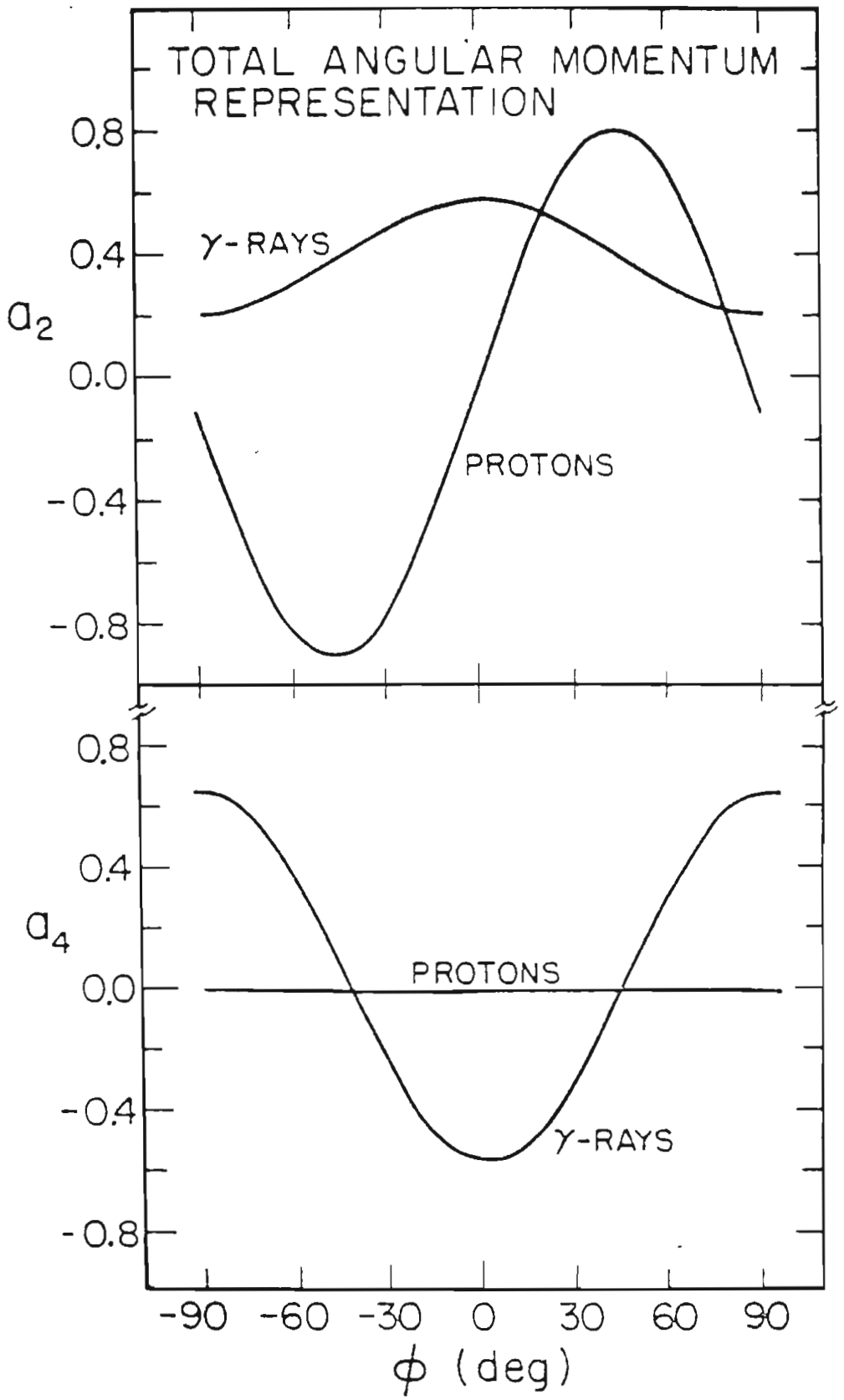
TOTAL ANGULAR MOMENTUM
REPRESENTATION
0.8
0.4
0.0
-0.4
-0.8
a_2
γ-RAYS
PROTONS
0.8
0.4
0.0
-0.4
-0.8
a_4
PROTONS
γ-RAYS
-90
-60
-30
0
30
60
90
φ (deg)

Figure 2.5 Graph of the a_2 and a_4 Coefficients Versus Arctangent of Mixing Ratio for Gamma-Ray and Proton Angular Distributions of the $5/2^-$ Compound State in the Channel Spin Representation.

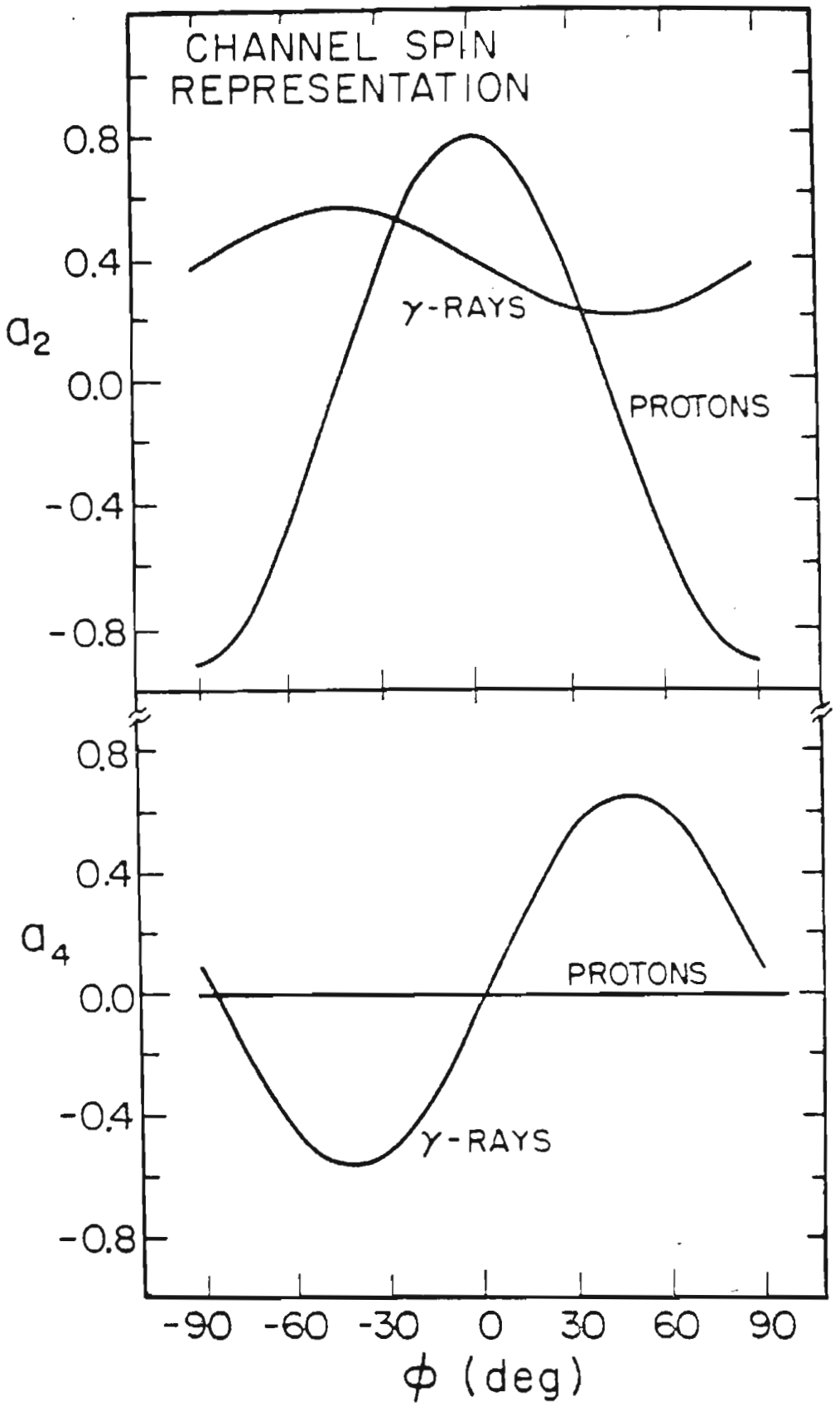
CHANNEL SPIN
REPRESENTATION
0.8
0.4
0.0
-0.4
-0.8
a_2
γ-RAYS
PROTONS
0.8
0.4
0.0
-0.4
-0.8
a_4
PROTONS
γ-RAYS
-90 -60 -30 0 30 60 90
φ (deg)

Chapter 3

EXPERIMENTAL EQUIPMENT AND PROCEDURES

3.1 3 MV Van de Graaff Accelerator

This experiment was performed on the 3 MV Van de Graaff accelerator and associated high-resolution system at the Triangle Universities Nuclear Laboratory.

The accelerator and associated analyzer-homogenizer system are shown in Fig. 3.1. This system is described in detail by Parks et al. (1969). Recently the homogenizer has been redesigned and rebuilt to provide more reliability.

The accelerator produces a beam composed of the hydrogen ions H^+ and HH^+. The two types of ions are separated by an analyzing magnet which directs the proton (H^+) and molecular (HH^+) beams into separate beam lines. The proton beam passes directly to a scattering chamber. The molecular beam passes first through two slits, called control slits, which sample the position of the beam. This sampling technique produces a signal representative of the difference between the two slit currents. The corona con-

Figure 3.1 Floor Plan of the 3 MV Van de Graaff Accelerator Laboratory.

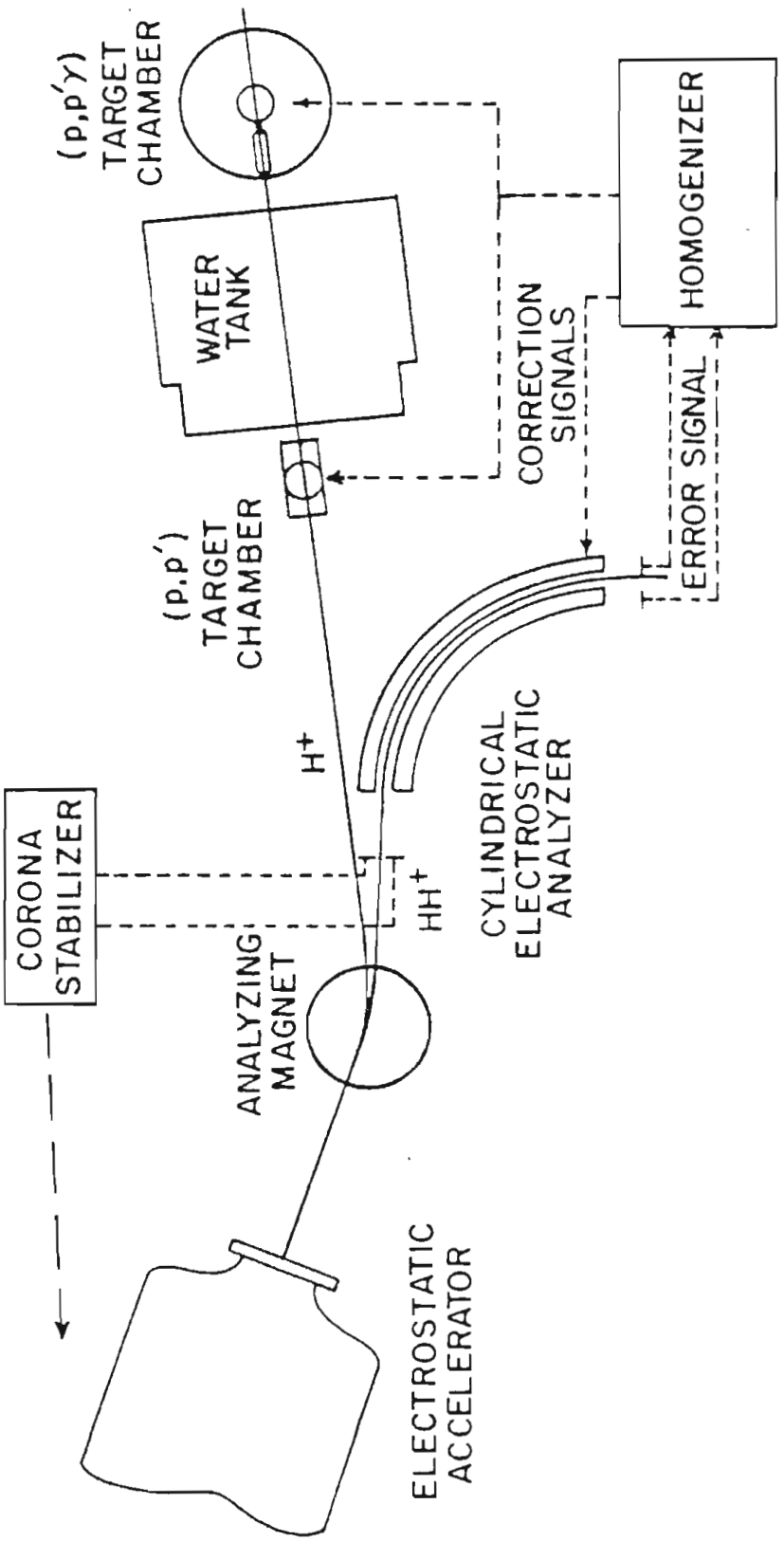
(p,p'γ)
TARGET
CHAMBER
WATER
TANK
(p,p')
TARGET
CHAMBER
CORRECTION
SIGNALS
HOMOGENIZER
ERROR SIGNAL
H+
HH+
CYLINDRICAL
ELECTROSTATIC
ANALYZER
CORONA
STABILIZER
ANALYZING
MAGNET
ELECTROSTATIC
ACCELERATOR

trol circuit uses this difference signal as a first order correction to the beam energy, and removes all low (<20Hz) frequency fluctuations. The signal from the corona control circuit must pass through an insulating gas to reach the accelerator dome. Since this signal requires a finite amount of time to reach the dome, fast fluctuations cannot be removed with this method.

After the control slits, the molecular beam passes through an electrostatic analyzer. The analyzer consists of two concentric quarter circle plates with a mean radius of one meter, and with a separation of 0.18". A well regulated negative high voltage (20-30 kV) is applied to the inner plate in order to steer the beam through the gap. At the entrance to the analyzer are two object slits used to initially center the beam in the analyzer. As it exits the analyzer, the beam passes through two image slits. Any change in energy will cause the beam to be off-center on the image slits. A Princeton Applied Research (PAR) Model 113 difference amplifier produces a difference signal from the signal on the image slits and sends this signal to the homogenizer.

The geometrical shape of the analyzer is such that the energy of a molecular beam centered on the image slits will be 111 times the voltage applied to the inner plate. The high voltage supply for the inner plate also sends an output signal to a precision resistance stack, where the

signal is divided by 111. The new signal is used by a differential voltmeter (DVM) as a check against the desired voltage. If the two voltages do not match, a signal is sent to the homogenizer.

The homogenizer sums the outputs from the DVM and the PAR, and sends this signal to the outer plate of the analyzer. The molecular beam has now been corrected for fast fluctuations in energy. At the same time, the homogenizer multiplies the PAR signal by 111 and sends this to the target rod. Normally the target rod is biased at +4 kV, but the correction signal can raise or lower this by 2 kV.

This completes the corrections necessary to maintain a constant beam energy. Any slow energy change will be detected on the control slits, and the correction will be made by the corona control circuit. Fast fluctuations are detected on the image slits of the analyzer, and the corrections are applied by the homogenizer. A schematic diagram of the analyzer-homogenizer system is given in Fig. 3.2.

Figure 3.2 Block Diagram of the Present Electrostatic Analyzer-Homogenizer Circuitry.

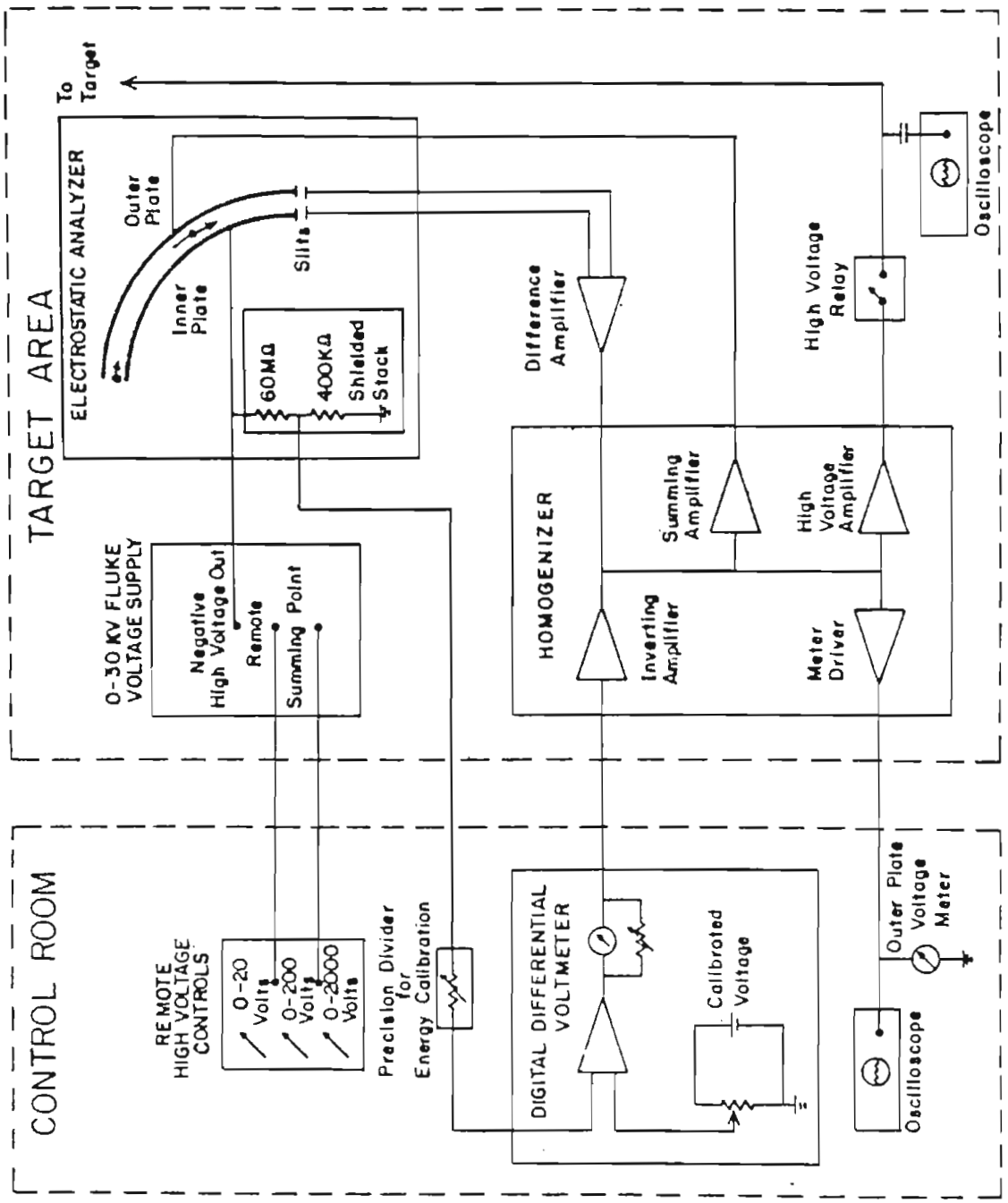
TARGET AREA
ELECTROSTATIC ANALYZER
To Target
Outer Plate
Inner Plate
Slits
60MΩ
400KΩ
Shielded Stack
Difference Amplifier
High Voltage Relay
Oscilloscope
0-30 KV FLUKE VOLTAGE SUPPLY
Negative High Voltage Out
Remote
Summing Point
HOMOGENIZER
Summing Amplifier
High Voltage Amplifier
Inverting Amplifier
Meter Driver
CONTROL ROOM
REMOTE HIGH VOLTAGE CONTROLS
0-20 Volts
0-200 Volts
0-2000 Volts
Precision Divider for Energy Calibration
DIGITAL DIFFERENTIAL VOLTMETER
Calibrated Voltage
Outer Plate Voltage Meter
Oscilloscope

3.2 Scattering Chambers

Two scattering chambers were used in this experiment. A chamber designed by Browne (1969) was used to study the particle angular distributions. The vacuum in this chamber was kept at 10^{-6} Torr in order to minimize the accumulation of deposits on the target.

Ortec surface barrier detectors located at angles 90°, 120°, 135°, and 160° were used to detect the inelastically scattered protons. All four detectors were placed at the same distance from the target, and all four detectors subtended a solid angle of 1.95 millisteradians. However, movement of the beam affected the area viewed by each detector. To account for small beam movement, elastic scattering was performed upon a gold target after data were taken for each 417 resonance. The gold data were compared with Rutherford scattering cross sections, and a normalization factor was determined for each detector. The worst problem concerned the 120° detector. Elastic scattering experiments performed in previous years used the angle 105°. Therefore, the chamber was not designed for a detector at 120°. A special plate was made to enable the 120° detector to be mounted, but the mount was not as rigid as desired. Therefore, the largest error occurred at 120°. The chamber and collimator assembly

Figure 3.3 Top View of the Proton Detection Chamber With Collimator Assembly.

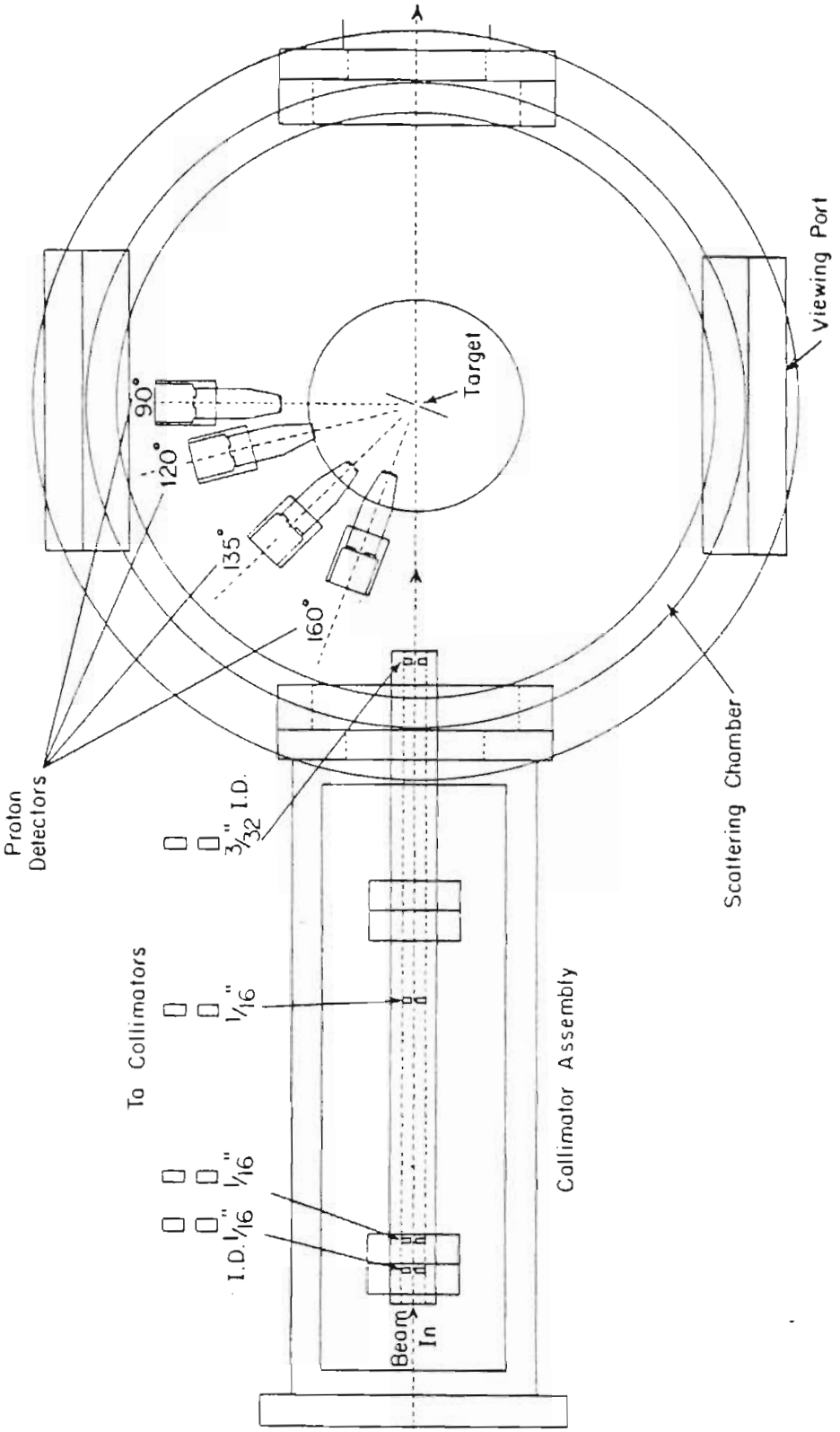
Viewing Port
Target
90°
120°
135°
160°
Proton Detectors
3/32" I.D.
Scattering Chamber
To Collimators
1/16"
I.D. 1/16"
Collimator Assembly
Beam In

preceding the chamber are shown in Fig. 3.3. The first three collimators actually collimate the beam, while the fourth acts as an antiscattering aperture to reduce background in the spectra.

A typical proton spectrum for this experiment is shown in Fig. 3.4. The spectrum shown was taken at an energy of 2.5680 MeV and an angle of 160°, and illustrates the typical relative size of the peaks of interest. Although the ^{12}C peak was gated out electronically, its relative position is shown in the figure.

The chamber used in measuring the gamma-ray angular distributions was designed by Wimpey (1974) and is shown schematically in Fig. 3.5. The chamber vacuum was kept at $5x10^{-7}$ Torr or less throughout the entire experiment. As in the particle measurements, the beam is collimated before it enters the second chamber.

Four 3"x3" NaI(Tl) Harshaw gamma-ray crystals were used in this experiment. The crystals were placed at 90°, 60°, 45°, and 30° and were shielded from stray radiation by two inch thick lead collars. The distances of the detectors from the target ranged from 5.44" to 5.85". Since the relative efficiencies of the four crystals were not equal, the distances were varied slightly so that a known isotropic distribution was measured to be isotropic. Relative efficiencies were determined with calibrated ^{22}Na and ^{137}Cs sources and used to correct the data. Absolute

Figure 3.4 Proton Spectrum for $^{46}Ti(p,p')^{46}Ti^*$ at E_p = 2.5680 MeV. Although the ^{12}C peak has been gated out of the spectrum, its relative position is shown. The solid line is to guide the eye.

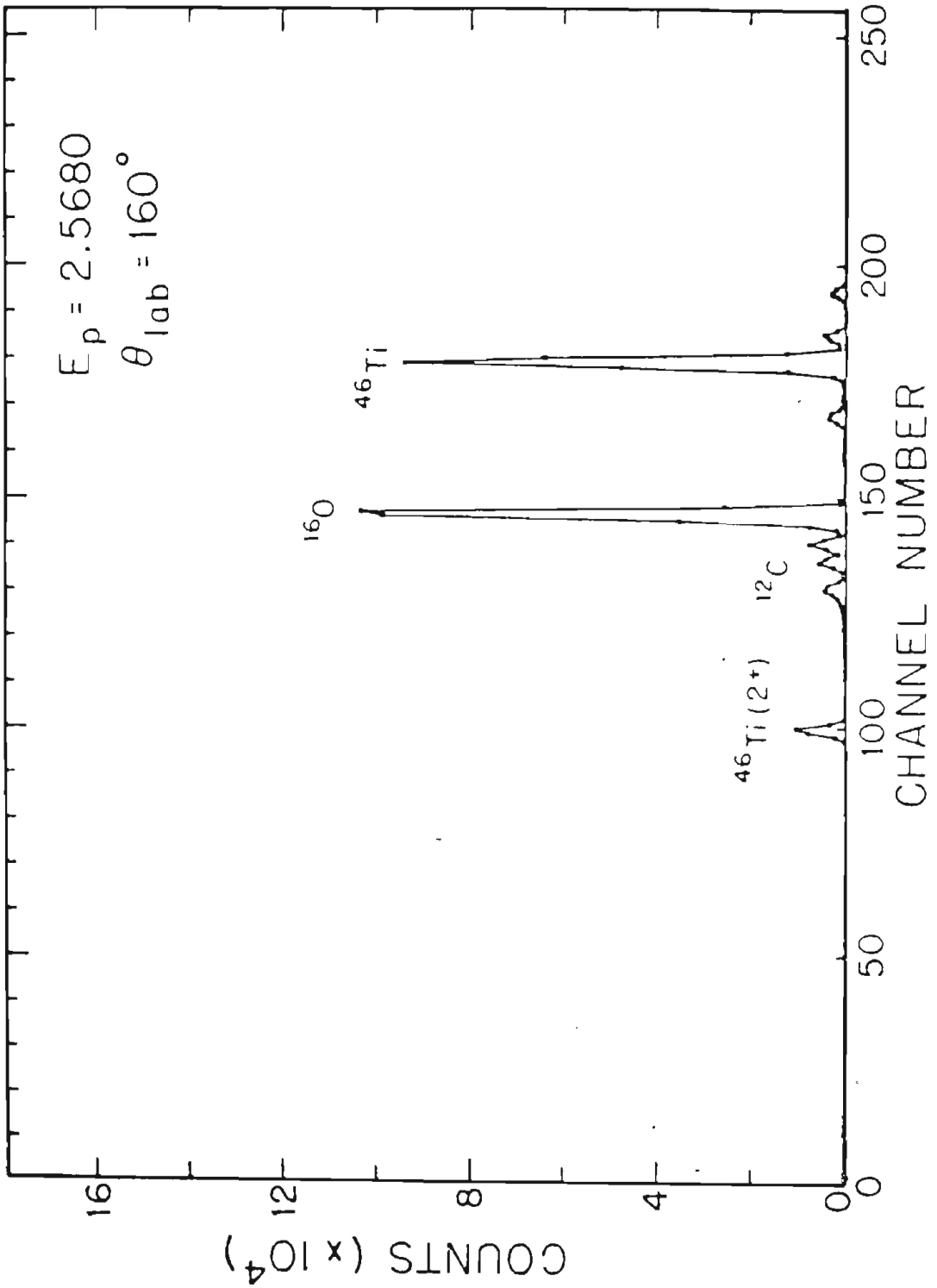
$E_p = 2.5680$
$\theta_{lab} = 160°$
^{46}Ti
^{16}O
^{12}C
$^{46}Ti(2^+)$
COUNTS ($\times 10^4$)
CHANNEL NUMBER
0
4
8
12
16
50
100
150
200
250

Figure 3.5 Gamma-Ray Detection Chamber With Collimator Assembly. A top view is shown in the upper drawing and a side view is shown in the lower drawing.

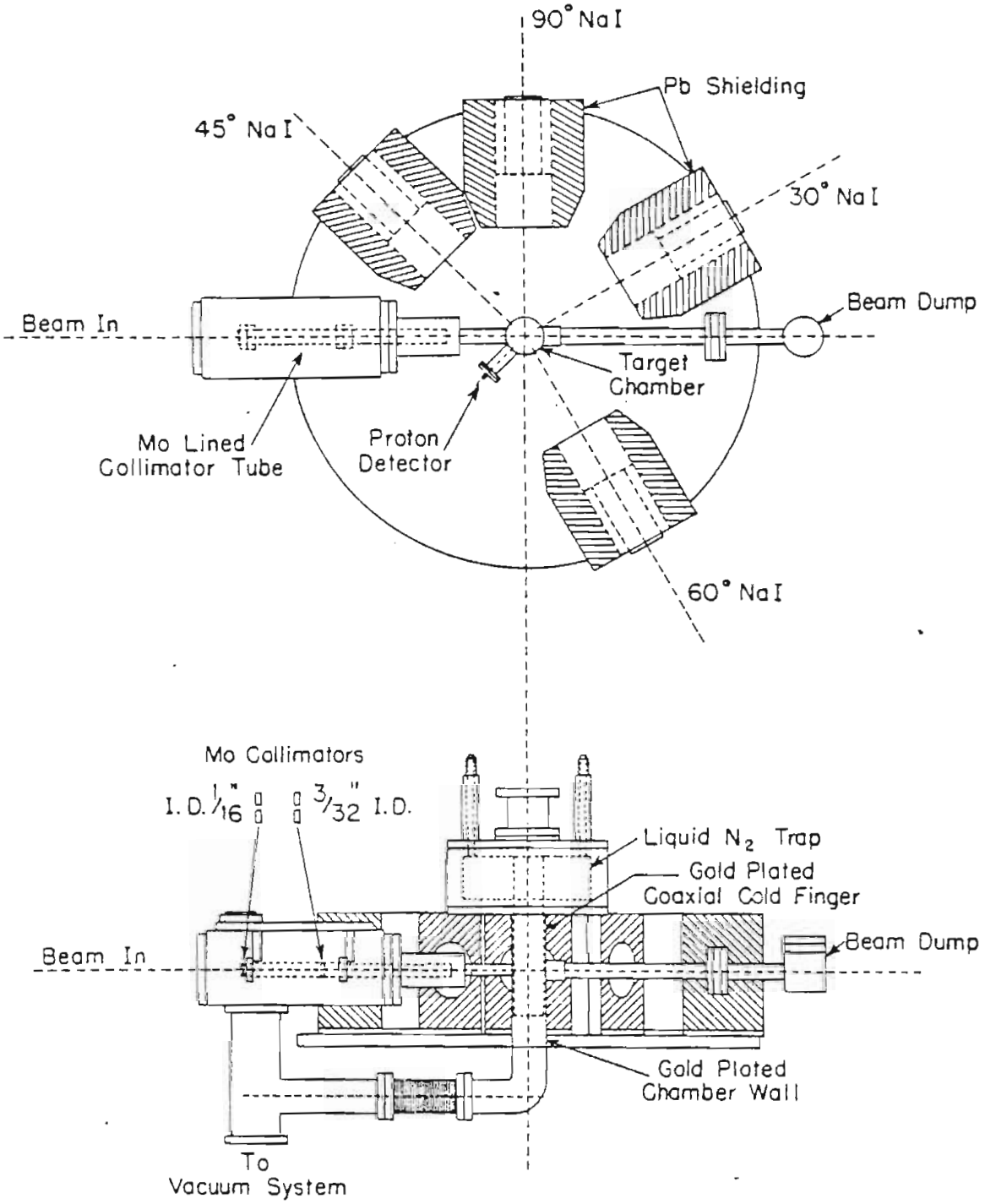
90° NaI
Pb Shielding
45° NaI
30° NaI
Beam In
Beam Dump
Target Chamber
Mo Lined Collimator Tube
Proton Detector
60° NaI
Mo Collimators
I.D. 1/16"
I.D. 3/32"
Liquid N2 Trap
Gold Plated Coaxial Cold Finger
Beam In
Beam Dump
Gold Plated Chamber Wall
To Vacuum System

efficiencies were also determined and utilized in measuring laboratory resonance widths.

Two additional detectors were also used in the gamma-ray study. An Ortec surface barrier detector was used to measure the proton elastic scattering yield. This insured that the resonances studied were the same as those studied in the inelastic proton distribution measurements. An 80cc Ge(Li) detector from Princeton Gamma-Tech was also used. The Ge(Li) detector has much better resolution than the NaI(Tl) detectors and was used to monitor the spectrum for contaminant gamma-rays.

A sample NaI(Tl) spectrum is shown in Fig. 3.6 for E_p = 2.5539 MeV and a detector angle of 30°. The ^{46}Ti peak occurs at 0.889 MeV. The 0.983 MeV gamma-ray was produced by the ^{48}Ti contaminant.

Figure 3.6 Gamma-Ray Spectrum for $^{46}Ti(p,p'\gamma)^{46}Ti$ at Energy 2.5539 MeV. The 0.889 MeV gamma-ray is from the decay of the first excited state in ^{46}Ti. The 0.983 MeV gamma-ray is from the decay of the ^{48}Ti contaminant. The solid line is a guide to the eye.

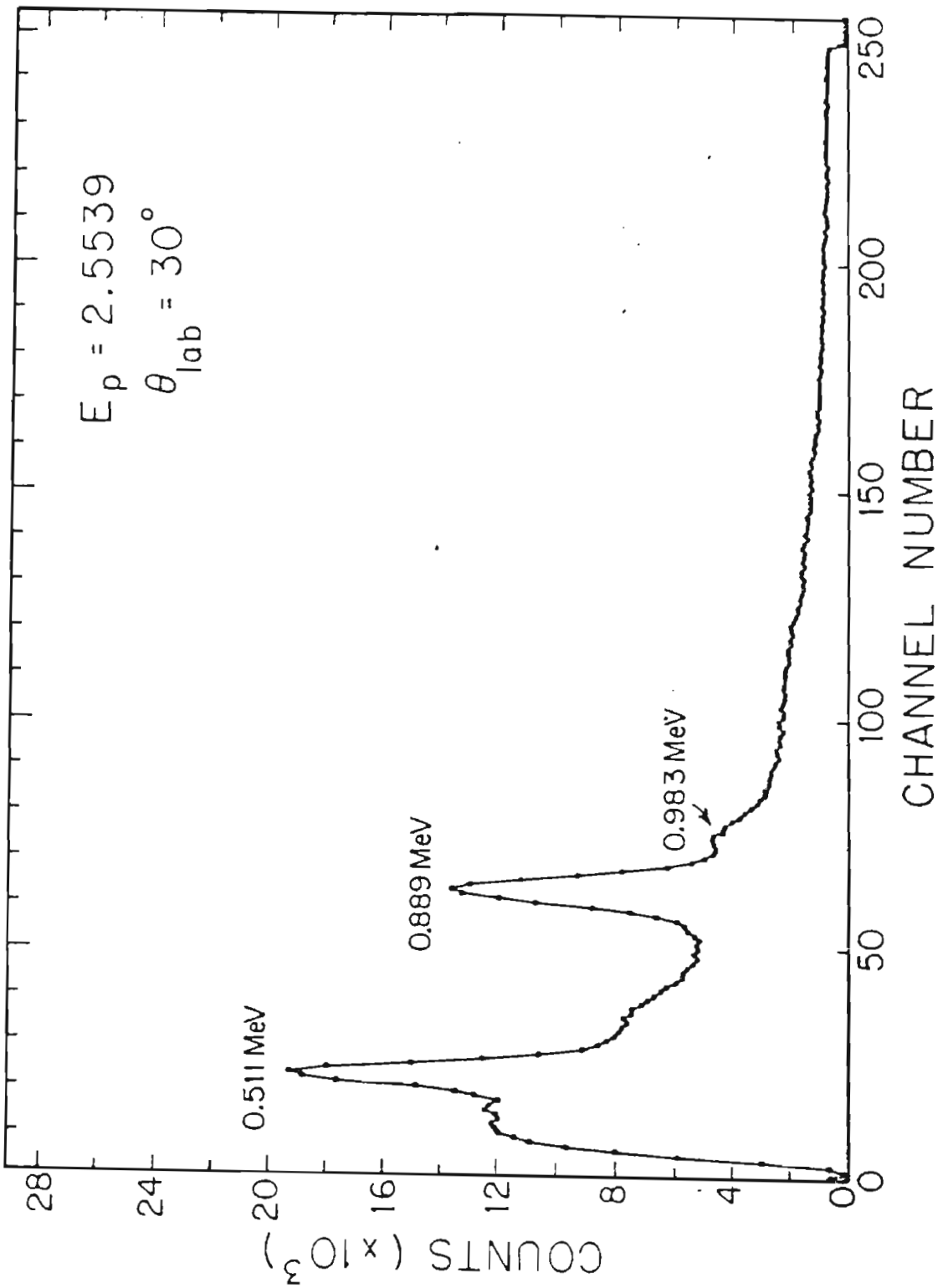
E_p = 2.5539
θ_{lab} = 30°
0.511 MeV
0.889 MeV
0.983 MeV
COUNTS (x 10³)
CHANNEL NUMBER
0
4
8
12
16
20
24
28
50
100
150
200
250

3.3 Electronics and Computer

The detection electronics used in this experiment are illustrated in Fig. 3.7. All of the electronics shown in the figure are located in the 3 MV laboratory. The computer, a Prime 300 with 32K of memory, is in the main Physics building. This experiment was the first to be carried out using the Prime computer. Therefore, a description of the computer interface and software is given in the Appendix.

Consider first the particle measurements. When a surface barrier detector outputs a pulse, the pulse is amplified by an Ortec (model 109A) preamplifier and by a Tennelec 203 spectroscopy amplifier. The spectroscopy amplifier outputs two signals; one unipolar and one bipolar. The four unipolar signals, one for each detector, were summed in an Ortec 433 Dual Sum and Inverter. The combined linear signal was then sent to a Northern Scientific (model 621) analogue to digital converter (ADC). Each bipolar signal was sent to an Ortec (model 420A) timing single channel analyzer (SCA), and also through a delay line and into a Hewlett Packard (model 558A) single channel analyzer. The output of the timing SCA was also input into the Hewlett Packard SCA as a gate signal. This system allowed the ^{12}C signals to be gated out by simply setting a

Figure 3.7 Block Diagram of the Proton and Gamma-Ray Detection Electronics.

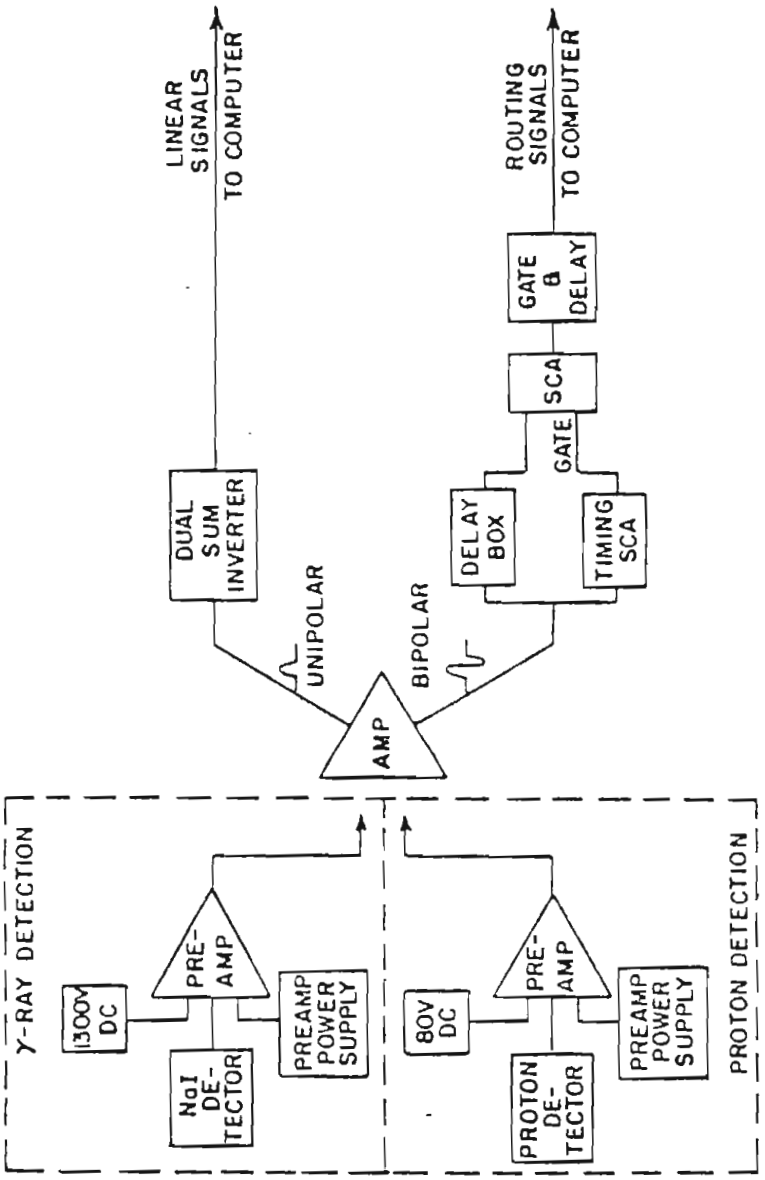
γ-RAY DETECTION
1300V DC
NaI DE-TECTOR
PRE-AMP
PREAMP POWER SUPPLY
80V DC
PROTON DE-TECTOR
PRE-AMP
PREAMP POWER SUPPLY
PROTON DETECTION
AMP
UNIPOLAR
BIPOLAR
DUAL SUM INVERTER
LINEAR SIGNALS TO COMPUTER
DELAY BOX
TIMING SCA
GATE
SCA
GATE & DELAY
ROUTING SIGNALS TO COMPUTER

window around the carbon pulses. The timing SCA would then output a signal only for carbon pulses, and the Hewlett Packard SCA would gate out the carbon upon receipt of the gate from the timing SCA. The outputs of the four Hewlett Packard SCA's were then sent to an Ortec (model 416A) gate and delay generator to be shaped and input to an eight input router.

The main function of the router was to construct a three bit word according to which input received the signal, and to set a fourth bit if two inputs received a signal at the same time. However, the router also output a gate and a busy signal. The router gate was used to gate the ADC which was operated in a coincidence mode. The output of the ADC was a twelve bit word, and along with the four bits from the router, comprised a sixteen bit word input into the computer.

The counting time for each data point was regulated by an Ortec (model 439) current digitizer. Beam was collected behind the target and sent to the current digitizer. A scalar was fed the output from the digitizer, and the counting time was preset on the scaler. A correction for dead time was made using the router busy signal to gate off the current digitizer.

The detection system was the same for the NaI(Tl) signals except that the Hewlett Packard SCA's were not gated.

3.4 Targets

Targets for this experiment were prepared from two different enriched ^{46}Ti samples obtained from Oak Ridge National Laboratory. One was in the form of a crystal bar; the second was a titanium dioxide powder. The enrichment of both samples was 81.2%. The major contaminant was ^{48}Ti, which was 14.5%. The other 4.3% consisted of ^{47}Ti, ^{49}Ti, and ^{50}Ti.

Preparation of targets proved easiest with the crystal bar. The bar was placed in a tantalum boat, which was heated in a high-current evaporator. The Ti was evaporated onto carbon foils of thickness 2 $\mu g/cm^2$. A glass slide was placed on top of the foils in order to prevent Ti from depositing onto the back side.

The titanium dioxide required a closed tantalum boat. This was made by crimping both ends of a 0.25" O. D. piece of tantalum tubing and drilling a small hole in the center of the tube. About 17 milligrams of carbon were placed in the boat along with 27 milligrams of titanium dioxide. The titanium dioxide was first reduced and then evaporated. Targets made by both methods were about 1 $\mu g/cm^2$ thick.

Chapter 4

EXPERIMENTAL RESULTS

4.1 Preliminary Analysis

Fifty-two p-wave and f-wave resonances were studied between the proton energies 2.25 MeV and 3.07 MeV for the reaction $^{46}Ti(p,p'\gamma)^{46}Ti$. These resonances are listed in Table 4.1, where the resonance energies are those given by Prochnow (1971). The compound nuclear resonances decay to the 2^+ excited state at 0.889 MeV. It was assumed that the decay of the compound state occurred only by $\ell'=1$ protons. This assumption seems valid for the inelastic channel because the ratio of the $\ell'=1$ and $\ell'=3$ penetrabilities is 117 to 1 at 2.0 MeV and 55 to 1 at 3.0 MeV. For the elastic channel, the ratio is 59 to 1 and 30 to 1 at 2.0 MeV and 3.0 MeV respectively.

Excitation curves were measured for an energy range of about 2 keV on either side of each resonance. Once the resonance was located and the accelerator energy set at the resonance energy, proton and gamma-ray spectra were accumulated. Two studies of each resonance were required

Table 4.1 ^{47}V Resonance Parameters

Res. No.	E_p (MeV)	J^π	Γ_p (eV)	γ_p^2 (keV)	$\Gamma_{p'}$ (eV)	$\gamma_{p'}^2$ (keV)
1	2.2508	3/2−	40 ± 5	0.98	2	2.33
2	2.2900	3/2−	330 ± 60	7.27	20	19.79
3	2.3163	3/2−	25 ± 5	0.51	weak	
4	2.3492	3/2−	220 ± 20	4.13	6	4.37
5	2.3720	3/2−	10 ± 5	0.18	2	1.45
6	2.3950	3/2−	50 ± 5	0.84	weak	
7	2.4812	1/2−	3100 ±200	41.92	weak	
8	2.4985	1/2−	110 ± 15	1.43	weak	
9	2.5087	3/2−	250 ± 75	3.17	weak	
10	2.5297	3/2−	35 ± 10	0.42	7	1.74
11	2.5333	1/2−	2600 ±300	31.14	weak	
12	2.5506	3/2−	20 ± 10	0.23	weak	
13	2.5539	5/2−	1 ± 1	0.47	1	1.43
14	2.5680	3/2−	20 ± 10	0.22	36	7.86
15	2.5801	1/2−	525 ± 50	5.66	weak	
16	2.5929	3/2−	130 ± 15	1.36	3	0.48
17	2.6322	3/2−	65 ± 10	0.63	weak	
18	2.6368	3/2−	60 ± 10	0.57	2	0.33
19	2.6842	3/2−	30 ± 10	0.26	11	1.41
20	2.6953	5/2−	4 ± 2	1.24	9	6.48

Table 4.1 (continued)

Res. No.	E_p (MeV)	J^π	Γ_p (eV)	γ_p^2 (keV)	$\Gamma_{p'}$ (eV)	$\gamma_{p'}^2$ (keV)
21	2.6992	3/2−	1450 ±150	12.15	weak	
22	2.7056	3/2−	1400 ±150	11.58	51	5.95
23	2.7096	3/2−	135 ± 25	1.11	52	5.97
24	2.7380	1/2−	215 ± 20	1.67	13	1.34
25	2.7411	3/2−	110 ± 15	0.85	1	0.13
26	2.7626	3/2−	25 ± 10	0.18	32	2.98
27	2.7972	1/2−	40 ± 10	0.28	weak	
28	2.8010	3/2−	10 ± 5	0.06	15	1.20
29	2.8206	3/2−	35 ± 10	0.23	23	1.72
30	2.8326	3/2−	55 ± 10	0.36	43	3.03
31	2.8397	5/2−	10 ± 5	2.12	19	7.39
32	2.8456	1/2−	1200 ±150	7.58	weak	
33	2.8459	5/2−	25 ± 10	5.23	weak	
34	2.8638	3/2−	600 ± 70	3.67	150	9.49
35	2.8708	5/2−	15 ± 5	2.95	42	14.43
36	2.8732	3/2−	240 ± 40	1.44	101	6.19
37	2.8977	3/2−	190 ± 30	1.09	38	2.11
38	2.9057	3/2−	1780 ±300	10.10	127	6.95
39	2.9307	1/2−	20 ± 10	0.11	9	0.44
40	2.9350	3/2−	150 ± 30	0.81	51	2.53

Table 4.1 (continued)

Res. No.	E_p (MeV)	J^π	Γ_p (eV)	γ_p^2 (keV)	Γ_p' (eV)	$\gamma_p^{2\prime}$ (keV)
41	2.9397	1/2−	1400 ±200	7.49	weak	
42	2.9463	(5/2−)	5 ± 3	0.82	weak	
43	2.9526	3/2−	50 ± 15	0.26	16	0.72
44	2.9562	1/2−	1800 ±200	9.36	73	3.37
45	2.9607	3/2−	110 ± 15	0.57	weak	
46	2.9655	1/2−	175 ± 20	0.90	7	0.32
47	2.9836	3/2−	75 ± 15	0.37	9	0.36
48	3.0047	1/2−	190 ± 25	0.91	41	1.60
49	3.0279	3/2−	20 ± 10	0.09	17	0.61
50	3.0490	1/2−	700 ± 75	3.12	weak	
51	3.0605	3/2−	70 ± 15	0.31	23	0.74
52	3.0654	1/2−	550 ± 75	2.39	weak	

since the inelastic proton data and gamma-ray data were measured in separate chambers. Excitation curves were measured in each case, however, to insure that the same resonance was being studied. In both studies, data were accumulated until there were ten thousand counts in the peak of interest, or until thirty thousand microcoulombs of integrated charge had been accumulated (see Sec. 3.3).

Spectra from four detectors (see Sec. 3.2) were accumulated at each resonance energy for both protons and gamma-rays. The areas under the inelastic proton and gamma-ray peaks were found by subtracting an exponential background from a region including the peaks. These areas were then normalized as described in Sec. 3.2. The major error in these areas arose from two sources; counting statistics and changes in effective solid angle due to movement of the proton beam. The statistical error was normally less than one percent for gamma-ray data and two percent for proton data. The error due to beam movement was estimated in two ways. For protons, the standard deviation was calculated from the normalization factors. This was assumed to be the worst possible beam movement. The results of this analysis yielded errors of about six percent for the proton angles 90°, 135°, and 160°. The error for 120° was estimated to be sixteen percent; this was larger due to the manner in which the detector was mounted (see Sec. 3.2). The gamma-ray errors were deter-

mined by assuming that the beam moves no more than 0.05" horizontally. The 0.05" movement would cause a two percent change in NaI(Tl) detector solid angle. The final errors were then assumed to be three percent for gamma-rays; seven percent for proton angles 90°, 135°, and 160°; and sixteen percent for the proton angle 120°.

Once the normalized peak areas were obtained, they were fitted to a Legendre polynomial expansion of the form $a_0(1+a_2P_2(\theta)+a_4P_4(\theta))$, and a_2 and a_4 values were obtained. From the results of Chap. 2, two solutions for the mixing ratios for both protons and gamma-rays can be determined. However, for the $3/2^-$ and $5/2^-$ resonances the data from the proton and gamma-ray experiments have a common solution. The results for the $3/2^-$ compound states are listed in Table 4.2 and for the $5/2^-$ compound states in Table 4.3. If the a_2 value from both proton and gamma-ray data was zero, the compound state was assigned a spin and parity of $1/2^-$. Of the fifty-two resonances between 2.25 MeV and 3.07 MeV, eighteen were too weak for study. The other thirty-four resonances were studied, and five were determined to be $1/2^-$ resonances. Only five spin assignments were in disagreement with Prochnow's assignments (1971). The disagreements are for resonance Nos. 4, 5, 39, 47, and 49. Of these, only No. 4 has a large elastic width. A common mistake made in the fitting of elastic data is to misassign a $3/2^-$ resonance as $1/2^-$. This is also true for

Table 4.2 Angular Distribution Parameters for 3/2⁻ Resonances in ^{47}V

Res. No.		a_2	$\delta_{j'}$	$\Phi_{j'}$	$\delta_{s'}$	$\Phi_{s'}$
1	P	0.19	-0.39	-21.1°	-10.42	-84.5°
		+0.01	+0.21	+11.4°	+ 7.13	+11.4°
		-0.08	-0.01	- 5.5°	large	- 5.5°
	G	0.46	-0.31	-17.2°	- 6.08	-80.7°
		±0.03	+0.18	+ 9.6°	+ 3.16	+ 9.6°
			-0.12	- 6.2°	-11.99	- 6.2°
2	P	0.20	-0.50	-26.6°	large	-90.0°
		+0.00	+0.32	+16.2°		+16.2°
		-0.06	-0.00	- 0.0°		- 0.0°
	G	0.41	-0.47	-25.4°	-48.73	-88.8°
		±0.04	+0.12	+ 5.7°	+40.48	+ 5.7°
			-0.11	- 4.9°	-64.04	- 1.2°
4	P	-0.46	0.53	27.9°	-0.71	-35.5°
		±0.06	+0.08	+3.6°	+0.09	+ 3.6°
			-0.07	-3.4°	-0.09	- 3.4°
	G	0.35	0.65	33.1°	-0.58	-30.3°
		±0.04	+0.11	+4.3°	+0.10	+ 4.3°
			-0.11	-4.6°	-0.11	- 4.6°
5	P	-0.21	-2.28	-66.3°	1.20	50.3°
		±0.07	+0.38	+ 4.0°	+0.19	+ 4.0°
			-0.50	- 3.9°	-0.16	- 3.9°
	G	0.07	-2.55	-68.6°	1.11	48.0°
		±0.04	+0.57	+ 5.4°	+0.24	+ 5.4°
			-1.32	- 6.9°	-0.24	- 6.9°
10	P	0.20	-0.50	-26.6°	large	-90.0°
		+0.00	+0.31	+16.1°		+16.1°
		-0.02	-0.00	- 0.0°		- 0.0°
	G	0.41	-0.45	-24.4°	-27.00	-87.9°
		±0.04	+0.13	+ 6.3°	+20.22	+ 6.3°
			-0.12	- 5.2°	-45.38	- 2.1°

Table 4.2 (continued)

Res. No.		a_2	δ_j'	Φ_j'	δ_s'	Φ_s'
14	P	0.19	-0.46	-24.6°	-29.31	-88.0°
		+0.01	+0.28	+14.2°	+25.86	+14.2°
		-0.08	-0.04	- 2.0°	-large	- 2.0°
	G	0.42	-0.44	-23.7°	-19.76	-87.1°
		±0.04	+0.12	+ 6.1°	+13.44	+ 6.1°
			-0.11	- 5.1°	-46.08	- 2.0°
16	P	0.05	-1.17	-49.6°	2.35	66.9°
		±0.08	+0.25	+ 6.9°	+1.11	+ 6.9°
			-0.26	- 5.6°	-0.52	- 5.6°
	G	0.37	-0.60	-30.8°	13.65	85.9°
		±0.04	+0.11	+ 4.9°	+ 7.08	+ 4.4°
			-0.11	- 4.5°	- 7.04	- 4.4°
18	P	0.01	-1.30	-52.5°	2.06	64.1°
		±0.07	+0.25	+ 6.0°	+0.70	+ 6.0°
			-0.27	- 5.1°	-0.40	- 5.1°
	G	0.16	-1.43	-55.1°	1.84	61.5°
		±0.04	+0.21	+ 4.3°	+0.38	+ 4.3°
			-0.27	- 4.5°	-0.30	- 4.5°
19	P	0.20	-0.50	-26.6°	large	90.0°
		+0.00	+0.31	+16.0°		+16.0°
		-0.05	-0.00	- 0.0°		- 0.0°
	G	0.41	-0.47	-25.0°	-37.27	-88.5°
		±0.03	+0.12	+ 5.7°	+29.41	+ 5.7°
			-0.11	- 4.9°	-54.41	- 5.7°
22	P	-0.24	-2.52	-68.4°	1.12	48.2°
		±0.07	+0.43	+ 3.9°	+0.16	+ 3.9°
			-0.59	- 3.8°	-0.14	- 3.8°
	G	0.04	-3.38	-73.5°	0.93	43.0°
		±0.04	+1.01	+ 6.4°	+0.24	+ 6.4°
			-6.88	-10.9°	-0.31	-10.9°

Table 4.2 (continued)

Res. No.		a_2	δ_j'	Φ_j'	δ_s'	Φ_s'
23	P	-0.10	0.11	6.4°	-1.54	-57.0°
		±0.08	+0.08	+4.6°	+0.24	+ 4.6°
			-0.09	-4.9°	-0.34	- 4.9°
	G	0.50	0.00	0.0°	-2.00	-63.4°
		+0.00	+0.25	+14.2°	+0.84	+14.2°
		-0.25	-0.00	- 0.0°	-0.00	- 0.0°
25	P	-0.03	-1.46	-55.5°	1.81	61.1°
		±0.07	+0.25	+ 5.3°	+0.48	+ 5.3°
			-0.29	- 4.7°	-0.31	- 4.7°
	G	0.36	-0.64	-32.4°	9.71	84.1°
		±0.03	+0.11	+ 4.5°	+31.43	+ 4.5°
			-0.11	- 4.2°	- 4.07	- 4.2°
26	P	-0.17	-2.07	-64.2°	1.30	52.4°
		±0.07	+0.33	+ 4.2°	+0.22	+ 4.2°
			-0.43	- 4.0°	-0.17	- 4.0°
	G	0.04	-3.64	-74.6°	0.90	42.0°
		±0.04	+1.17	+ 6.7°	+0.24	+ 6.7°
			-1.17	- 6.7°	-0.24	- 6.7°
28	P	-0.18	-2.11	-64.7°	1.28	51.9°
		±0.07	+0.35	+ 4.2°	+0.22	+ 4.2°
			-0.46	- 4.1°	-0.17	- 4.1°
	G	0.14	-1.59	-57.8°	1.65	58.8°
		±0.04	+0.24	+ 4.3°	+0.32	+ 4.3°
			-0.33	- 4.7°	-0.27	- 4.7°
29	P	-0.58	0.71	35.3°	-0.53	-28.1°
		±0.05	+0.10	+ 3.6°	+0.08	+ 3.6°
			-0.08	- 3.3°	-0.08	- 3.3°
	G	0.30	0.83	39.6°	-0.44	-23.9°
		±0.03	+0.12	+ 3.9°	+0.08	+ 3.9°
			-0.11	- 4.1°	-0.09	- 4.1°

Table 4.2 (continued)

Res. No.		a_2	δ_j'	Φ_j'	δ_s'	Φ_s'
30	P	-0.24	-2.46	-67.9°	1.14	48.7°
		±0.07	+0.42	+ 4.0°	+0.17	+ 4.0°
			-0.58	- 3.9°	-0.15	- 3.9°
	G	0.03	-3.67	-74.8°	0.89	41.8°
		±0.03	+1.20	+ 6.8°	+0.24	+ 6.8°
			-1.20	- 6.8°	-0.24	- 6.8°
34	P	-0.72	5.48	79.7°	0.29	16.2°
		±0.04	+3.29	+ 3.8°	+0.07	+ 3.8°
			-1.81	- 4.9°	-0.09	- 4.9°
	G	0.00	large	90.0°	0.50	26.6°
		+0.03		+ 0.0°	+0.00	+ 0.0°
		-0.00		-15.4°	-0.40	-15.4°
36	P	-0.80	2.00	63.5°	0.00	0.0°
		+0.03	+1.43	+10.3°	+0.18	+10.3°
		-0.00	-0.00	- 0.0°	-0.00	- 0.0°
	G	0.00	large	90.0°	0.50	26.6°
		+0.04		+ 0.0°	+0.00	+ 0.0°
		-0.00		-15.5°	-0.40	-15.5°
37	P	-0.79	2.25	66.1°	0.05	2.6°
		+0.04	+1.33	+ 8.3°	+0.15	+8.3°
		-0.01	-0.25	- 2.7°	-0.05	-2.6°
	G	0.05	2.86	70.7°	0.13	7.3°
		±0.03	+2.16	+ 8.0°	+0.15	+8.0°
			-0.72	- 5.8°	-0.10	-5.8°
38	P	-0.44	-5.56	-79.8°	0.75	36.8°
		±0.06	+1.44	+ 3.5°	+0.10	+ 3.5°
			-3.08	- 3.6°	-0.09	- 3.6°
	G	0.10	-2.06	-64.1°	1.30	52.5°
		±0.03	+0.36	+ 4.6°	+0.24	+ 4.6°
			-0.59	- 5.2°	-0.22	- 5.2°

Table 4.2 (continued)

Res. No.		a_2	δ_j'	Φ_j'	δ_s'	Φ_s'
45	P	-0.09	-1.67	-59.1°	1.57	57.4°
		±0.07	+0.28	+ 4.8°	+0.33	+ 4.8°
			-0.34	- 4.4°	-0.24	- 4.4°
	G	0.29	-0.85	-40.5°	4.03	76.1°
		±0.03	+0.11	+ 4.0°	+1.69	+ 4.0°
			-0.13	- 3.9°	-0.93	- 3.9°
43	P	-0.72	5.80	80.2°	0.30	16.8°
		±0.04	+3.72	+ 3.8°	+0.07	+ 3.8°
			-1.95	- 4.8°	-0.09	- 4.8°
	G	0.09	2.14	64.9°	0.03	1.5°
		±0.04	+0.73	+ 5.8°	+0.10	+5.8°
			-0.41	- 5.0°	-0.09	-5.0°
47	P	-0.50	0.59	30.4°	-0.65	-33.1°
		±0.05	+0.08	+ 3.5°	+0.08	+ 3.5°
			-0.07	- 3.3°	-0.08	- 3.3°
	G	0.49	0.08	4.5°	-1.66	-58.9°
		+0.01	+0.20	+11.3°	+0.56	+11.3°
		-0.03	-0.08	- 4.5°	-0.26	- 4.5°
49	P	-0.27	0.30	16.5°	-1.07	-46.9°
		±0.07	+0.07	+ 3.8°	+0.13	+ 3.8°
			-0.07	- 3.8°	-0.15	- 3.8°
	G	0.50	0.00	0.0°	-2.00	-63.4°
		+0.00	+0.27	+14.9°	+2.84	+14.9°
		-0.03	-0.00	- 0.0°	-0.00	- 0.0°
51	P	-0.69	8.26	83.1°	0.36	19.7°
		±0.04	+8.76	+ 3.5°	+0.07	+ 3.5°
			-3.16	- 4.2°	-0.08	- 4.2°
	G	0.00	large	90.0°	0.50	26.6°
		+0.04		+ 0.0°	+0.00	+ 0.0°
		-0.00		-15.3°	-0.40	-15.3°

Table 4.3 Angular Distribution Parameters for $5/2^-$ Resonances in ^{47}V

Res. No.		a_2	a_4	$\delta_{j'}$	$\Phi_{j'}$	$\delta_{s'}$	$\Phi_{s'}$
13	P	-0.85	0.00	-1.58	-57.7°	5.27	79.3°
		±0.03	±0.00	+0.18	+ 3.1°	+2.21	+ 3.1°
				-0.16	- 2.4°	-1.00	- 2.4°
	G	0.31	-0.04	-1.53	-56.9°	5.67	80.0°
		±0.04	±0.06	+0.35	+ 7.0°	+13.49	+ 7.0°
				-0.59	- 7.9°	- 2.57	- 7.9°
20	P	-0.23	0.00	-0.13	-7.6°	-1.22	-50.7°
		±0.07	±0.00	+0.04	+2.3°	+0.09	+ 2.3°
				-0.04	-2.3°	-0.11	- 2.3°
	G	0.46	-0.60	-0.65	-32.9°	-4.00	-76.0°
		±0.04	+0.06	+0.19	+ 8.2°	+1.56	+ 8.2°
			-0.00	-0.20	- 7.2°	-4.41	- 7.2°
31	P	-0.64	0.00	-0.43	-23.4°	-2.30	-66.5°
		±0.05	±0.00	+0.04	+ 2.0°	+0.20	+ 2.0°
				-0.04	- 2.1°	-0.25	- 2.1°
	G	0.44	-0.50	-0.76	37.1°	- 5.81	-80.2°
		±0.04	±0.06	+0.19	+ 7.5°	+ 2.59	+ 7.5°
				-0.21	- 7.0°	-14.71	- 7.0°
35	P	-0.22	0.00	-0.13	-7.6°	-1.22	-50.6°
		±0.07	±0.00	+0.04	+2.3°	+0.09	+ 2.3°
				-0.04	-2.3°	-0.11	- 2.3°
	G	0.50	-0.59	-0.50	-26.7°	-2.72	-69.8°
		±0.04	±0.06	+0.21	+10.2°	+1.02	+10.2°
				-0.19	- 8.0°	-1.89	- 8.0°

these five resonances. It is easy to understand that the spin of a resonance with a small elastic width could be misassigned. However, resonance No. 4 has an elastic width of 220 eV. The excitation curve originally taken by Prochnow and the curve measured in this experiment were both fit with a multi-level, multi-channel R-matrix computer program (MULTI) written by D. L. Sellin (1969). In both the old and new data, a $3/2^-$ spin assignment best fit the data for resonance No. 4.

The resonance numbers in Tables 4.2 and 4.3 refer to those in Table 4.1. The first line of each resonance gives the results obtained from the inelastic proton data, and the two lines following this give the errors. The last three lines of each resonace give similar results for the de-excitation gamma-rays.

It should be noted that the error bars given in Tables 4.2 and 4.3 are not always symmetric. This occurs mainly in regions where the a_2 or a_4 value is near a maximum or a minimum. In these cases, the coefficient plus one of the errors may yield a nonphysical result; thus the error in that particular direction is reduced in order that the coefficient plus error gives a physical result. If the coefficient itself was nonphysical but the error bars brought the coefficient within physical limits, the maximum physical value was assumed. It should also be pointed out that the Legendre polynomial fitting routine

weights the data points according to the error estimates. The gamma-ray data are weighted equally, but the 120° proton data is weighted less than data at the other three proton angles.

The results of the proton and gamma-ray studies usually do not agree exactly. Therefore, it is necessary to combine the common solutions and weight the relative errors. This weighting was accomplished in the following manner:

$$\delta_{s'} = \frac{\Delta P \delta_{\gamma_{s'}} + \Delta G \delta_{p'_{s'}}}{\Delta P + \Delta G} \qquad 4.1.1$$

$$\delta_{j'} = \frac{\Delta P \delta_{\gamma_{j'}} + \Delta G \delta_{p'_{j'}}}{\Delta P + \Delta G} \qquad 4.1.2$$

where ΔP and ΔG are the size of the errors on the mixing ratio measured in the proton and gamma-ray data, respectively. The errors determined in the two individual methods were also weighted in the same fashion. The final values obtained from combining gamma-ray and proton data are listed in Tables 4.4 and 4.5.

The values for Γ_p were obtained by Prochnow (1971). The present values for Γ_p are the same except for resonance Nos. 34, 36, 37, and 38. In these four cases, Prochnow obtained doublets, but no doublets were observed

Table 4.4 Mixing Ratios
for 3/2⁻ Resonances in ^{47}V

Res. No.	$\delta_{j'}$	$\Phi_{j'}$	$\delta_{s'}$	$\Phi_{s'}$
1	-0.35 +0.19 -0.12	-19.1° +10.5° - 5.8°	- 6.08 + 3.16 -27.13	-80.7° + 9.6° - 7.6°
2	-0.49 +0.20 -0.06	-25.9° +10.0° - 2.9°	-large	-89.6° + 6.5° - 2.9°
4	0.58 +0.10 -0.09	30.1° + 3.9° - 3.9°	-0.65 +0.09 -0.10	-33.2° + 3.9° - 4.0°
5	-2.36 +0.44 -0.76	-67.1° + 4.5° - 5.2°	1.16 +0.21 -0.19	49.3° + 4.6° - 5.1°
10	-0.47 +0.21 -0.07	-25.4° +10.5° - 3.0°	-92.55 +85.77 -large	-89.4° + 7.8° - 3.0°
14	-0.45 +0.19 -0.08	-24.1° + 9.5° - 3.8°	-19.76 +13.45 -large	-87.1° + 6.1° - 2.4°
16	-0.77 +0.15 -0.16	-37.6° + 5.9° - 5.2°	2.53 +1.20 -0.55	68.4° + 6.6° - 5.2°
18	-1.37 +0.23 -0.27	-53.9° + 5.0° - 4.8°	1.92 +0.50 -0.34	62.5° + 5.1° - 4.8°
19	-0.48 +0.20 -0.06	-25.7° + 9.9° - 2.9°	46.51 +large -33.79	88.8° + 9.9° - 2.9°
22	-2.62 +0.49 -1.30	-69.1° + 4.3° - 6.6°	1.05 +0.19 -0.20	46.4° + 4.7° - 6.0°

Table 4.4 (continued)

Res. No.	$\delta_{j'}$	$\Phi_{j'}$	$\delta_{s'}$	$\Phi_{s'}$
23	0.07	3.8°	-1.73	-60.0°
	+0.15	+8.4°	+0.48	+ 8.7°
	-0.05	-3.0°	-0.20	- 2.6°
25	-0.86	-40.8°	1.98	63.2°
	+0.15	+ 5.2°	+1.14	+ 9.1°
	-0.16	- 4.8°	-0.39	- 5.4°
26	-2.07	-64.2°	1.15	48.9°
	+0.33	+ 4.2°	+0.22	+ 5.0°
	-1.20	- 8.8°	-0.26	- 7.3°
28	-1.80	-61.0°	1.42	54.9°
	+0.28	+ 4.4°	+0.26	+ 4.4°
	-0.39	- 4.5°	-0.21	- 4.4°
29	0.76	37.2°	-0.49	-26.1°
	+0.11	+ 3.8°	+0.08	+ 3.8°
	-0.10	- 3.7°	-0.08	- 3.7°
30	-2.46	-67.9°	1.06	46.5°
	+0.42	+ 4.0°	+0.20	+ 4.8°
	-1.58	- 8.2°	-0.23	- 7.0°
34	10.59	84.6°	0.36	20.0°
	+ 3.29	+ 1.3°	+0.05	+ 2.4°
	- 6.92	- 9.8°	-0.17	- 8.8°
36	2.67	69.4°	0.16	8.9°
	+5.14	+13.3°	+0.25	+13.3°
	-1.34	-16.3°	-0.03	-16.3°
37	2.00	63.4°	0.08	4.7°
	+0.59	+ 5.5°	+0.15	+8.2°
	-0.53	- 7.7°	-0.07	-4.0°

Table 4.4 (continued)

Res. No.	δ_j,	Φ_j,	δ_s,	Φ_s,
38	-2.66	-69.4°	0.91	42.3°
	+0.55	+ 4.7°	+0.14	+ 4.1°
	-1.02	- 5.4°	-0.13	- 4.4°
40	-1.09	-47.3°	2.01	63.5°
	+0.16	+ 4.6°	+0.57	+ 5.3°
	-0.19	- 4.5°	-0.36	- 4.8°
43	2.78	70.0°	0.17	9.9°
	+1.23	+ 5.9°	+0.09	+4.8°
	-0.67	- 5.6°	-0.09	-4.9°
47	0.40	22.0°	-0.81	-39.0°
	+0.13	+ 6.0°	+0.16	+ 5.9°
	-0.08	- 3.8°	-0.12	- 4.1°
49	0.19	10.9°	-1.30	-52.4°
	+0.14	+ 7.6°	+0.32	+ 7.9°
	-0.05	- 2.6°	-0.12	- 2.3°
51	20.18	87.2°	0.41	22.1°
	+94.41	+ 2.3°	+0.05	+ 2.3°
	-15.07	- 8.2°	-0.15	- 8.0°

Table 4.5 Mixing Ratios
for $5/2^-$ Resonances in ^{47}V

Res. No.	$\delta_{j'}$	$\Phi_{j'}$	$\delta_{s'}$	$\Phi_{s'}$
13	-1.57	-57.5°	5.34	79.4°
	+0.29	+ 5.4°	+4.08	+ 4.6°
	-0.21	- 3.2°	-1.26	- 3.2°
20	-0.22	-12.6°	-1.50	-56.4°
	+0.07	+ 3.6°	+0.67	+16.7°
	-0.07	- 3.7°	-0.55	- 7.6°
31	-0.49	-26.1°	-2.39	-67.3°
	+0.07	+ 3.0°	+0.26	+ 2.5°
	-0.07	- 3.0°	-0.63	- 4.4°
35	-0.20	-11.1°	-1.32	-52.7°
	+0.07	+ 3.9°	+0.15	+ 3.5°
	-0.07	- 3.6°	-0.22	- 4.2°

in this experiment. The excitation curves from the original data of Prochnow were refit using MULTI to obtain the parameters listed in Table 4.1 for these resonances.

The $\Gamma_{p'}$ values were determined from the following equation from Peters (1972):

$$(2J+1)\Gamma_p\Gamma_{p'}/\Gamma = 4Y/(B\lambda^2 t) \qquad 4.1.3$$

This is the thin target yield for protons on spin zero targets where: J is the spin of the compound nuclear state; Γ is the elastic scattering width in eV; $\Gamma_{p'}$ is the inelastic scattering width; Γ is the total scattering width; Y is the yield in eV-reactions per incident proton; the B parameters are from the stopping power equation and are tabulated by Marion (1960); λ is the center of mass wavelength of the incident protons in centimeters; and t is the target thickness in $\mu g/cm^2$. To obtain the values listed in Table 4.1, the approximation $\Gamma_p/\Gamma = 1$ was made. This approximation is reasonable since the inelastic widths are much smaller than the elastic widths. The inelastic widths in Table 4.1 are generally slightly smaller than those found by Prochnow.

4.2 Inelastic Reduced Widths and Amplitudes

The reduced widths were calculated using the relation

$$\gamma^2_{\lambda c} = \frac{\Gamma_{\lambda c}}{2P_c} \qquad 4.2.1$$

where $\Gamma_{\lambda c}$ is the partial width of resonance λ in channel c, and P_c is the Coulomb penetrability for channel c. The penetrability was evaluated at the channel radius $R = 1.25(A_1^{1/3} + A_2^{1/3})$ Fermi, where A_1 and A_2 are the mass numbers of the nuclei. The total inelastic reduced widths are listed in Table 4.1.

It is expected that the width distribution should have a Porter-Thomas form if no analogue states are included. The Porter-Thomas distribution is

$$W(\gamma^2) = \frac{1}{\sqrt{2\pi\gamma^2\langle\gamma^2\rangle}} \exp(-\gamma^2/2\langle\gamma^2\rangle) \qquad 4.2.2$$

Fig. 4.1 shows the 3/2$^-$ compound state data compared to a normalized Porter-Thomas distribution. The three analogue states studied are composed of resonance Nos. 2, 22, 23, 29, 30, 34, 36, 37, 38, 40, and 43, with the latter eight comprising the 2.87 MeV state. Therefore, the widths from these resonances are not included in Fig. 4.1. The areas

Figure 4.1 Distribution of Reduced Widths for the $3/2^-$ Levels in ^{47}V Excluding Analogue States. The smooth curve is a normalized Porter-Thomas distribution.

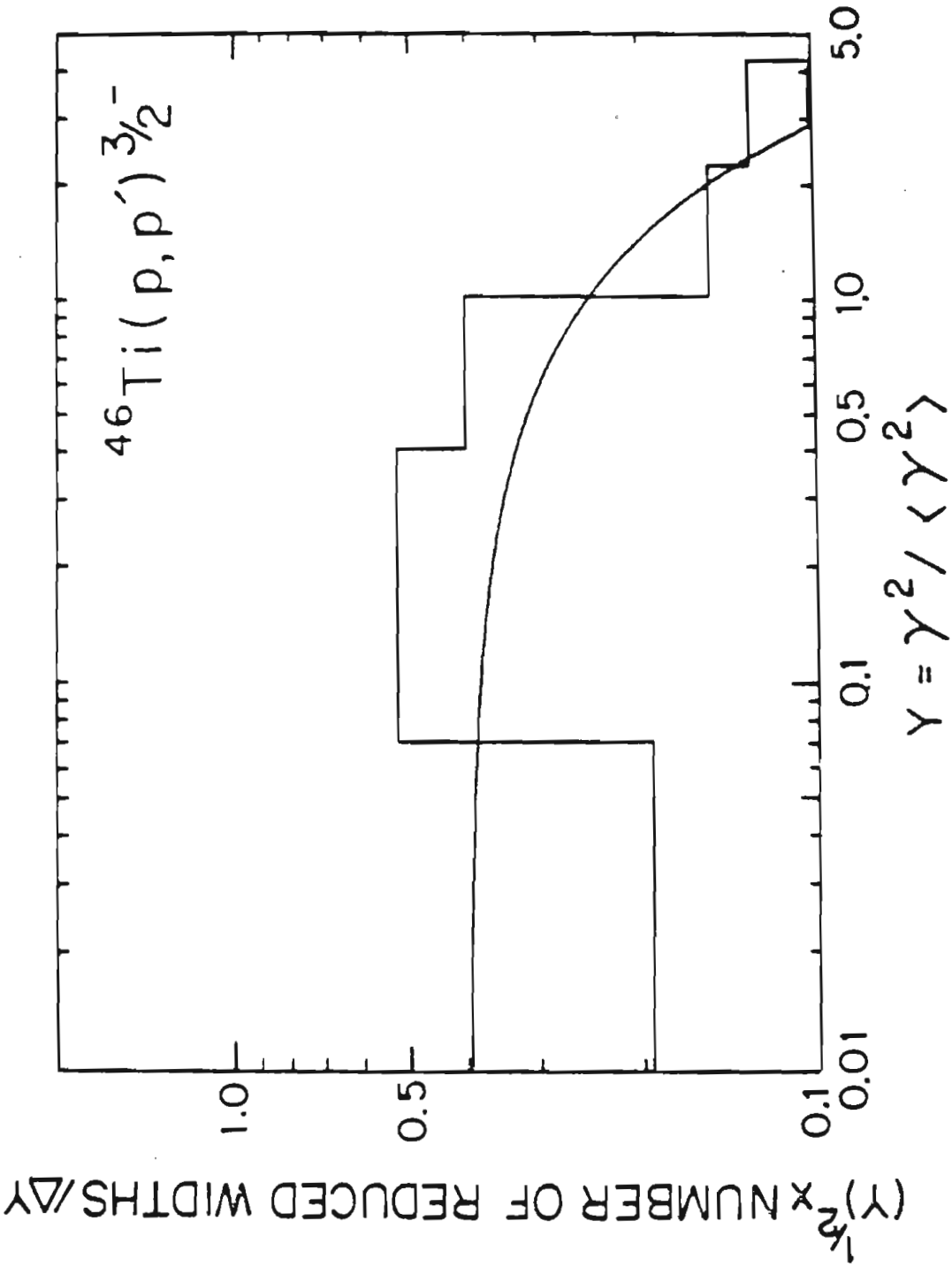
$^{46}Ti(p,p')\,3/2^-$
$(\gamma)^{-\frac{1}{2}}$ x NUMBER OF REDUCED WIDTHS /$\Delta\gamma$
1.0
0.5
0.1
0.01
0.1
0.5
1.0
5.0
$\gamma = \gamma^2 / \langle \gamma^2 \rangle$

under both curves have been normalized to one. The plot is on a log-log scale in order to accentuate the missing smaller levels; for convenience a change of variable has been made. From the graph it appears that no levels above Y=.07 were missed.

Additional information can be obtained from the reduced widths by considering the separate channels. These values are obtained using the mixing ratios and relative phases given in Table 4.2 and the widths from Table 4.1. The final reduced widths for each decay channel of the 3/2⁻ compound nuclear state are listed in Table 4.6 in the total angular momentum representation. Inelastic reduced widths are plotted in Fig. 4.2, along with the elastic reduced widths. The plots show the analogues at 2.29, 2.70, and 2.87 MeV. The strong states at 2.35 and 2.57 MeV are not analogues. The inelastic plots illustrate how the total widths of the lower two analogues are split between the two channels. On the other hand, the analogue state near 2.87 MeV occurs mainly in the j'=3/2 channel.

The square root of the reduced width is the magnitude of the reduced width amplitude. The relative phase of the amplitudes in the two channels is determined from the sign of the mixing ratio. Lynn (1968) discusses the conventional Gaussian assumption for the distribution of the reduced width amplitudes, where the Gaussian distribution is given by

$$P(\gamma) = \frac{1}{\sqrt{2\pi\langle\gamma^2\rangle}} \exp(-\gamma^2/2\langle\gamma^2\rangle) \qquad 4.2.3$$

Using the change in variable $Y = |\gamma|/\sqrt{\langle\gamma^2\rangle}$ Eq. 4.2.3 becomes

$$P(Y) = 1/\sqrt{2\pi} \exp(-1/2\ Y^2) \qquad 4.2.4$$

The total inelastic data are plotted along with a half Gaussian distribution in Fig. 4.3; absolute values were used so that all values are positive. Fig. 4.3 also suggests that an excessive number of large widths exist. Fig. 4.4 shows a similar plot for the separate channels. All plots show an excessive number of large widths, while three of the four plots indicate that some small levels are missed.

Table 4.6 Reduced Widths
for $3/2^-$ Resonances in ^{47}V

Res. No.	$\gamma^2_{j',1}$ (keV)	$\gamma^2_{j',3}$ (keV)	$\gamma_{j',1}\gamma_{j',3}$ (keV)	$\gamma^2_{s',3}$ (keV)	$\gamma^2_{s',5}$ (keV)	$\gamma_{s',3}\gamma_{s',5}$ (keV)
1	2.07	0.25	-0.72	0.06	2.26	-0.37
2	16.02	3.77	-7.77	0.00	19.79	-0.14
4	3.27	1.10	+1.90	3.06	1.31	-2.00
5	0.22	1.23	-0.52	0.62	0.83	+0.72
10	1.42	0.32	-0.68	0.00	1.74	-0.02
14	6.55	1.31	-2.93	0.02	7.84	-0.40
16	0.30	0.18	-0.23	0.07	0.41	+0.16
18	0.12	0.21	-0.16	0.07	0.26	+0.14
19	1.14	0.27	-0.55	0.00	1.41	+0.03
22	0.76	5.19	-1.99	2.82	3.12	+2.97
23	5.94	0.03	+0.42	1.50	4.47	-2.59
25	0.07	0.06	-0.07	0.03	0.10	+0.05
26	0.57	2.41	-1.17	1.29	1.69	+1.48
28	0.28	0.92	-0.51	0.40	0.80	+0.57
29	1.09	0.63	+0.83	1.39	0.33	-0.68
30	0.43	2.60	-1.06	1.43	1.60	+1.51

Table 4.6 (continued)

Res. No.	$\gamma^2_{j,1}$ (keV)	$\gamma^2_{j,3}$ (keV)	$\gamma_{j,1}\gamma_{j,3}$ (keV)	$\gamma^2_{s,3}$ (keV)	$\gamma^2_{s,5}$ (keV)	$\gamma_{s,3}\gamma_{s,5}$ (keV)
34	0.09	9.40	+0.89	8.37	1.12	+3.06
36	0.76	5.43	+2.04	6.04	0.15	+0.94
37	0.42	1.69	+0.83	2.09	0.02	+0.19
38	0.86	6.09	-2.29	3.80	3.15	+3.46
40	1.16	1.37	-1.26	0.50	2.03	+1.01
43	0.08	0.64	+0.23	0.70	0.02	+0.12
47	0.31	0.05	+0.13	0.22	0.14	-0.18
49	0.59	0.02	+0.11	0.23	0.38	-0.29
51	0.00	0.74	+0.04	0.64	0.10	+0.26

Figure 4.2 Reduced Widths for the $^{46}Ti(p,p)^{46}Ti$ and $^{46}Ti(p,p')^{46}Ti^*$ Reactions.

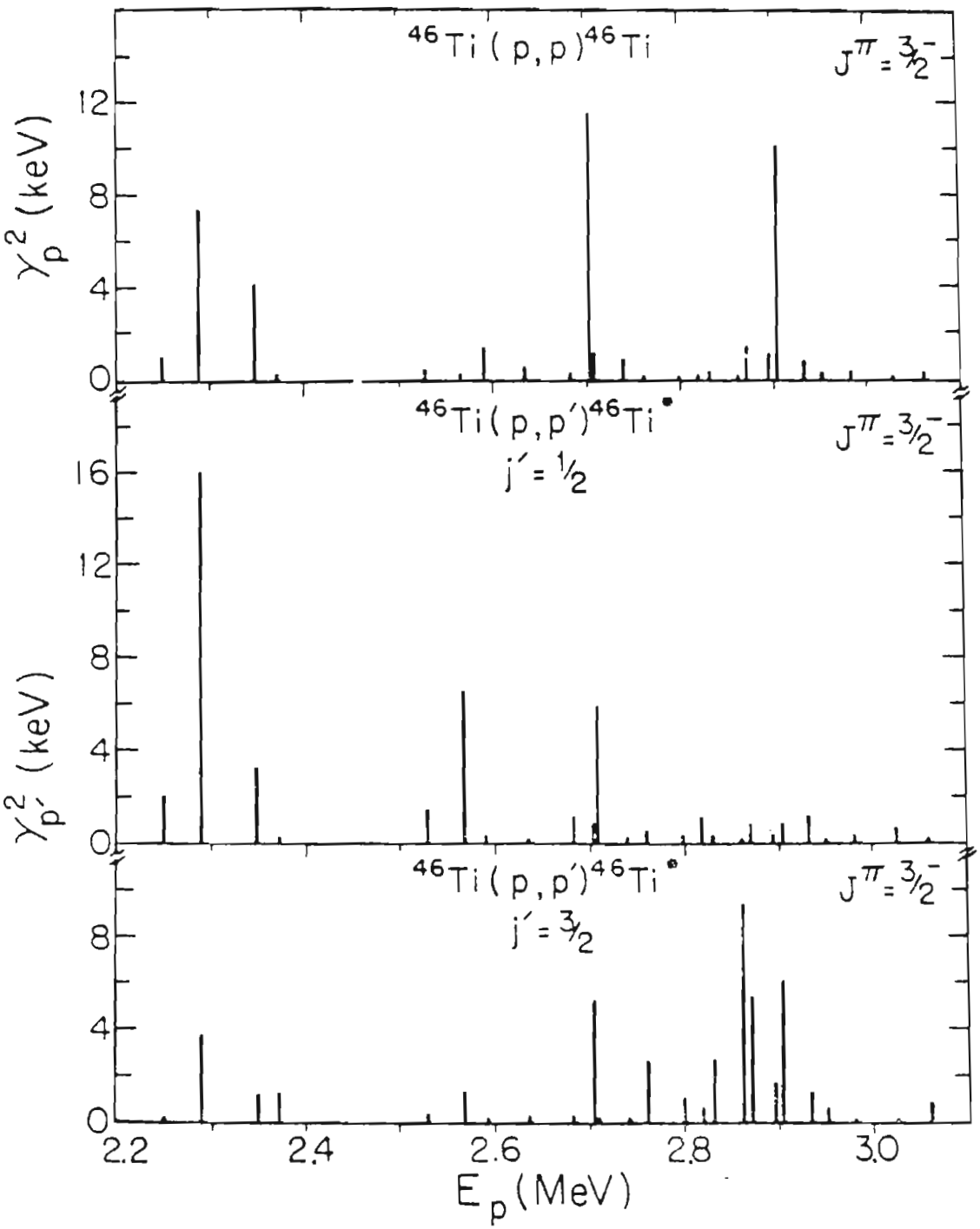
$^{46}Ti(p,p)^{46}Ti$
$J^\pi = 3/2^-$
γ_p^2 (keV)
$^{46}Ti(p,p')^{46}Ti^*$
$j' = 1/2$
$J^\pi = 3/2^-$
$\gamma_{p'}^2$ (keV)
$^{46}Ti(p,p')^{46}Ti^*$
$j' = 3/2$
$J^\pi = 3/2^-$
E_p (MeV)

Figure 4.3 Distribution of Reduced Width Amplitudes from $^{46}Ti(p,p')^{46}Ti^*$.

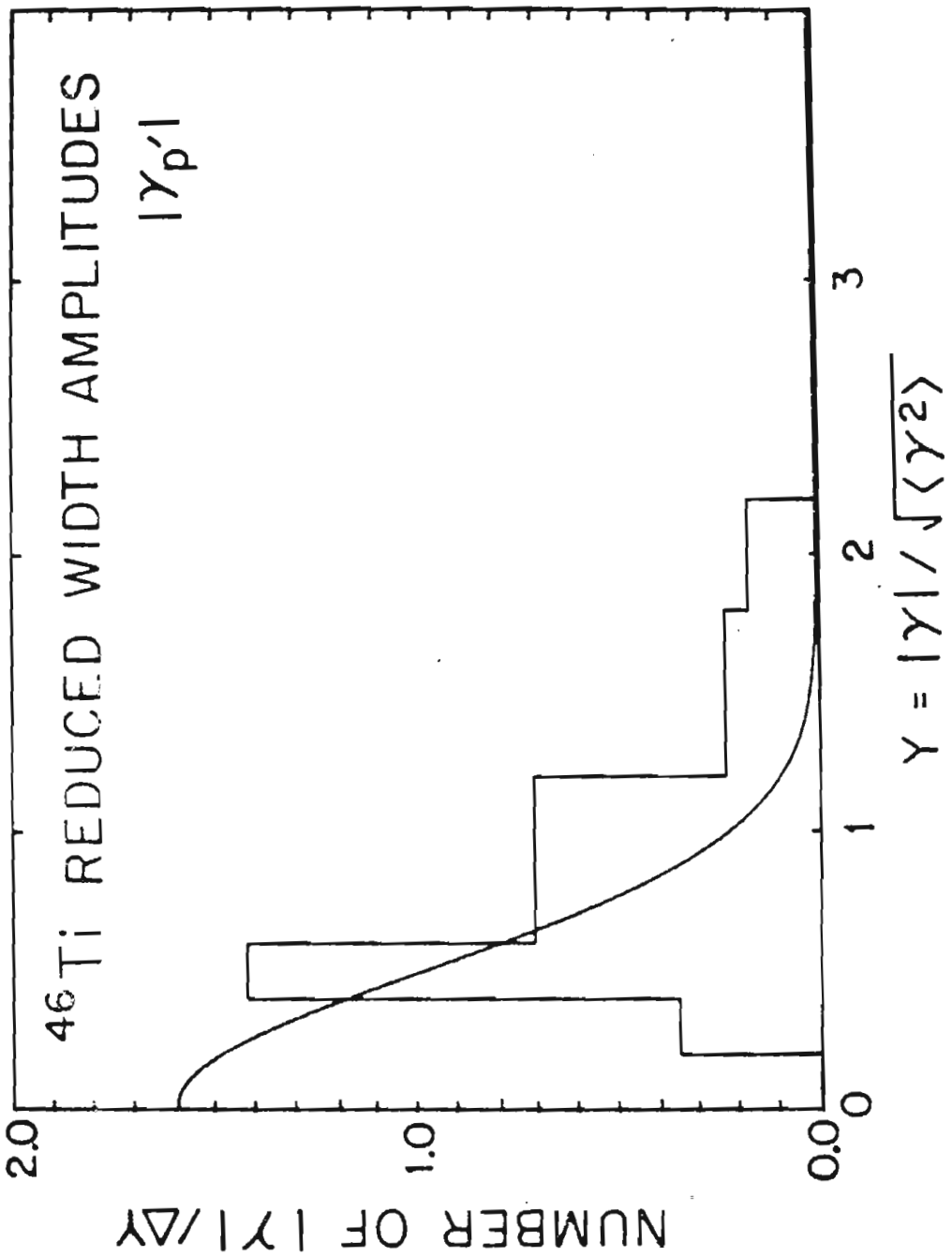
^{46}Ti REDUCED WIDTH AMPLITUDES
$|\gamma_{p'}|$
NUMBER OF $|\gamma|/\Delta\gamma$
2.0
1.0
0.0
0
1
2
3
$Y = |\gamma| / \sqrt{\langle \gamma^2 \rangle}$

Figure 4.4 Distribution of Reduced Width Amplitudes for $^{46}Ti(p,p')^{46}Ti^*$ in Both Channel Spin and Total Angular Momentum Representations.

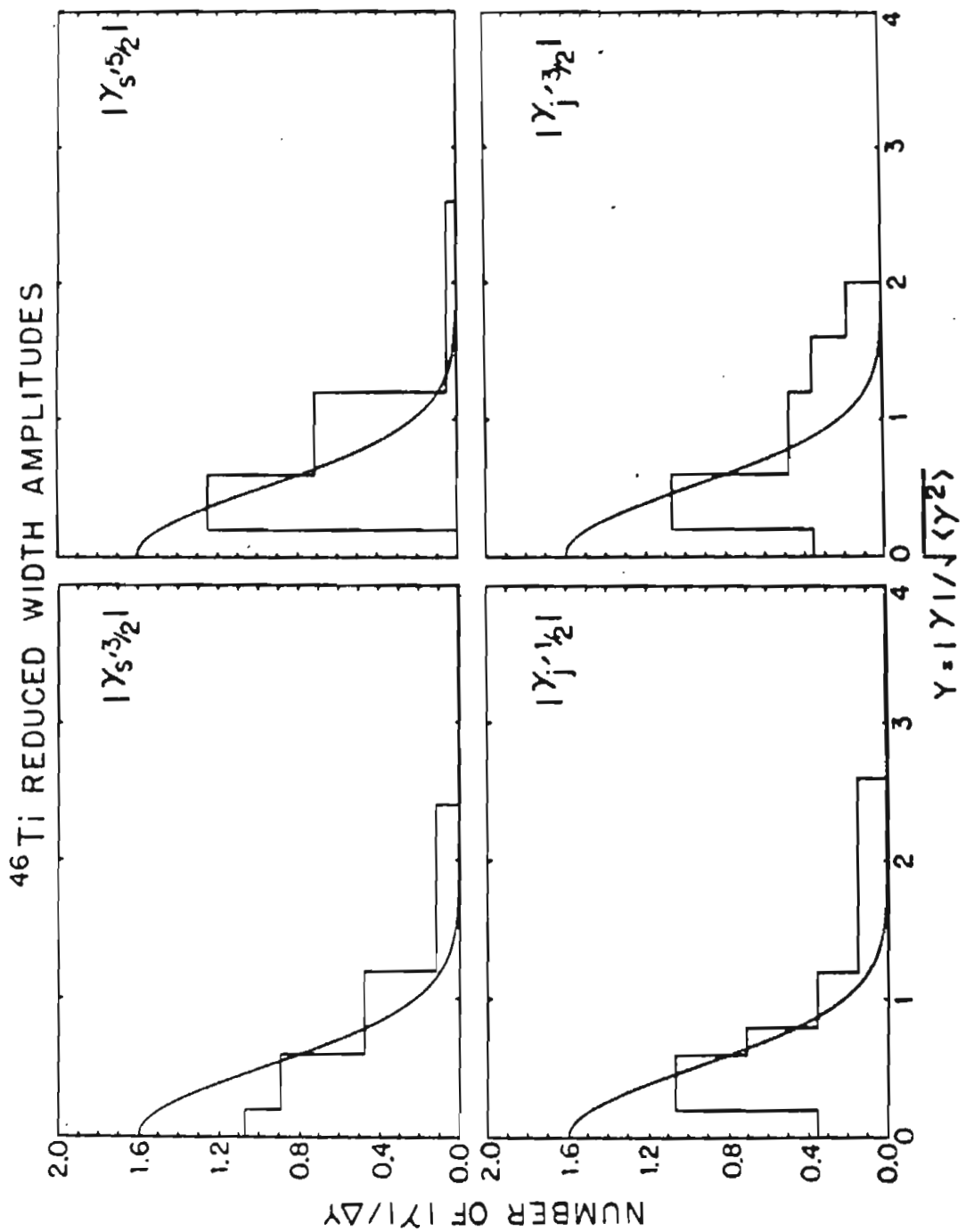
^{46}Ti REDUCED WIDTH AMPLITUDES
$|\gamma_{s,5/2}|$
$|\gamma_{s,3/2}|$
$|\gamma_{j,3/2}|$
$|\gamma_{j,1/2}|$
NUMBER OF $|\gamma|/\Delta\gamma$
$Y = |\gamma|/\sqrt{\langle\gamma^2\rangle}$
0.0
0.4
0.8
1.2
1.6
2.0
0
1
2
3
4

4.3 Statistical Results

Kendall and Stuart (1958) have shown that the ratio of two independent normal variables with zero mean and unit variance will be given by the Cauchy distribution

$$P(\delta)d\delta = \frac{1}{\pi(1 + \delta^2)}\, d\delta \qquad 4.3.1$$

This means that the ratio of the reduced width amplitudes will be given by the Cauchy distribution. Let

$$\delta = \tan \Phi \qquad 4.3.2$$

Therefore

$$\frac{d\delta}{d\Phi} = \frac{d(\tan \Phi)}{d\Phi} = \sec^2 \Phi \qquad 4.3.3$$

The probability distribution is

$$W(\Phi)d\Phi = P(\delta)\left|\frac{d\delta}{d\Phi}\right| d\Phi \qquad 4.3.4$$

From Eq. 4.3.1 this is

$$W(\Phi)d\Phi = \frac{1}{\pi(1 + \delta^2)} \sec^2 \Phi \, d\Phi \qquad 4.3.5$$

Or

$$W(\Phi)d\Phi = \frac{1}{\pi(1 + \tan^2 \Phi)} \sec^2 \Phi \, d\Phi \qquad 4.3.6$$

This can be written

$$W(\Phi)d\Phi = \frac{1}{\pi} \frac{\cos^2 \Phi}{\cos^2 \Phi} \frac{\sec^2 \Phi}{1 + \tan^2 \Phi} d\Phi \qquad 4.3.7$$

But this is just

$$W(\Phi)d\Phi = \frac{1}{\pi} \frac{1}{\cos^2 \Phi + \sin^2 \Phi} d\Phi \qquad 4.3.8$$

or

$$W(\Phi)d\Phi = \frac{1}{\pi} d\Phi \qquad 4.3.9$$

Therefore all values of Φ have an equal probability of occurring, and all ratios of the reduced width amplitudes are equally likely. An exception to this should occur in the region of a doorway state. Lane (1971) states that the reduced width amplitudes of a doorway should have the same phase for all levels instead of fluctuating randomly.

Figs. 4.5 and 4.6 show the results of this experiment for the $3/2^-$ compound state. Careful examination of Fig. 4.5 discloses that for the fourteen resonances below 2.81 MeV, twelve have arctangents of mixing ratios between -10° and -70°. This result can also be seen in Fig. 4.7. Here, Region 1 refers to proton energies below 2.81 MeV and Region 2 to energies above 2.81 MeV. The resonances in Region 2 have mostly positive mixing ratios. For the channel spin representation, Fig. 4.8 gives a similar illustration.

Figs. 4.9 and 4.10 give number plots on and off the analogues. It is clear from Region 1 of Fig. 4.9 that the off-analogue resonances have Φ in the -10° to -70° range. Only one off-analogue resonance has a different Φ. In order to understand Region 2, it is most convenient to consider the channel spin representation in Fig. 4.10. Here, the analogue near 2.87 MeV has Φ values ranging from -30° to +70°.

Linear correlation coefficients were calculated using the widths and relative phases obtained in this experiment. These results are given in Tables 4.7, 4.8, 4.9, 4.10, and 4.11. The linear correlation coefficients were calculated using standard methods as discussed in Bevington (1969). Table 4.12 gives the confidence levels of a few selected linear correlation coefficients. The first column gives the number of resonances, while the other

Figure 4.5 Arctangent of Mixing Ratio Versus Energy for the $3/2^-$ Compound State in the Total Angular Momentum Representation.

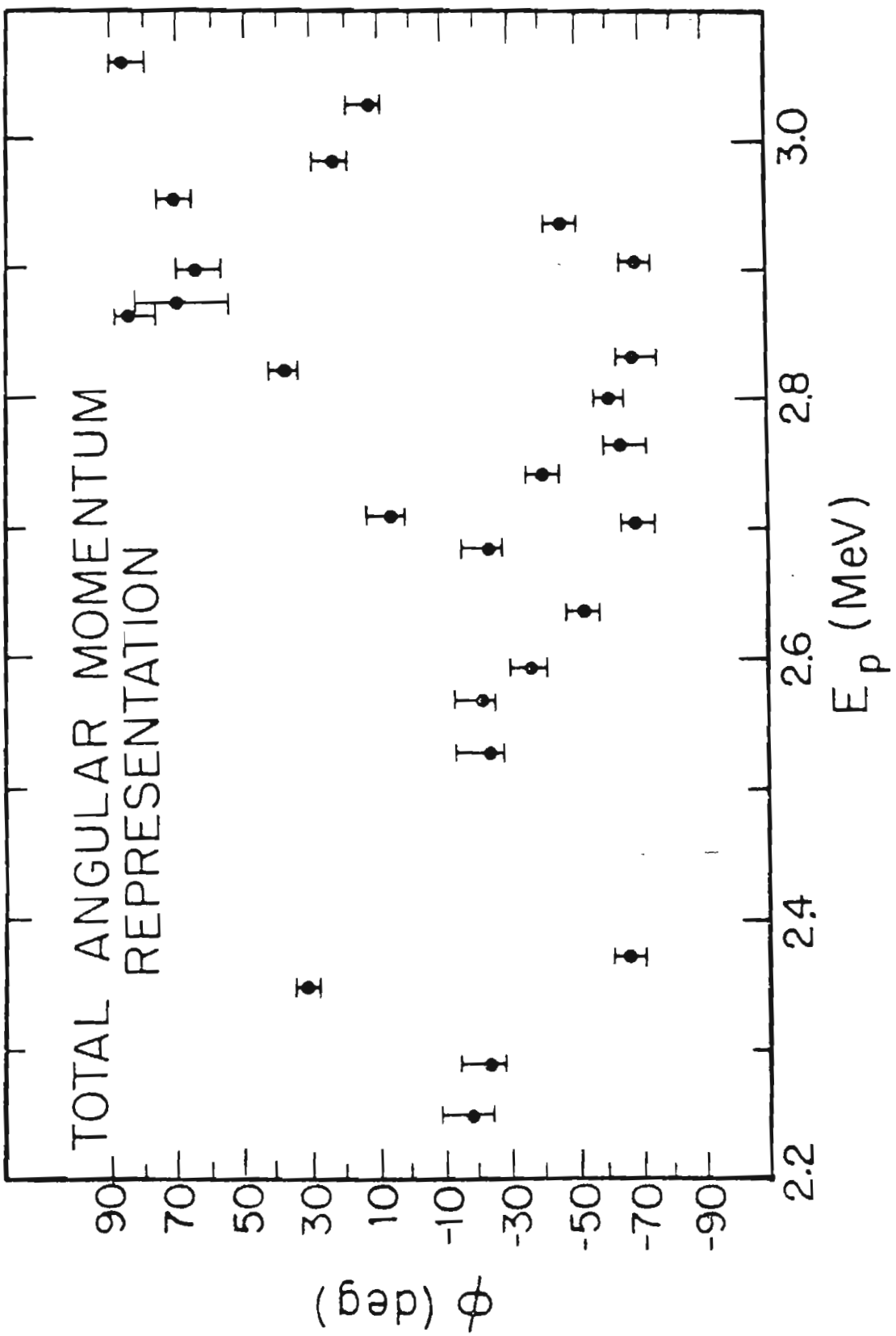
TOTAL ANGULAR MOMENTUM
REPRESENTATION
90
70
50
30
10
-10
-30
-50
-70
-90
φ (deg)
2.2
2.4
2.6
2.8
3.0
E_p (MeV)

Figure 4.6 Arctangent of Mixing Ratio Versus Energy for the $3/2^-$ Compound State in the Channel Spin Representation.

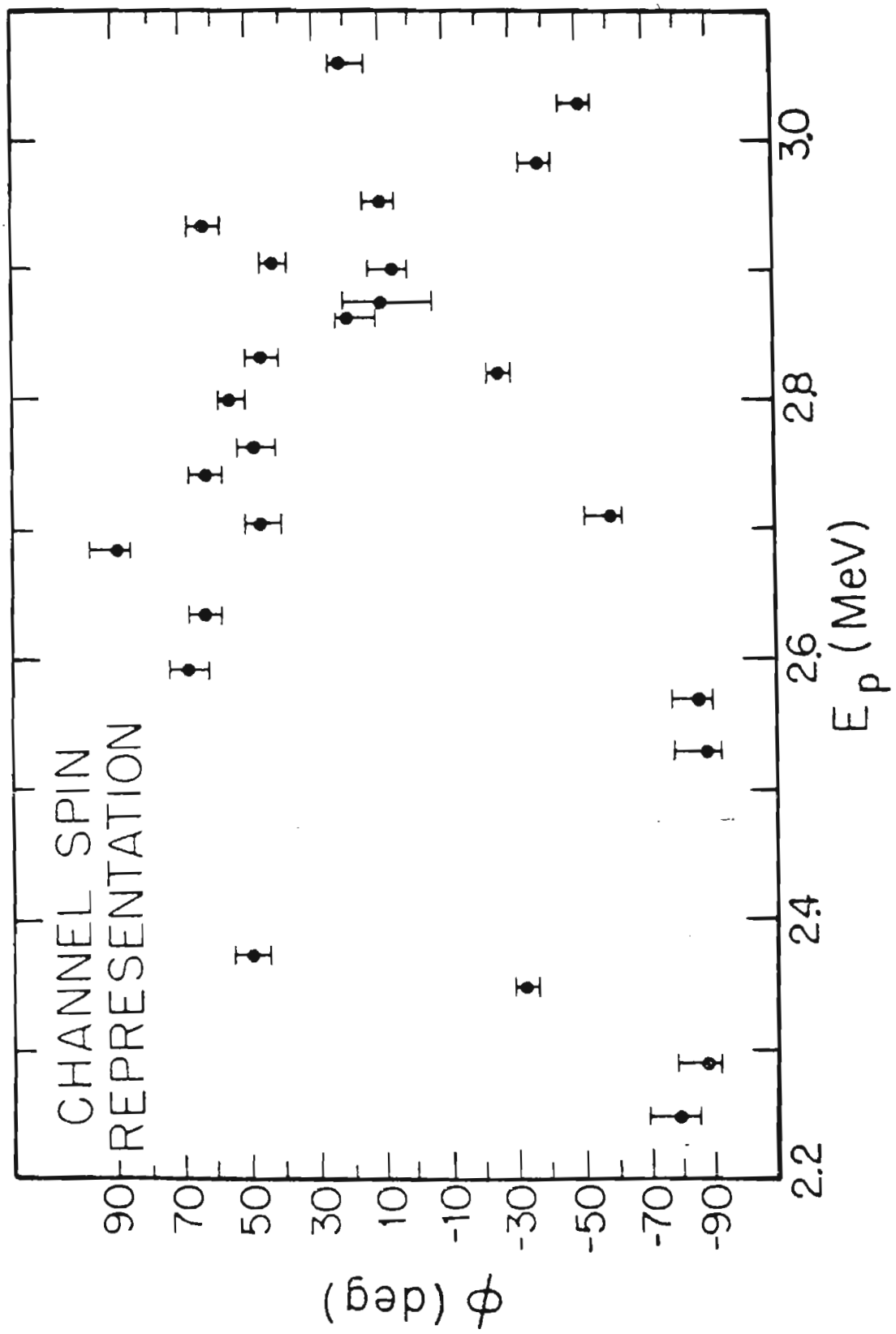
CHANNEL SPIN
REPRESENTATION
90
70
50
30
10
-10
-30
-50
-70
-90
φ (deg)
2.2
2.4
2.6
2.8
3.0
E_p (MeV)

Figure 4.7 Number of Resonances Versus Arctangent of Mixing Ratio for All $3/2^-$ Compound States in the Total Angular Momentum Representation. Region 1 refers to proton energies below 2.81 MeV, and Region 2 refers to energies above 2.81 MeV.

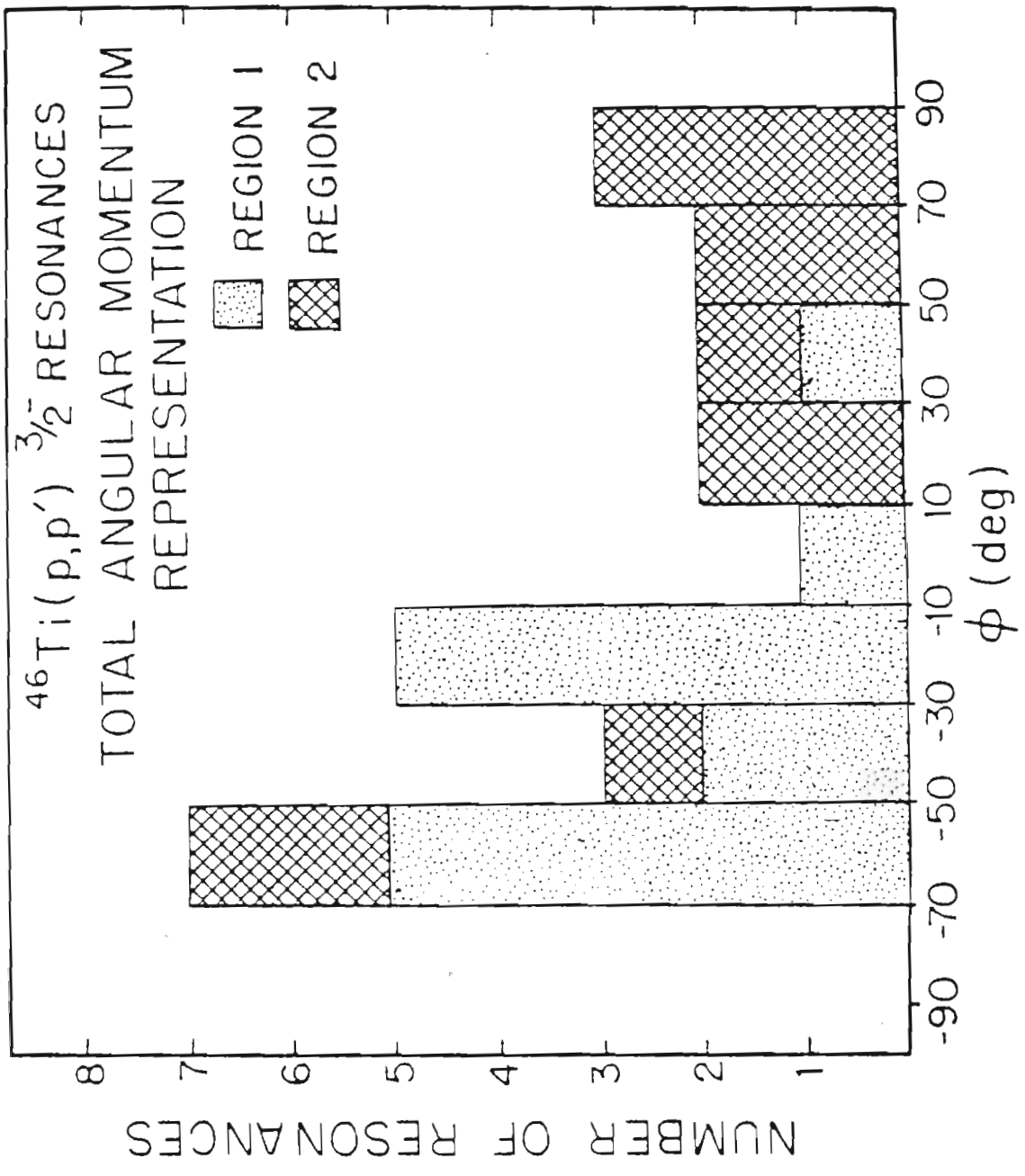
$^{46}Ti(p,p')$ $^{3}/_{2}^{-}$ RESONANCES
TOTAL ANGULAR MOMENTUM REPRESENTATION
REGION 1
REGION 2
NUMBER OF RESONANCES
1
2
3
4
5
6
7
8
-90 -70 -50 -30 -10 10 30 50 70 90
ϕ (deg)

Figure 4.8 Number of Resonances Versus Arctangent of Mixing Ratio for All $3/2^-$ Compound States in the Channel Spin Representation. Region 1 refers to proton energies below 2.81 MeV, and Region 2 refers to energies above 2.81 MeV.

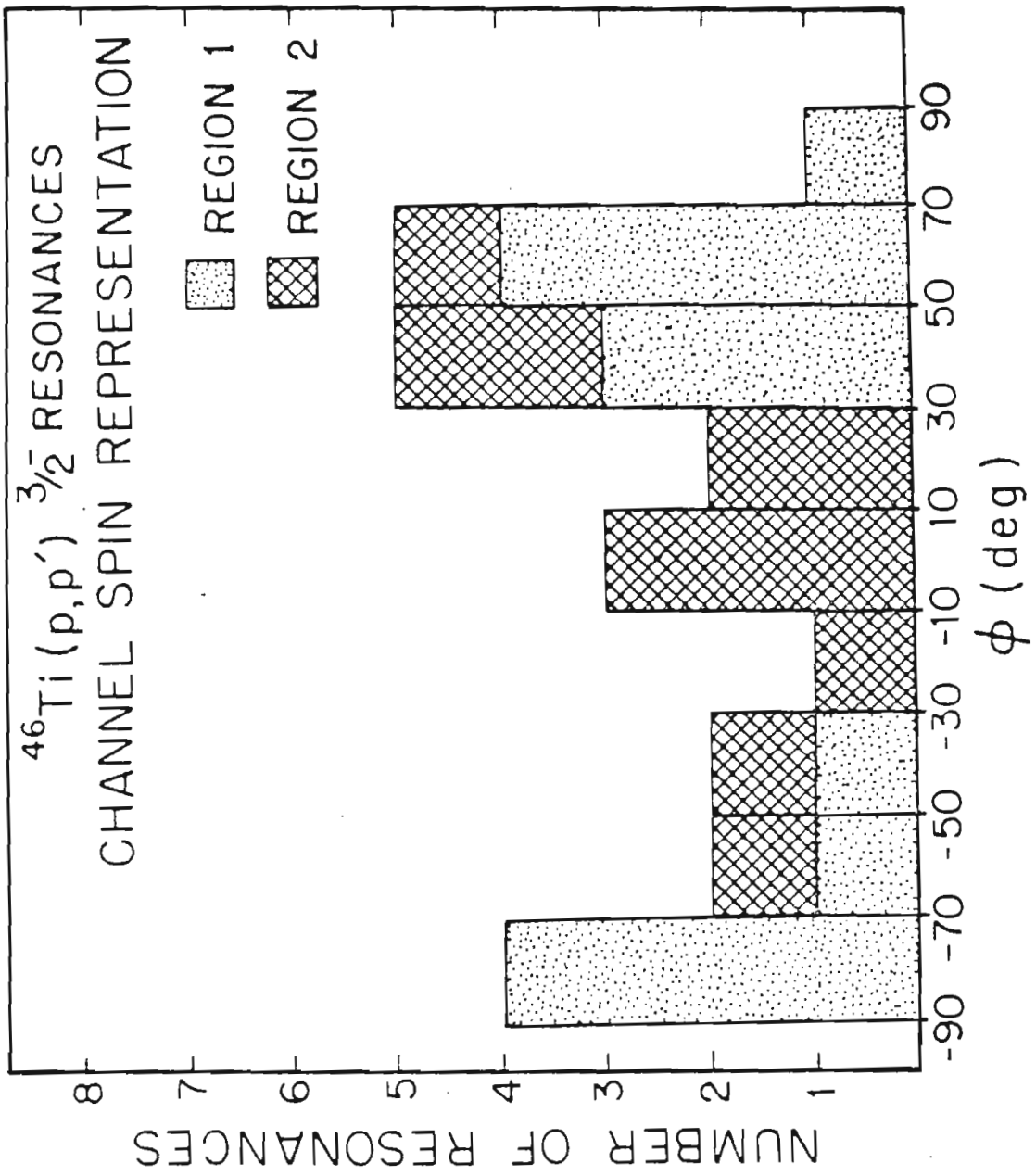
^{46}Ti (p,p′) $^{3}/_{2}^{-}$ RESONANCES
CHANNEL SPIN REPRESENTATION
REGION 1
REGION 2
NUMBER OF RESONANCES
1
2
3
4
5
6
7
8
-90
-70
-50
-30
-10
10
30
50
70
90
φ (deg)

Figure 4.9 Number of Resonances Versus Arctangent of Mixing Ratio for the 3/2⁻ Compound States in Each Energy Region, and in the Total Angular Momentum Representation. Region 1 refers to the energy range below 2.81 MeV, and Region 2 refers to the energy range above 2.81 MeV.

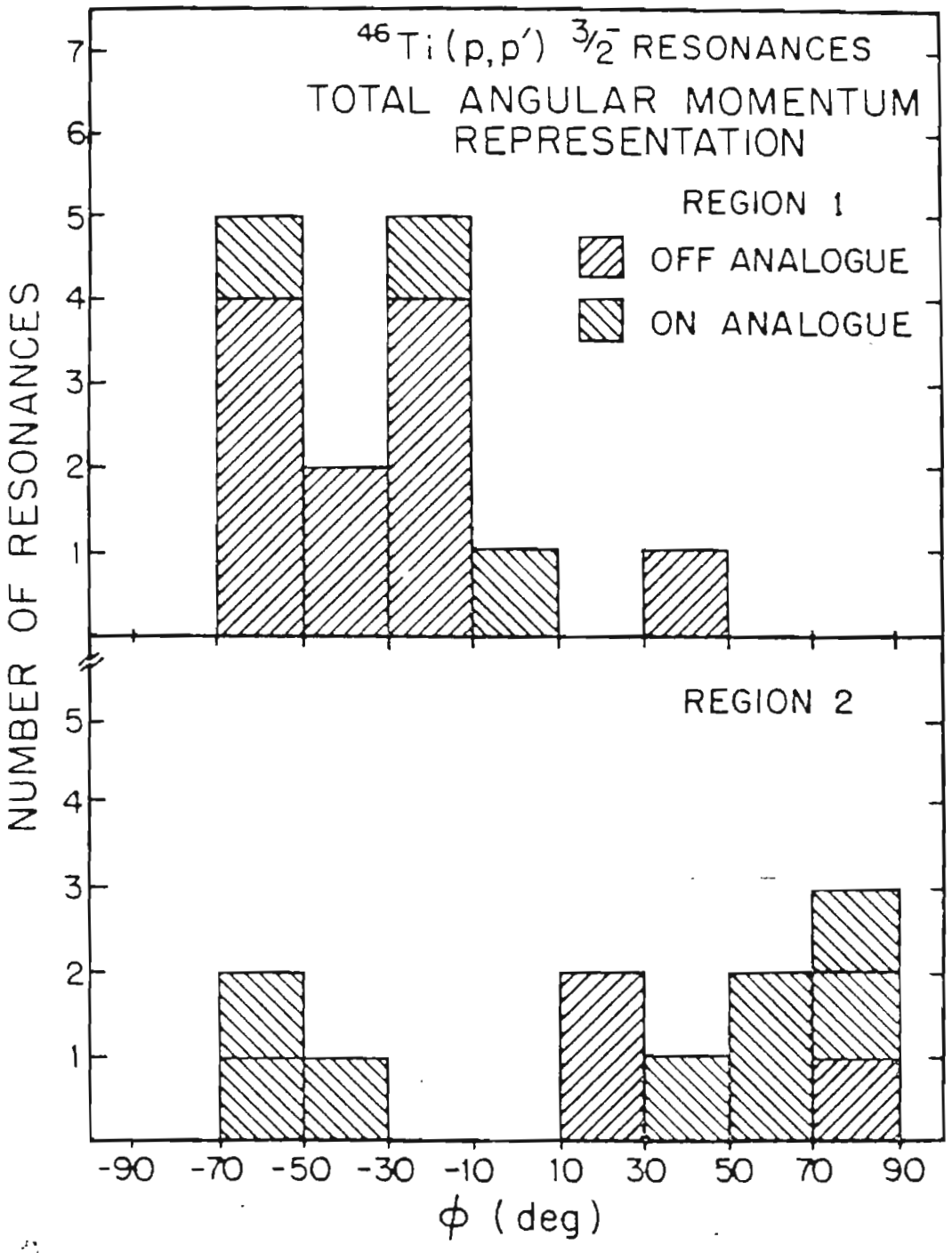
$^{46}Ti(p,p')\ 3/2^-$ RESONANCES
TOTAL ANGULAR MOMENTUM REPRESENTATION
REGION 1
OFF ANALOGUE
ON ANALOGUE
REGION 2
NUMBER OF RESONANCES
1
2
3
4
5
6
7
-90
-70
-50
-30
-10
10
30
50
70
90
ϕ (deg)

Figure 4.10 Number of Resonances Versus Arctangent of Mixing Ratio for the $3/2^-$ Compound States in Each Energy Region, and in the Channel Spin Representation. Region 1 refers to the energy range below 2.81 MeV, and Region 2 refers to the energies above 2.81 MeV.

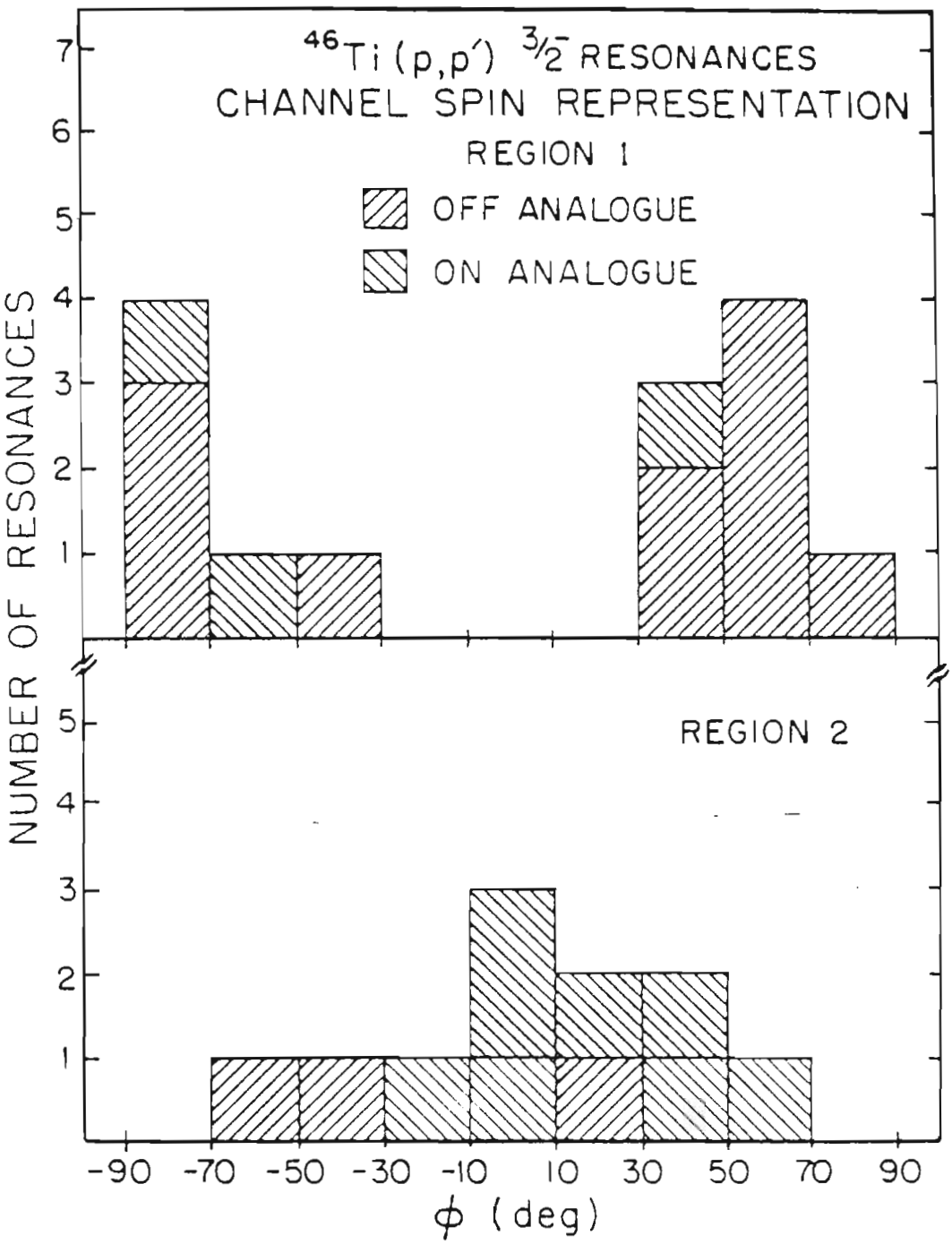
^{46}Ti (p,p′) 3/2⁻ RESONANCES
CHANNEL SPIN REPRESENTATION
REGION 1
OFF ANALOGUE
ON ANALOGUE
REGION 2
NUMBER OF RESONANCES
1
2
3
4
5
6
7
-90 -70 -50 -30 -10 10 30 50 70 90
φ (deg)

Table 4.7 Linear Correlation Coefficients

All $3/2^-$ Resonances (N = 25)

	γ_p^2	$\gamma_{p'}^2$	$\gamma_{j_1'}^2$	$\gamma_{j_3'}^2$	$\gamma_{s_3'}^2$	$\gamma_{s_5'}^2$
γ_p^2	1.00	0.53	0.32	0.49	0.24	0.44
$\gamma_{p'}^2$		1.00	0.83	0.61	0.35	0.88
$\gamma_{j_1'}^2$			1.00	0.06	----	----
$\gamma_{j_3'}^2$				1.00	----	----
$\gamma_{s_3'}^2$					1.00	-0.14

$\rho(\gamma_{j_1'}\gamma_{j_3'}) = -0.32$ $\rho(\gamma_{s_3'}\gamma_{s_5'}) = 0.23$

Table 4.8 Linear Correlation Coefficients

With Analogue States Excluded (N = 14)

	γ_p^2	$\gamma_{p'}^2$	$\gamma_{j_1'}^2$	$\gamma_{j_3'}^2$	$\gamma_{s_3'}^2$	$\gamma_{s_5'}^2$
γ_p^2	1.00	0.24	0.27	0.02	0.77	-0.07
$\gamma_{p'}^2$		1.00	0.95	0.57	0.32	0.92
$\gamma_{j_1'}^2$			1.00	0.28	----	----
$\gamma_{j_3'}^2$				1.00	----	----
$\gamma_{s_3'}^2$					1.00	-0.08

$\rho(\gamma_{j_1'}\gamma_{j_3'}) = -0.43$ $\rho(\gamma_{s_3'}\gamma_{s_5'}) = 0.01$

Table 4.9 Linear Correlation Coefficients for Region 1 (N = 14)

	γ_p^2	$\gamma_{p'}^2$	$\gamma_{j_1'}^2$	$\gamma_{j_3'}^2$	$\gamma_{s_3'}^2$	$\gamma_{s_5'}^2$
γ_p^2	1.00	0.57	0.36	0.85	0.57	0.44
$\gamma_{p'}^2$		1.00	0.96	0.61	0.07	0.98
$\gamma_{j_1'}^2$			1.00	0.37	----	----
$\gamma_{j_3'}^2$				1.00	----	----
$\gamma_{s_3'}^2$					1.00	-0.14

$\rho(\gamma_{j_1'}\gamma_{j_3'}) = -0.58$ $\rho(\gamma_{s_3'}\gamma_{s_5'}) = 0.03$

Table 4.10 Linear Correlation Coefficients for Region 1 Without Analogue States (N = 11)

	γ_p^2	$\gamma_{p'}^2$	$\gamma_{j_1'}^2$	$\gamma_{j_3'}^2$	$\gamma_{s_3'}^2$	$\gamma_{s_5'}^2$
γ_p^2	1.00	0.18	0.23	-0.06	0.78	-0.16
$\gamma_{p'}^2$		1.00	0.95	0.53	0.31	0.91
$\gamma_{j_1'}^2$			1.00	0.24	----	----
$\gamma_{j_3'}^2$				1.00	----	----
$\gamma_{s_3'}^2$					1.00	-0.11

$\rho(\gamma_{j_1'}\gamma_{j_3'}) = -0.49$ $\rho(\gamma_{s_3'}\gamma_{s_5'}) = 0.03$

Table 4.11 Linear Correlation Coefficients for Region 2 (N = 11)

	γ_p^2	$\gamma_{p'}^2$	$\gamma_{j_1'}^2$	$\gamma_{j_3'}^2$	$\gamma_{s_3'}^2$	$\gamma_{s_5'}^2$
γ_p^2	1.00	0.45	0.32	0.41	0.23	0.73
$\gamma_{p'}^2$		1.00	0.07	0.99	0.94	0.51
$\gamma_{j_1'}^2$			1.00	-0.06	----	----
$\gamma_{j_3'}^2$				1.00	----	----
$\gamma_{s_3'}^2$					1.00	0.19

$\rho(\gamma_{j_1'}, \gamma_{j_3'}) = 0.04$ $\rho(\gamma_{s_3'}, \gamma_{s_5'}) = 0.62$

Table 4.12 Linear Correlation Confidence Levels

N	99.9%	99%	95%	90%
25	0.54	0.44	0.33	0.26
14	0.66	0.56	0.43	0.35
11	0.72	0.61	0.48	0.40

columns list the linear correlation coefficients corresponding to confidence levels of 99.9%, 99%, 95%, and 90%. The confidence levels were calculated using the equation

$$F = \int_{-\infty}^{x} 1/\sqrt{2\pi}\ \exp(-1/2\ t^2)\ dt \qquad 4.3.10$$

where F is the confidence level and

$$x^2 = \frac{(N - 2)r^2}{1 - r^2} \qquad 4.3.11$$

Here N is the number of resonances and r is the linear correlation coefficient. From Table 4.7 it is seen that the reduced widths are not correlated in general, but that there is a relatively large correlation between the reduced width amplitudes of the channels j'=1/2 and j'=3/2. Table 4.8 lists correlations for all off-analogue resonances and shows that the reduced width amplitudes are still correlated at the 95% significance level. Tables 4.9, 4.10, and 4.11 subdivide the data into the two energy regions defined earlier. Region 1 has reduced width amplitudes which are also correlated in the j'=1/2 and j'=3/2 channels. In Region 2, however, the only correlation is between s'=3/2 and s'=5/2 near the analogue. It

should be noted that the elastic reduced widths and the total inelastic reduced widths are correlated, but this correlation is reduced when the analogue states are removed.

4.4 Analogue State Parameters

It has been shown (Robson, 1969) that analogue state widths approximately satisfy

$$\Gamma_A = \frac{S_n}{2T_o + 1} \Gamma_{sp} \qquad 4.4.1$$

Here Γ_A is the total analogue state width, S_n is the spectroscopic factor of the parent state, T_o is the z-component of the isospin of the target nucleus, and Γ_{sp} is the single particle width of the proton plus core state. The widths and spectroscopic factors of the three analogue states studied in this experiment are given in Table 4.13. The single particle widths were calculated using the methods described by Bilpuch et al. (1976), and the results in the table are from the ZDH method. Results of the MM method agreed within one percent. Results of the TAP method, however, were ten to fifteen percent lower.

Table 4.13 Spectroscopic Factors

	Γ (keV)	$\frac{\Gamma_{sp}}{2T_0+1}$ (keV)	S_p	
E_p = 2.290 MeV	Γ_p = 0.330	10.0	0.033	
E_x = 3.275 MeV				
V_p =-53.597 MeV	$\Gamma_{p'}$ = 0.016	.162	0.099	j'=1/2
V_n =-49.608 MeV				
	$\Gamma_{p'}$ = 0.004	.167	0.024	j'=3/2
E_p = 2.702 MeV	Γ_p = 1.535	25.3	0.061	
E_x = 3.764 MeV				
V_p =-52.850 MeV	$\Gamma_{p'}$ = 0.058	1.90	0.031	j'=1/2
V_n =-48.863 MeV				
	$\Gamma_{p'}$ = 0.045	1.95	0.023	j'=3/2
E_p = 2.894 MeV	Γ_p = 1.780	36.5	0.049	
E_x = 3.916 MeV				
V_p =-52.390 MeV	$\Gamma_{p'}$ = 0.037	4.03	0.009	j'=1/2
V_n =-48.401 MeV				
	$\Gamma_{p'}$ = 0.378	4.13	0.092	j'=3/2

The analogue near 2.87 MeV was also fit for fine structure parameters using the procedure of Bilpuch et al. (1976). This procedure extracts parameters for the strength function, where the strength function is defined as the average reduced width divided by the average level spacing. As shown by Bilpuch et al. (1976), the strength function can be written

$$S_c(E) = S_c^{pot} - \frac{(2S_c^{pot}\Delta_{\lambda c})(E_\lambda - E)}{(E_\lambda - E)^2 + W_\lambda^2/4} + \frac{\gamma_{\lambda c}^2 W_\lambda/2\pi}{(E_\lambda - E)^2 + W_\lambda^2/4} \qquad 4.4.2$$

The three terms in Eq. 4.4.2 are from left to right: background, asymmetric, and symmetric terms.

From the mixing ratios, it is clear that the strength of the 2.87 MeV analogue is predominantly in one channel. For that reason, only one channel was fit in the channel spin and total angular momentum representations. Figs. 4.11 and 4.12 show the fits, along with the reduced widths, for the two channels. The fits were made to the cumulative sum of the strength of all $3/2^-$ resonances except the analogue states at 2.29 MeV and 2.70 MeV. The results are listed in Table 4.14. For the $j'=3/2$ channel, values for the background strength, analogue energy, and

Figure 4.11 Differential and Integral Plots of Reduced Widths for j'=3/2. The fit is made to the cumulative sum of the strength function.

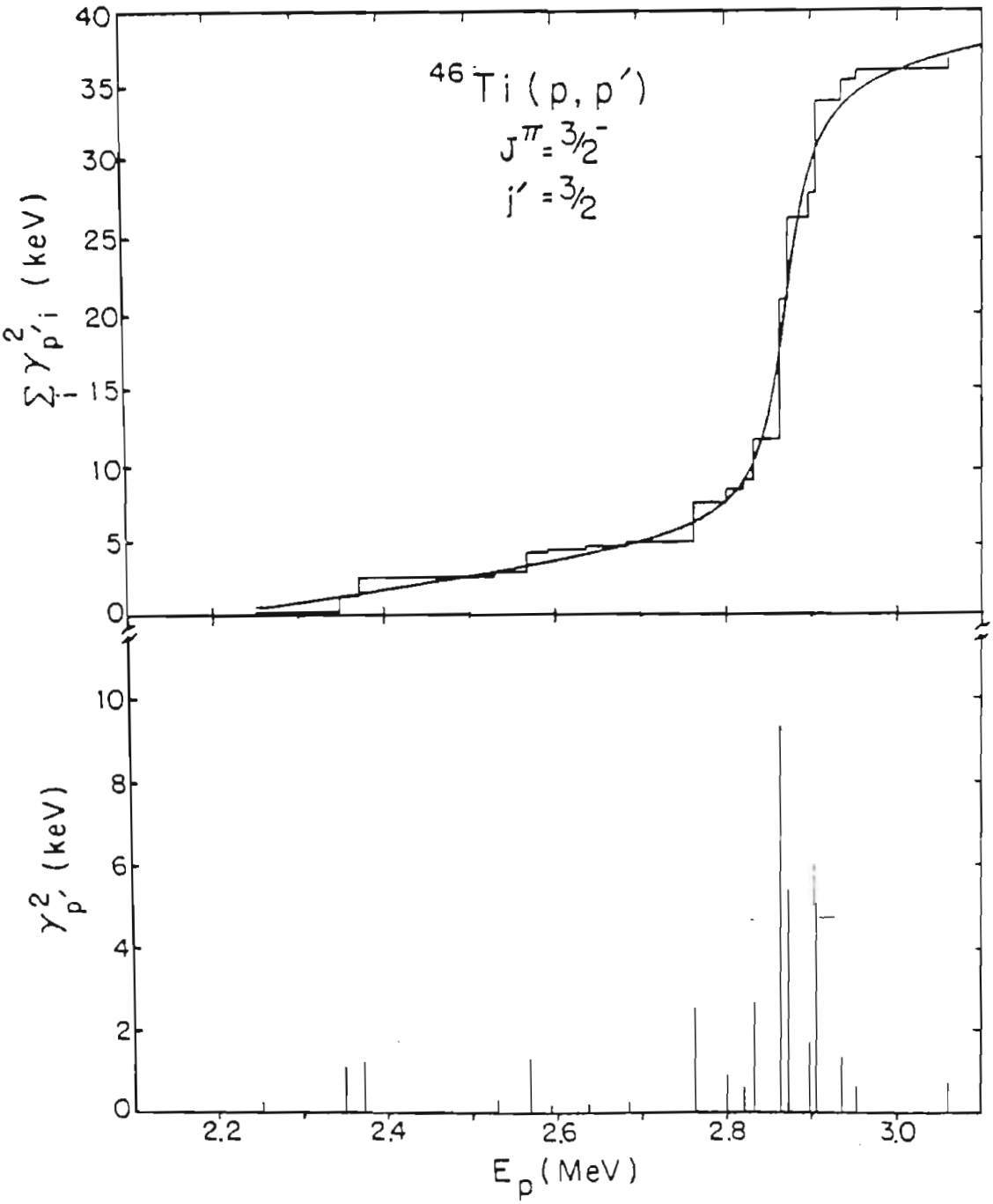
^{46}Ti (p, p′)
$J^{\pi} = 3/2^-$
$j' = 3/2$
$\sum_i \gamma^2_{p'i}$ (keV)
$\gamma^2_{p'}$ (keV)
E_p (MeV)
0
5
10
15
20
25
30
35
40
2
4
6
8
10
2.2
2.4
2.6
2.8
3.0

Figure 4.12 Differential and Integral Plots of Reduced Widths for s'=3/2. The fit is made to the cumulative sum of the strength function.

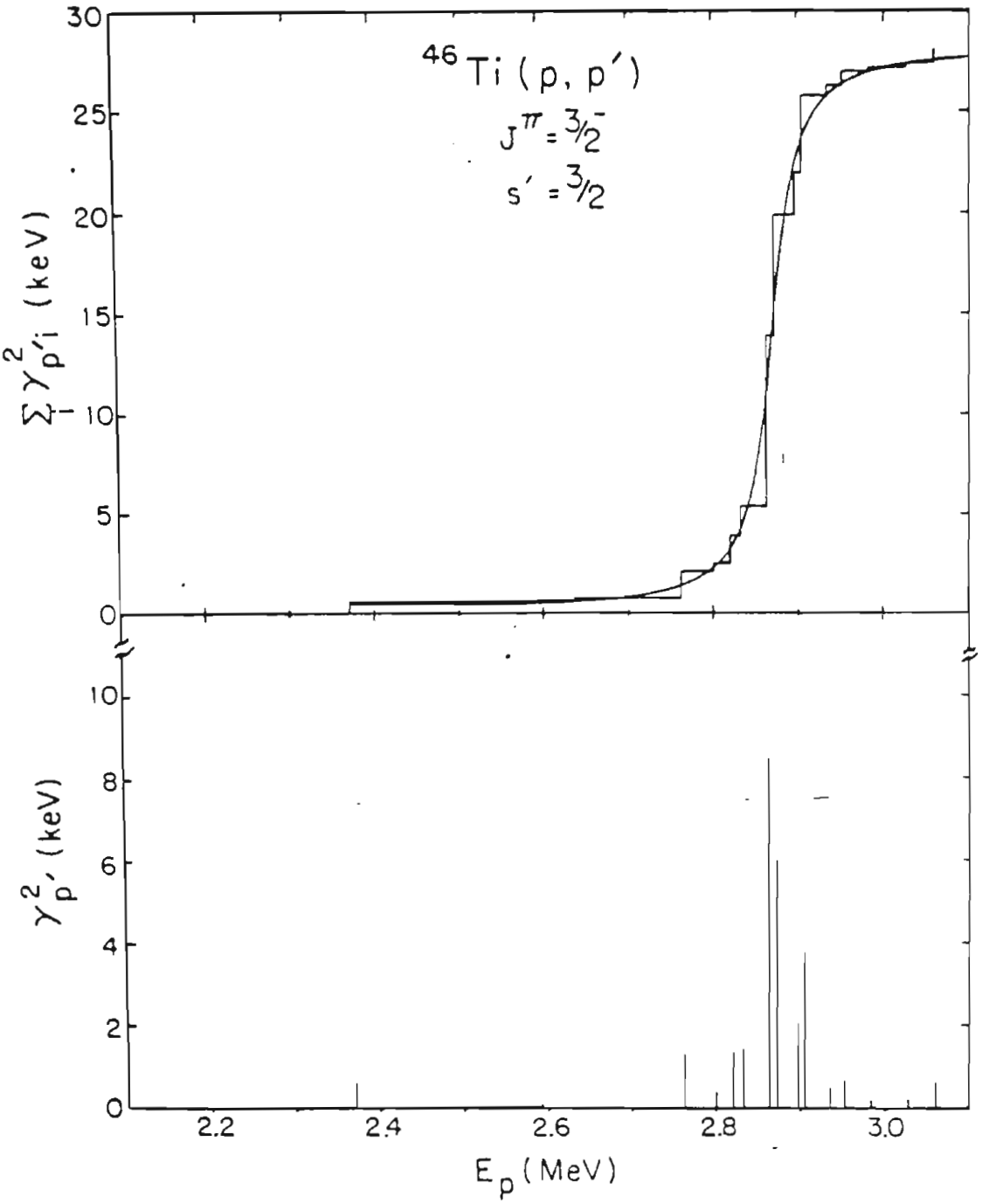
^{46}Ti (p, p′)
$J^{\pi} = 3/2^-$
$s' = 3/2$
$\sum_i \gamma^2_{p'i}$ (keV)
$\gamma^2_{p'}$ (keV)
E_p (MeV)
30
25
20
15
10
5
0
10
8
6
4
2
0
2.2
2.4
2.6
2.8
3.0

Table 4.14 Fine Structure Parameters for E = 2.87 MeV

Channel	S^{pot}	E_λ (MeV)	Δ_λ (keV)	γ_A^2 (keV)	W_λ (keV)
j'=3/2	.0079	2.871	-6.2	32.4	48.4
s'=3/2	-.0011	2.871	0.0	29.3	42.3

analogue reduced width agree with the values estimated from the data in Table 4.6. Results from the s'=3/2 channel for the analogue energy and analogue reduced width also agree with estimates, although the value for the s'=3/2 background strength function does not. The background in the channel spin representation is almost completely in the s'=5/2 channel. Therefore, it is not too surprising that the background found by fitting the s'=3/2 data appears to be nonphysical.

One last series of calculations was performed with the 2.87 MeV analogue state data. This involves using an off-diagonal strength function defined by

$$S_{cc'} = \langle \gamma_{\nu c} \gamma_{\nu c'} \rangle / D \qquad 4.4.3$$

where ν represents the fine structure level, c the channel, and D the average spacing between levels. Here, the reduced width amplitudes are averaged over ν in order to remove effects from Porter-Thomas fluctuations. The idea of off-diagonal strength functions was recently developed by A. M. Lane (1978), and can be illustrated using the data from this experiment.

Lane has shown that

$$S_{cc'} = A_{cc'} + \frac{1}{\pi} \text{Im.} \frac{\gamma_{\lambda c}\gamma_{\lambda c'}}{E_\lambda - E - iW_\lambda/2} \qquad 4.4.4$$

Eq. 4.4.4 can be written in a form similar to Eq. 4.4.2

$$S_{cc'} = A_{cc'} + \frac{B_{cc'}(E_\lambda - E) + C_{cc'}}{(E_\lambda - E)^2 + W_\lambda^2/4} \qquad 4.4.5$$

where

$$2C_{cc'}/W_\lambda + iB_{cc'} = 1/\pi\ \gamma_{\lambda c}\gamma_{\lambda c'} \qquad 4.4.6$$

From Eq. 4.4.6, it can be shown that

$$(C_{cc'} + iW_\lambda B_{cc'}/2)^2 = (C_{c'c'} + iW_\lambda B_{c'c'}/2)$$

$$\cdot(C_{cc'} + iW_\lambda B_{cc'}/2) \qquad 4.4.7$$

Separating the real and imaginary parts of Eq. 4.4.7,

$$C^2_{cc'} - W^2_\lambda B^2_{cc'}/4 = C_{cc}C_{c'c'} - W^2_\lambda B_{cc}B_{c'c'}/4 \qquad 4.4.8$$

$$2B_{cc'}C_{cc'} = B_{c'c'}C_{cc} + B_{cc}C_{c'c'} \qquad 4.4.9$$

Eqs. 4.4.8 and 4.4.9 then yield the off-diagonal matrix elements in terms of the diagonal elements.

For an illustration of off-diagonal elements, consider the product of reduced width amplitudes in two different channels. Figs. 4.13 and 4.14 show the product of the j'=1/2 and j'=3/2 channels, and the product of the s'=3/2 and s'=5/2 channels. Since the relative phase of each pair of channels is known, the signs of the products are determined. Further calculations were made using the channel spin representation of the product. Consider Fig. 4.15 where the points represent the off-diagonal strength as calculated from the product data. In order to reduce fluctuations, the strengths were averaged over energy with a Lorentzian envelope of width 40 keV. The solid curve in the figure is a theoretical calculation made from Eq. 4.4.5 with A=-.002, B=50 keV, C=8.1 keV^2, and W=42.3 keV. The theoretical calculation has also been averaged over energy with a Lorentzian of width 40 keV. As can be seen

Figure 4.13 The Product of Reduced Width Amplitudes Versus Energy in the Total Angular Momentum Representation.

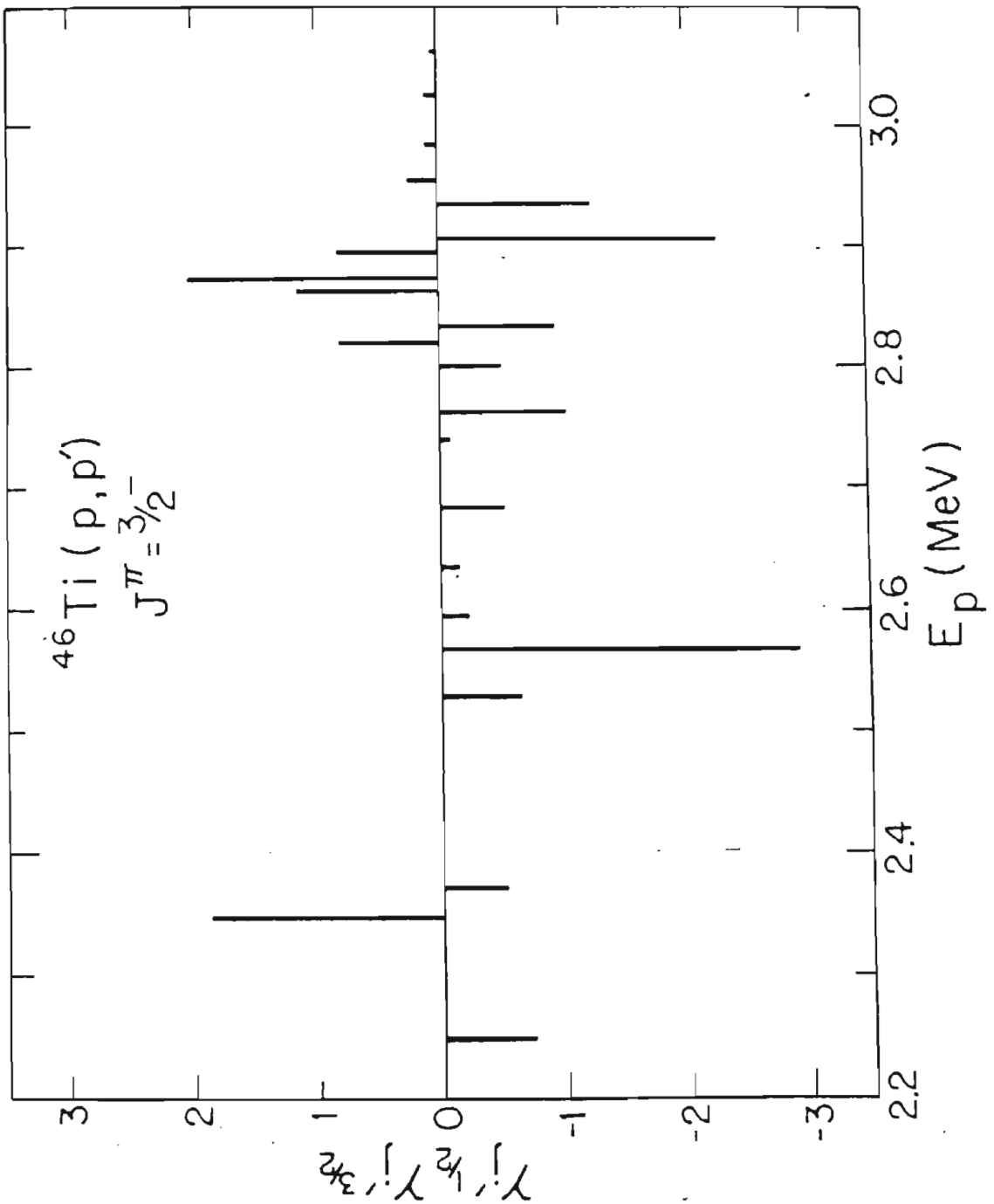
^{46}Ti (p, p′)
$J^{\pi} = 3/2^-$
E_p (MeV)
3.0
2.8
2.6
2.4
2.2
3
2
1
0
-1
-2
-3
$\gamma_{j'} \cdot \frac{1}{2} \gamma_{j'} \cdot \frac{3}{2}$

Figure 4.14 The Product of Reduced Width Amplitudes Versus Energy in the Channel Spin Representation.

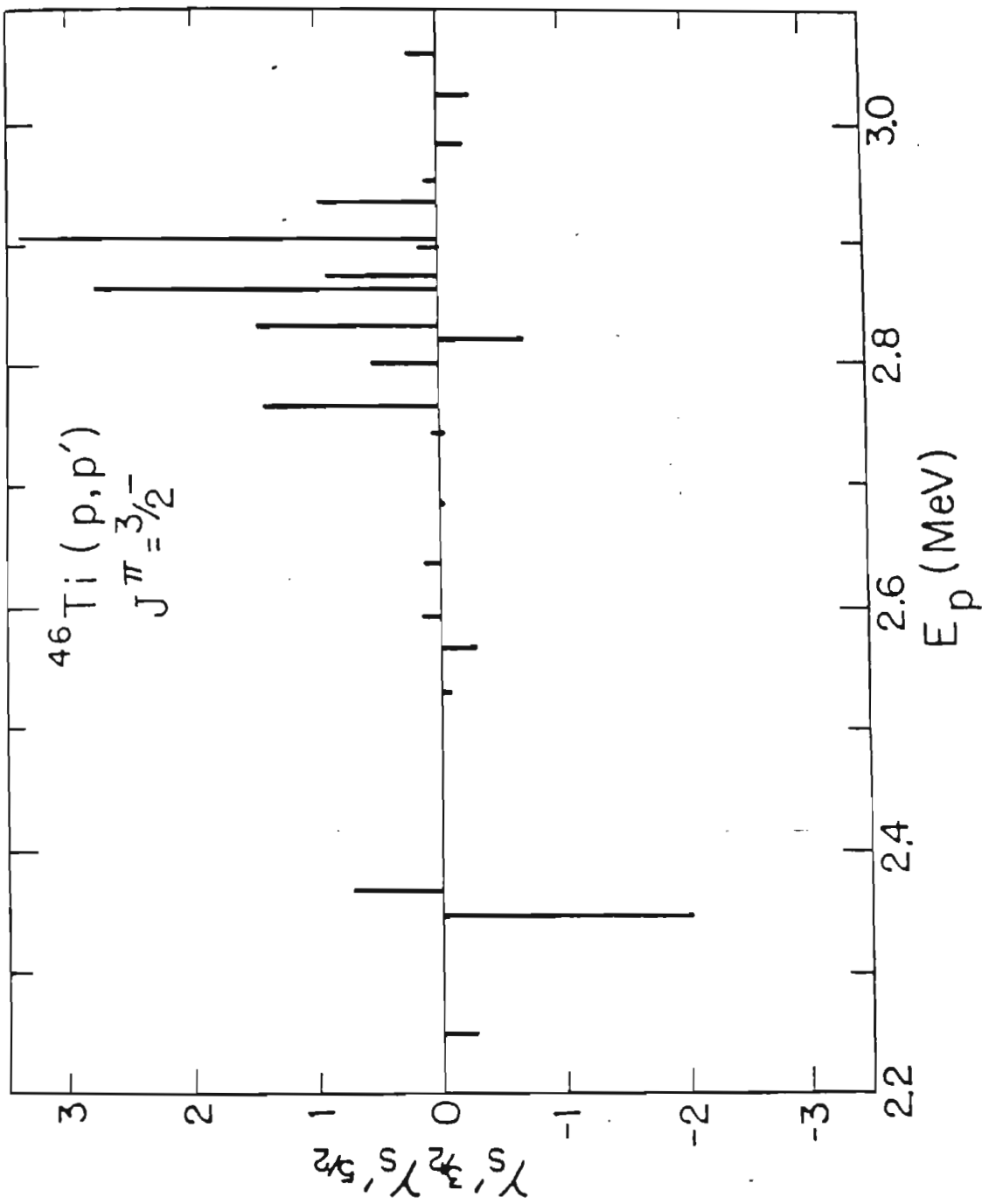
^{46}Ti (p,p')
$J^\pi = 3/2^-$
$\gamma_{s_{1/2}}, \gamma_{s_{3/2}}$
3
2
1
0
-1
-2
-3
2.2
2.4
2.6
2.8
3.0
E_p (MeV)

Figure 4.15 The Theoretical Fit to Off-Diagonal Strength Function for Channel Spin Representation. Both the data and fit were averaged over energy with a Lorentzian envelope of width 40 keV. The parameters used in the theoretical fit were: A=-.002; B=50 keV; C=8.1 keV^2; and W=42.3 keV.

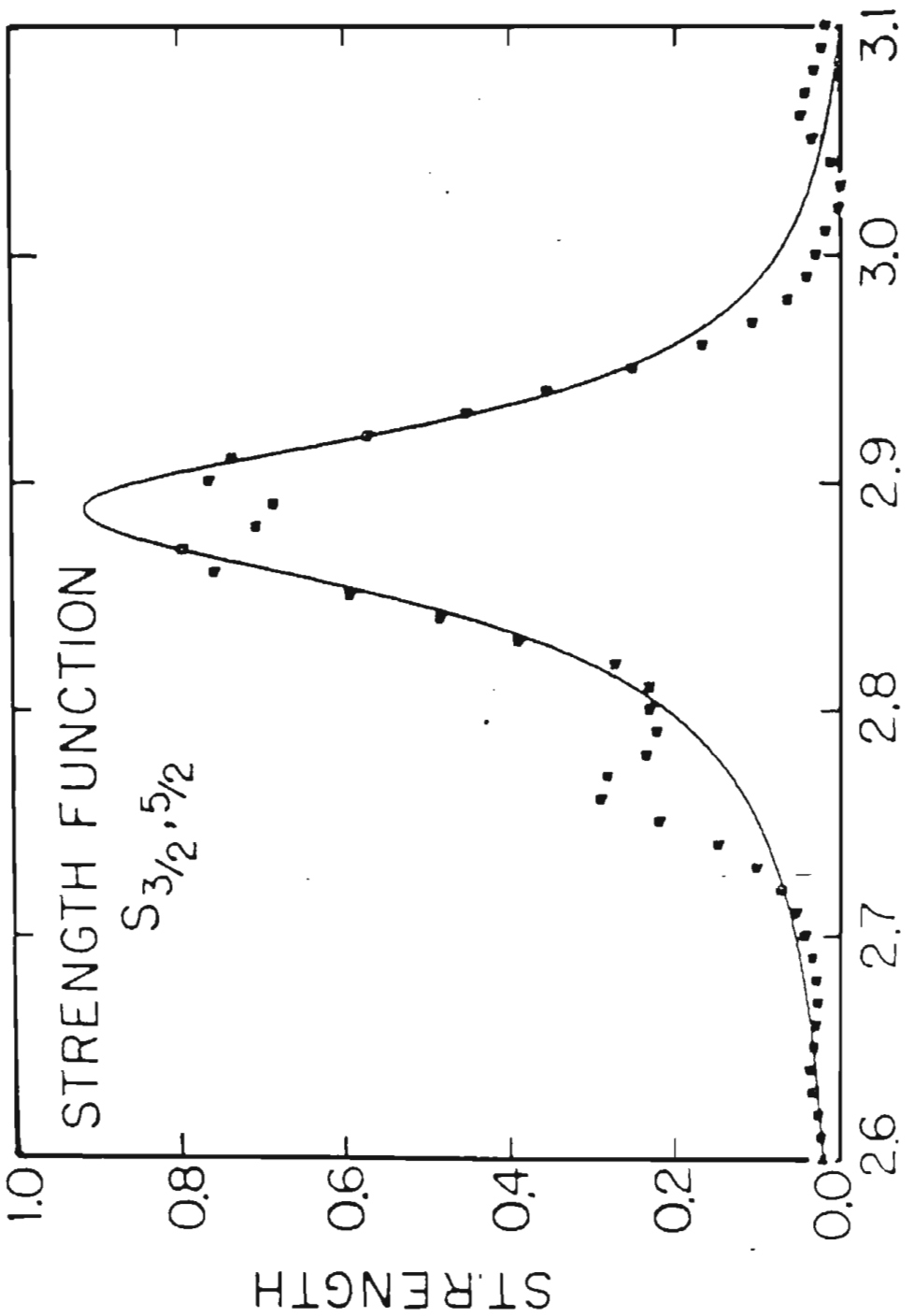
STRENGTH FUNCTION
$S_{3/2,5/2}$
STRENGTH
1.0
0.8
0.6
0.4
0.2
0.0
2.6
2.7
2.8
2.9
3.0
3.1
E_p (MeV)

in Fig. 4.15, the fit near the peak is very good. This then determines the off-diagonal elements of Eq. 4.4.7.

In order to compute a set of diagonal elements from Eq. 4.4.7, the results from the fit in Fig 4.12 were used. This gives for s'=3/2, B=0.0 keV and C=20.8 keV². Combining results from s'=3/2 and the product of s'=3/2 and s'=5/2, the strength function in the channel s'=5/2 can be determined from Eq. 4.4.7. The results are B=39 keV and C=3.1 keV². Fig. 4.16 shows the s'=5/2 data and the theoretical strength as calculated from Eq. 4.4.5. The analogue strength is small in this channel and cannot be clearly seen above the background. Therefore, using Lane's ideas on off-diagonal strength functions, the data for the 2.87 MeV analogue state appear internally consistent.

Figure 4.16 The Theoretical Fit to the Strength Function for the Channel Spin Representation in Channel $s'=5/2$. Both the data and fit were averaged over energy with a Lorentzian envelope of width 40 keV. The parameters used in the theoretical fit were: $A=.006$; $B=39$ keV; $C=3.1$ keV^2; and $W=42.3$ keV.

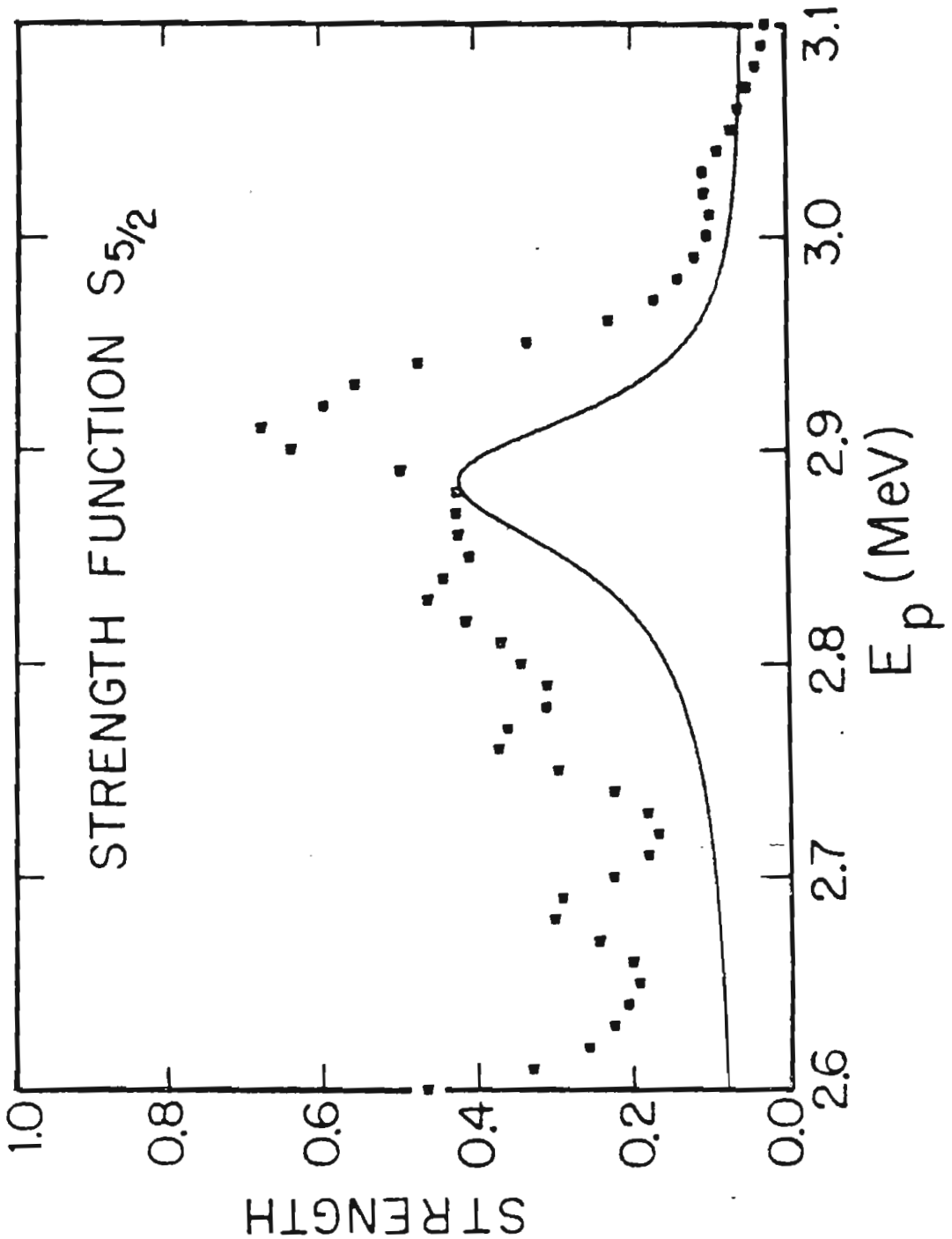
STRENGTH FUNCTION $S_{5/2}$
STRENGTH
1.0
0.8
0.6
0.4
0.2
0.0
2.6
2.7
2.8
2.9
3.0
3.1
E_p (MeV)

Chapter 5

SUMMARY

Inelastic proton and de-excitation gamma-ray angular distributions were measured for the reaction $^{46}Ti(p,p'\gamma)^{46}Ti$. Fifty-two p-wave and f-wave resonances were examined in ^{47}V between the proton bombarding energies 2.25 and 3.10 MeV. The current work demonstrated a simple method that can be used to obtain channel spin mixing ratios for both p-wave and f-wave resonances. This method also yields resonance spin assignments and detailed information about the magnitudes and relative phases of the exit channel amplitudes.

General angular distribution equations were given describing the particle and gamma-ray decays in two different angular momentum representations. The specific equations relevant to the present experiment were also listed in both representations, and transformations were provided to convert between the two representations.

Of the fifty-two resonances investigated, thirty-four were studied in detail. Five spin assignments were in disagreement with previous work. The channel spin mixing ratios were obtained for all $3/2^-$ and $5/2^-$ resonances, and

the magnitudes and relative phases of the reduced widths were determined. Evidence was presented for nonstatistical behavior of the mixing ratios and for the amplitudes. Spectroscopic factors were determined for the three analogue states observed. Data from one of the analogue states were used to evaluate new ideas about off-diagonal strength functions.

APPENDIX

6.1 Computer Hardware

This appendix will describe the computer hardware and software used in this experiment. The explanation is intended for users who have a limited knowledge of the Prime 300 computer and the CAMAC interface. Other descriptions of CAMAC are given by Costrell (1973) and Kirsten (1973).

The computer used in this experiment was a Prime 300 with thirty-two thousand words of memory and sixteen bits per word. The computer was interfaced to the 3 MV laboratory through a CAMAC interface designed and built at T. U. N. L. using a standard CAMAC crate and Bi Ra model 1260 branch driver.

CAMAC, which is short for Computer Aided Measurements and Control, is a standardized instrumentation system developed by the ESONE Committee of European laboratories. It features a data highway, called dataway, whereby modules can communicate with each other or with the computer. The CAMAC system is comprised of a branch driver, one or more twenty-four slot crates, and one or more modules. The branch driver handles communication between the central processing unit (CPU) of the computer and the CAMAC

crates. The branch driver can operate in two modes; programmed input and output, and direct memory addressing. The T. U. N. L. system uses programmed input and output. In order for the CAMAC system to perform a function, a command register and a data register in the branch driver must be loaded, and an output control pulse (OCP) must be given.

The command word consists of five bits specifying the function to be performed, five bits specifying the slot in the crate to which the command should be directed, four bits giving the subaddress of the module, and two modifier bits for automatically incrementing the station number and subaddress. The function and subaddress codes are specified for each module by the manufacturer. The bits of the command word are set as illustrated in Table 6.1. The MA and MN bits can be used to increment the station number or subaddress at the end of a CAMAC cycle. At the present time, these are not used. The F, N, and A bits make up the function code, station number, and subaddress. For example, the command F26 N28 A9 will cause the crate controller to clear the dataway. The F26 is made by setting the bits for F16, F8, and F2 since the sum of 16, 8, and 2 is 26. Similarly, setting N16, N8, and N4 will make N28; and the combination of A8 and A1 will make A9.

The data register actually consists of two registers. One corresponds to CAMAC bits one through sixteen. The

Table 6.1 CAMAC Command Word

Prime Bit	Command Bit
1	MA
2	MN
3	F16
4	F8
5	F4
6	F2
7	F1
8	N16
9	N8
10	N4
11	N2
12	N1
13	A8
14	A4
15	A2
16	A1

second has CAMAC bits seventeen through twenty-four, plus the crate address and X bit from the last CAMAC cycle. The X bit set after a CAMAC cycle means that the last CAMAC operation was able to be performed. The crate address portion of the second data register is called the branch crate register (BCR) and is loaded with the number of the crate performing the CAMAC operation. The user must be careful, however, when reading or writing the data registers. The bits in the data registers are reversed in the A register of the computer; that is, the most significant bit in a branch driver data register is the least significant bit in the A register. The branch driver is assigned the address code of '47 octal by Prime. The vector address for a branch driver interrupt is location '147.

The branch highway connects the branch driver with the crate and consists of the following: twenty-four data lines for reading and writing; five lines for the function code; five lines for the station number; four lines for the subaddress; one line for the branch demand signal; and one line for the crate address. Whenever the crate needs to be serviced, it generates a branch demand signal (BD) and outputs this to the branch driver. The branch driver then uses the other lines to perform the operation.

All operations within the crate are controlled by the crate controller which resides in the first two slots of the crate. The dataway is the system which interconnects

all slots within the crate. It consists of twenty-four read and twenty-four write lines common to all slots; function and subaddress lines common to all; lines for strobes, clear, initialize, inhibit, response, and busy signals; and a pair of lines between the crate controller and each slot. This pair has one line to carry a "look at me" signal generated when a module wants to request service, and one line to carry a signal when the crate controller requests the module to perform some function. This latter line is called an N line and the former an L line. The signal on the L line is called a LAM.

When a module requests attention, it sends a LAM to the crate controller. The crate controller in turn sends a branch demand to the branch driver. The common lines within the crate are then used to pass information from the module to the branch driver. In addition, the crate controller assembles a graded-L word. The bits of this word correspond to the LAM signals from each slot; a bit set means that slot is generating a LAM. The user may choose the correspondence between the devices and the bits of the graded-L word by means of the LAM board. However, this freedom is limited to crate slots and graded-L bits eleven through twenty. The LAM board consists of ten rows and ten columns of push buttons. The rows represent the graded-L bits eleven through twenty, and the columns correspond to the crate slot numbers. If a user wishes the

device in slot twelve to set the sixteenth bit of the graded-L, he pushes the button in the row numbered sixteen and the column labeled twelve. The LAM board can also be used for coincidence data. To do so, the board should be set up so that the devices in coincidence correspond to the same graded-L bit. When this is done, the LAM will not be generated until all coincident devices have accepted data.

At T. U. N. L. three Bi Ra model 2322 dual input registers, one EG&G model R1224 dual input register, one Bi Ra model 4301 graphic display driver, one Bi Ra model 6102A CAMAC test module, and one Bi Ra model 3222 output register are used. The crate controller is a Bi Ra model 1310 type A-1. Two input registers are used for ADC-router combinations, a third is used for a light pen, and the last one is used to read a panel of switches. Also, the two input registers used in conjunction with ADC's have a card interface between each register and ADC.

The light pen and switch panel were built by the T. U. N. L. electronics shop. The light pen is used in conjunction with a graphic oscilloscope to interact with the software. A pulse from the light pen causes the software to change the first bit of the last data point displayed on the oscilloscope. The switches also allow interaction with the software. They were designed to output a signal onto twenty-four lines leading to the associated

input register. Each switch corresponds to different bits of the output word; whenever a switch is moved, a new value appears on the data lines. Table 6.2 gives the bits of the CAMAC word and their associated functions. CAMAC bit 16 indicates whether the switch is a rotary (function A) or a toggle (function B). Bit 15 set denotes that the full 24 bits of the CAMAC word must be read. If the input register has been enabled, it generates a LAM signal and the software reads the new switch position.

The current software is designed to set a flag indicating the new position of the switches. The possible values of the flag and the corresponding switches are given in Table 6.3. The operator switches are numbered 1 to 15 from right to left when the multiply switch is down, and numbered 16 to 30 from right to left when the multiply switch is up. The flag values in Table 6.3 for rotary switch positions increase in the clockwise direction, and the toggle switch values are the minimum when the switch is down. For example, if the block switch is turned to position 1, or the position where the switch is as far counterclockwise as possible, the flag will be set equal to 38. If, for example, toggle switch A1 is pushed up, the value of the flag will be set equal to 51.

The switch panel also has a digital thumbwheel. The thumbwheel has a separate cable but uses the same input register as the switches. Whenever the button centered

Table 6.2 Switch Panel Word

CAMAC Bit	Function A Bit	Function B Bit
1	Range Switch Bit 1	Operator Switch Bit 1
2	Range Switch Bit 2	Operator Switch Bit 2
3	Range Switch Bit 3	Operator Switch Bit 3
4	Range Switch Bit 4	Operator Switch Bit 4
5	Group Switch Bit 1	Multiply Switch
6	Group Switch Bit 2	1D-2D Switch
7	Subgroup Sw. Bit 1	2D-4D Switch
8	Subgroup Sw. Bit 2	Times 2 Push Button
9	Subgroup Sw. Bit 3	Center Push Button
10	Utility Sw. Bit 1	Divide 2 Push Button
11	Utility Sw. Bit 2	Toggle Switch A1
12	Block Switch Bit 1	Toggle Switch A2
13	Block Switch Bit 2	Toggle Switch A3
14		Toggle Switch A4
15		Set to read 24 bits
16	Always reset	Always set
17		Toggle B1
18		Toggle B2
19		Toggle B3
20		Toggle B4

Table 6.3 Switches' Flag

Switch	Flag Value
Operator	1-30
Group	31-34
Times 2 Button	35
Center Button	36
Divide 2 Button	37
Block	38-41
1D-2D	42-43
2D-4D	44-45
Utility	46-49
Toggle A1	50-51
Toggle A2	52-53
Toggle A3	54-55
Toggle A4	56-57
Toggle B1	58-59
Toggle B2	60-61
Toggle B3	62-63
Toggle B4	64-65

below the thumbwheel is pushed, the binary coded decimal equivalent of the thumbwheel reading is output onto the data lines (see Table 6.4). The software permits the user either to read the thumbwheel whenever he desires or to establish the thumbwheel on an interrupt level. In the latter case, an interrupt will be generated whenever the button is pushed, and the setting will automatically be read.

Currently the 3 MV lab uses two Northern Scientific (model 621) ADC's. Each ADC is used in conjunction with an eight input router. The routers, built at T. U. N. L., provide three bit signals corresponding to the eight inputs. A fourth bit is set whenever two or more events reach a router at the same time. These four bits from each router and twelve bits from each ADC form sixteen bit words which go to the associated input registers.

There are two outputs on the front of each router. One is a router busy signal set to +12 volts while an event is taking place. The busy signal returns to ground when the input register accepts the on-line data. The other output is a 100 nanosecond gate. This gate is shaped with a linear gate and stretcher, and then input into the card interface panel. The interface checks the timing between the linear and gate signals; if they do not match, all data lines are reset. The interface also sends the gate back out with little delay. The gate then goes

Table 6.4 Thumbwheel Word

CAMAC Bit	BCD No.
1	1
2	2
3	4
4	8
5	10
6	20
7	40
8	80
9	100
10	200
11	400
12	800
13	1000
14	2000
15	4000
16	8000
17	10000
18	20000
19	40000
20	80000

Table 6.4 (continued)

CAMAC Bit	BCD No.
21	100000
22	200000
23	400000
24	800000

to the ADC coincidence input, and the ADC analyzes the linear signal. The timing of these signals, plus the PSB, is illustrated in Fig. 6.1. The pulse stretcher busy (PSB) signal is a +2.5 volt signal generated by the ADC, which verifies that the ADC is analyzing data. Once the ADC has finished analyzing, a store signal is output to the input register. This store signal causes the input register to accept the data and output a data accepted signal. The ADC interprets the data accepted signal as a clear command and resets the PSB.

For a check on signal timing, the user should watch the zero channel count rate. There are four ways in which a zero channel count can be generated. If the ADC gate signal and linear signal are not timed correctly, the in-

Figure 6.1 Timing of the Computer Interface Signals.

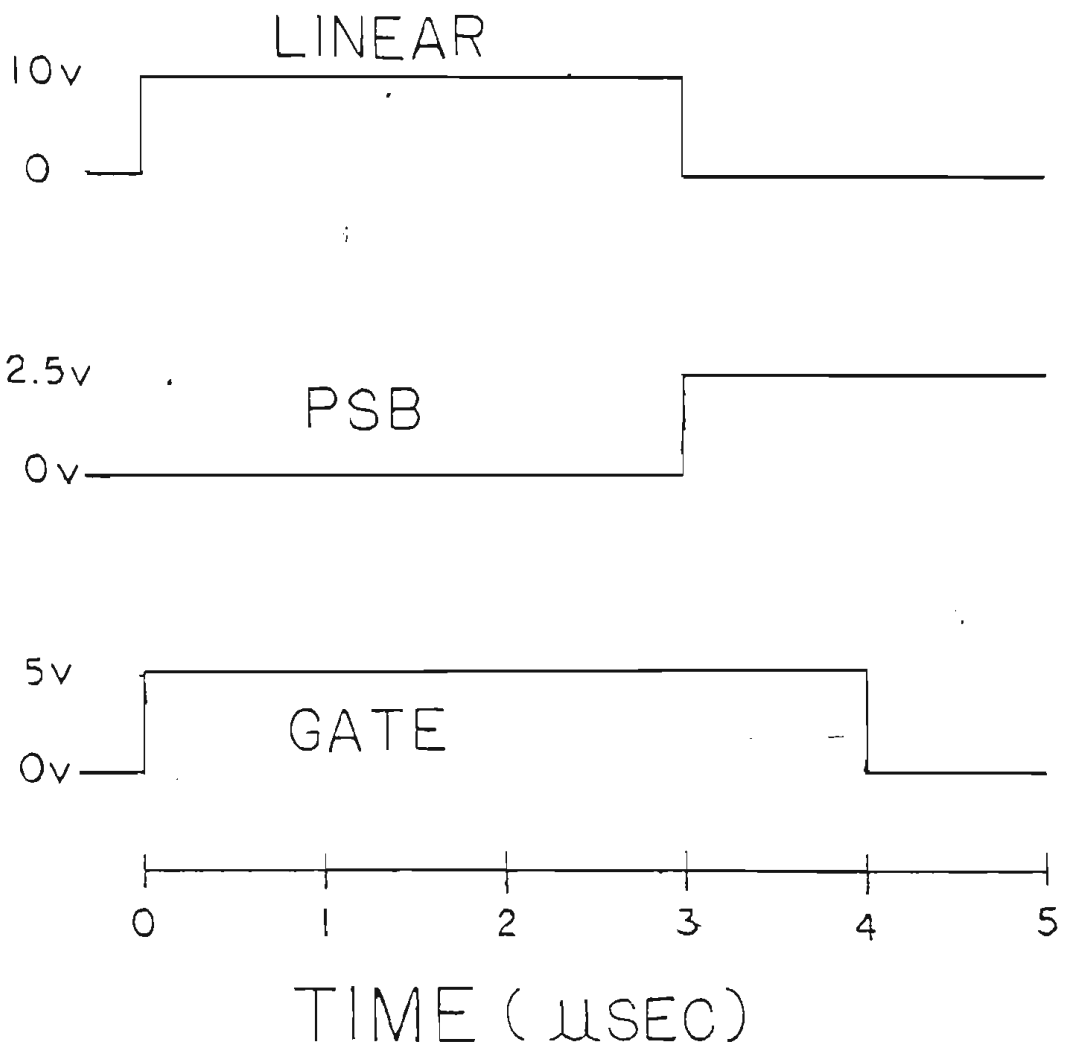
LINEAR
10v
0
2.5v
PSB
0v
5v
GATE
0v
0
1
2
3
4
5
TIME (μSEC)

terface will reset the ADC data lines. Also, a gate signal without a linear signal will cause a channel zero. Third, the ADC will output a channel zero if the amplitude of the linear signal is greater than the upper discriminator setting or less then the lower discriminator setting. Finally, the current software will generate a channel zero if the pile-up bit from the router is set.

To turn an ADC off, the user can input a 0 volt signal into the external control input of the card interface panel. In this experiment, the interval out signal from a preset scalar was used, but it was also necessary to terminate the input to the external control. Otherwise, the interval out was not quite able to pull the control to ground.

A general method to control any external device is the devices' control on the LAM panel. This consists of two columns of ten push buttons and two external stop inputs, one for each column. Each column of buttons correspond to the graded-L word bits eleven through twenty. To stop a device, the button corresponding to that device's graded-L must be pushed in and the external stop for that column must be pulled to ground. If several buttons in the same column are pushed, those devices will all be controlled by one external stop. Also, if the same two buttons in both columns are pushed, either external stop will control that device.

The steps taken when a data event or a user interaction takes place can now be traced (see Fig. 6.2). If the event is incoming data, a signal is input into the router and ADC. A sixteen bit word is formed and passed to the input register which generates a LAM. If the event is from the light pen or switch panel, the signal goes directly to an input register. Once the LAM is created, the crate controller sends a branch demand to the branch driver and the branch driver interrupts the computer program. Upon request, the crate controller will now return a graded-L word showing which devices created the LAM. The graded-L word will also reveal any additional LAM signals created after the initial LAM. After the software has decoded the graded-L information, a read operation can be executed. To do this, the branch driver command register must first be loaded with the proper function, station number, and subaddress bits; and the crate address must be loaded into the branch crate register. An OCP '47 will now start the CAMAC cycle. During the cycle, a busy signal is sent to the branch driver indicating that a dataway operation is in progress. The crate controller will put the function and subaddress bits onto their common busses. The controller then sets the proper N line, and the module executes the command. The X, or command accepted, response indicates the ability of the module to perform the function. If a read operation is required, the module

Figure 6.2 Block Diagram of the CAMAC Interface.

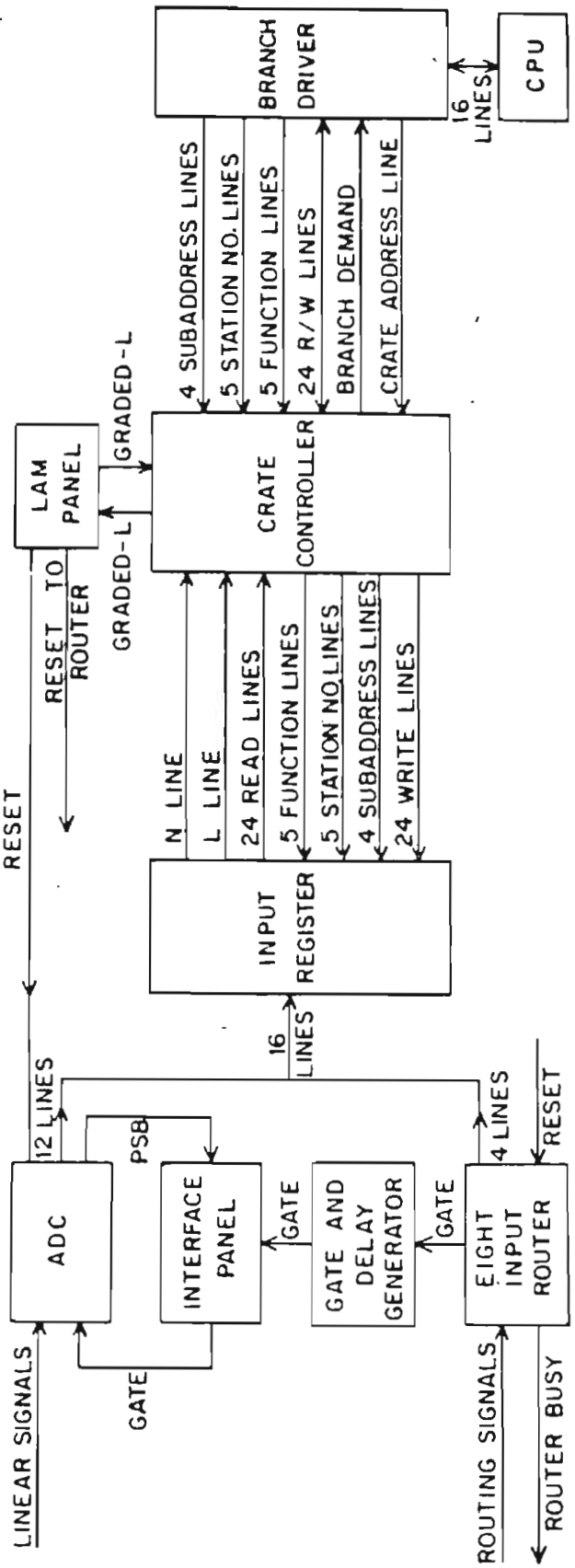
BRANCH DRIVER
CPU
16 LINES
4 SUBADDRESS LINES
5 STATION NO. LINES
5 FUNCTION LINES
24 R/W LINES
BRANCH DEMAND
CRATE ADDRESS LINE
LAM PANEL
GRADED-L
GRADED-L
RESET TO ROUTER
CRATE CONTROLLER
RESET
N LINE
L LINE
24 READ LINES
5 FUNCTION LINES
5 STATION NO LINES
4 SUBADDRESS LINES
24 WRITE LINES
INPUT REGISTER
16 LINES
12 LINES
PSB
4 LINES
RESET
ADC
INTERFACE PANEL
GATE
GATE AND DELAY GENERATOR
GATE
EIGHT INPUT ROUTER
LINEAR SIGNALS
GATE
ROUTING SIGNALS
ROUTER BUSY

will put the information onto the read busses. The crate controller passes the data to the branch driver data register, and the CAMAC cycle is complete.

6.2 Computer Software

To use the CAMAC hardware, the software must follow a few basic steps. First, the branch driver must be initialized through an OCP '1747. The CAMAC system can then be initialized with a BZ operation, which is started by an OCP '447. In a one crate system such as used in this experiment, the crate address can be loaded into the branch crate register and never changed. Once the crate address is established, the dataway inhibit within the crate should be removed. All CAMAC modules that will be allowed to generate interrupts should be enabled, and if necessary, modules can be cleared and loaded with initial values. Next, the branch driver is enabled with an OCP '1547, and the location of the interrupt handling software must be stored in location '147 of memory. At this point the CAMAC system has been initialized; however, the computer must be put into the vectored interrupt mode. If the computer is in this mode and is interrupted, program control passes to the interrupt handling subroutine; thus

the term vectored interrupt.

When an interrupt is generated and a CAMAC cycle is desired, the software should first inhibit computer interrupts. This is done because other computer peripherals such as teletype terminals, the tape drive, and the disk drive use interrupts, and all interrupts operate on an equal level. At the same time, the branch driver should be inhibited with an OCP '1647, and the branch demand should be disabled. The user must be careful to save the A register before executing the operation to disable the branch demand. Also, the X and B registers and the computer keys should be saved. If it is necessary to determine which module created the interrupt, a graded-L operation can be started with an OCP '147. After this cycle is completed, the graded-L word is in the data register of the branch driver and can be read into the A register with an INA command. Once the module requiring service has been located, CAMAC cycles to this module can be executed. To do so, the branch driver command register must be loaded with the proper function, station number, subaddress, and mode information. If necessary, the data register is loaded with a twenty-four bit word. An OCP '47 then starts the cycle and an SKS '147 checks to determine when the cycle is complete. If the CAMAC module has returned information to the branch driver, it will be in the data register and can be used as necessary.

After all interrupts have been processed, it is necessary to return the computer to its condition at the time of the interrupt. First, the branch driver is cleared with an OCP '347. Then, the computer's registers and keys are restored, and the computer interrupts are cleared and enabled. For a flow diagram of the software used in this experiment, see Fig. 6.3.

Other than CAMAC, the teletype terminal was the main device used for program interaction in this experiment. The terminal can operate in an interrupt mode and requires only a few steps. First, an OCP '1704 will initialize the terminal. The control word, described by Prime (1973), should be output to the terminal interface with an OCP '104 command and the interrupt mask set by an OCP '1504. The location of the interrupt handling software must be stored in location '104, and the keyboard interrupts must be enabled with an OCP '204. Finally, the computer must be put into the vectored interrupt mode and computer interrupts must be enabled.

Once the terminal is enabled, depressing any key will cause program control to pass to the terminal interrupt handling routine. This routine should first save the computer registers and keys just as the CAMAC routine does. Then the terminal can be read with an INA '1004. When finished, the software should restore the registers and keys to their initial states.

Figure 6.3 . Flow Diagram of the CAMAC Software.

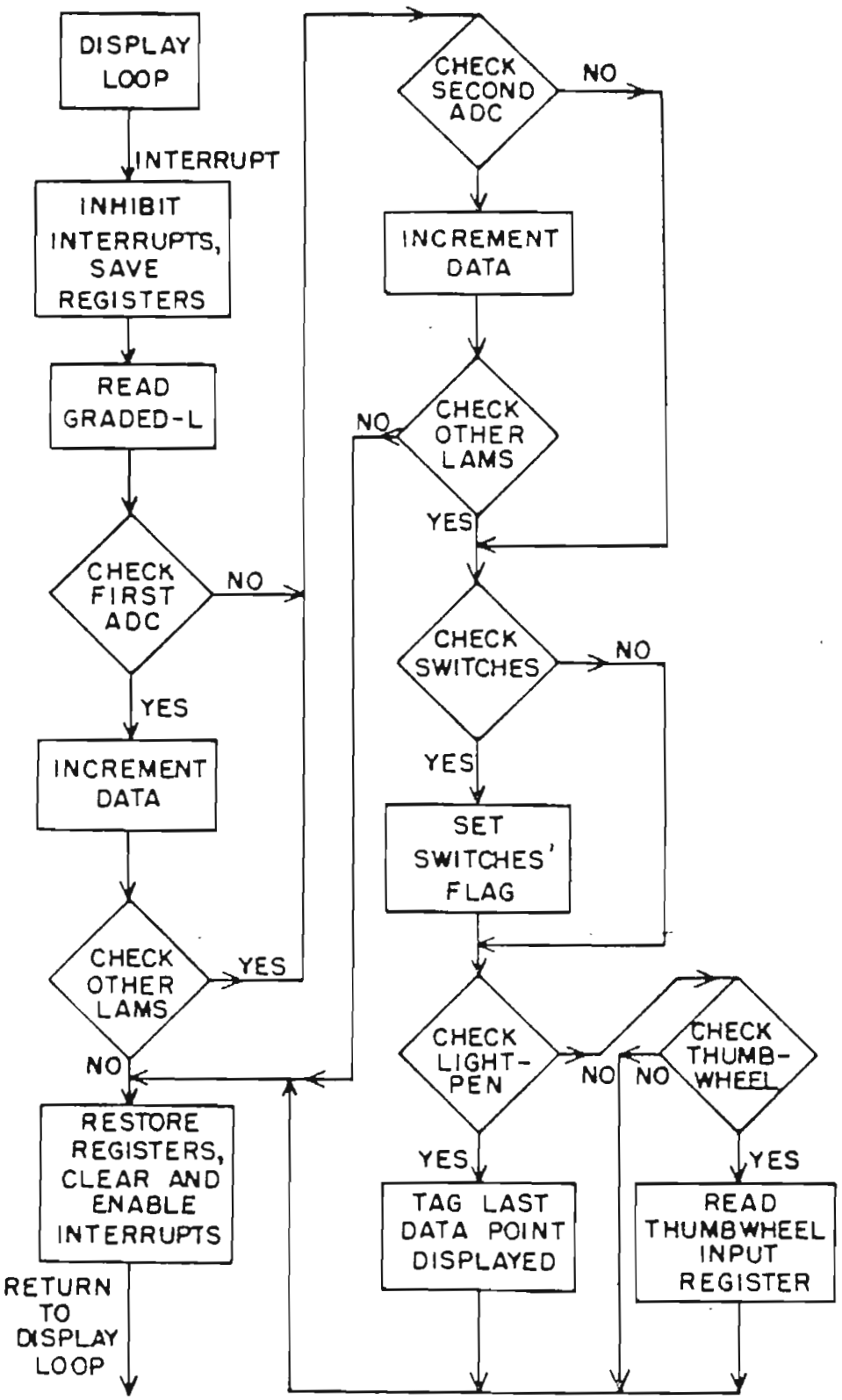
DISPLAY LOOP
INTERRUPT
INHIBIT INTERRUPTS, SAVE REGISTERS
READ GRADED-L
CHECK FIRST ADC
NO
YES
INCREMENT DATA
CHECK OTHER LAMS
YES
NO
RESTORE REGISTERS, CLEAR AND ENABLE INTERRUPTS
RETURN TO DISPLAY LOOP
CHECK SECOND ADC
NO
INCREMENT DATA
CHECK OTHER LAMS
NO
YES
CHECK SWITCHES
NO
YES
SET SWITCHES' FLAG
CHECK LIGHT-PEN
NO
YES
TAG LAST DATA POINT DISPLAYED
CHECK THUMB-WHEEL
NO
YES
READ THUMBWHEEL INPUT REGISTER

BIBLIOGRAPHY

Bevington, Phillip R., Data Reduction and Error Analysis for the Physical Sciences (McGraw-Hill Book Company, Inc., New York, 1969).

Biedenharn, L. C. and M. E. Rose, "Theory of Angular Correlation of Nuclear Radiations," Rev. Mod. Phys., Vol. 25, (1953), p. 729.

Bilpuch, E. G., A. M. Lane, G. E. Mitchell, and J. D. Moses, "Fine Structure of Analogue States," Phys. Reports, Vol. 28C, (1976), p. 147.

Blatt, John M. and L. C. Biedenharn, "The Angular Distribution of Scattering and Reaction Cross Sections," Rev. Mod. Phys., Vol. 24, (1952), p. 249.

Browne, J. C., Fine Structure of Analogue States in ^{61}Cu, ^{63}Cu, ^{65}Cu (Unpublished Ph. D. dissertation, 1969, Duke University, Durham, N. C., Department of Physics; University Microfilms, Ann Arbor, Michigan).

Costrell, Louis, "CAMAC Instrumentation System - Introduction and General Description," Nuc. Sci., Vol. NS-20, No. 2, (1973), p. 3.

Dittrich, T. R., Channel Spin Mixing Ratios in High Resolution Proton Inelastic Scattering on ^{50}Cr (Unpublished Ph. D. dissertation, 1976, N. C. State University, Raleigh, N. C., Department of Physics;

University Microfilms, Ann Arbor, Michigan).

Ferguson, A. J., Angular Correlation Methods in Gamma-Ray Spectroscopy (North-Holland Publishing Company, Amsterdam, 1965).

Halbert, M. L., "Nuclear Data Sheets for A=47," Nuclear Data Sheets, Vol. 22, No. 1, (1977), p. 59.

Kendall, M. G. and A. Stuart, The Advanced Theory of Statistics (Hafner Publishing Company, New York, 1958), p.215.

Kirsten, F. A., "Operational Characteristics of the CAMAC Dataway," Nuc. Sci., Vol. NS-20, No. 2, (1973), p. 9.

Kraus Jr., Alfred A., J. P. Schiffer, F. W. Prosser Jr., and L. C. Biedenharn, "Angular Correlation for the (a,bγ)-Type Nuclear Reaction," Phys. Rev., Vol. 104, (1956), p. 1667.

Lane, A. M., "Partial Width Correlations and Common Doorway States," Ann. of Phys. (N. Y.), Vol. 63, (1971), p. 179.

Lane, A. M., private communication, (1978).

Lynn, J. E., The Theory of Neutron Resonance Reactions (Oxford University Press, Ely House, London, 1968).

Marion, J. B., Nuclear Data Tables (National Academy of Sciences, Washington, D. C., 1960), p. 160.

Parks, P. B., H. W. Newson, and P. M. Williamson, "Method of Canceling Energy Fluctuations of a Van de Graaff

Ion Beam," Rev. Sci. Instr., Vol. 29, (1958), p. 834.

Peters, W. C., Electromagnetic Decay of Fragmented Analogue States in ^{55}Mn and ^{59}Co, (Unpublished Ph. D. dissertation, 1972, Duke University, Durham, N. C., Department of Physics; University Microfilms, Ann Arbor, Michigan).

Prime, Prime 200 Reference Manual (Prime Computer, Inc., Natick, Massachusetts, 1973), p.3-5.

Prochnow, N. H., A High-Resolution Study of Proton Resonances in ^{47}V, ^{49}V, ^{51}V (Unpublished Ph. D. dissertation, 1971, Duke University, Durham, N. C., Department of Physics; University Microfilms, Ann Arbor, Michigan).

Robson, D., Isospin in Nuclear Physics Ed. by D. H. Wilkinson (North-Holland Publishing Company, Amsterdam, 1969), p. 461.

Sellin, P. L., Excited States in ^{19}F (Unpublished Ph. D. dissertation, 1969, Duke University, Durham, N. C., Department of Physics; University Microfilms, Ann Arbor, Michigan).

Thompson, W. J. and W. I. van Rij, Notes on Applied Angular Correlation Theory (1968).

Wimpey, J. F., Electromagnetic Decay of Fragmented Analogue States (Unpublished Ph. D. dissertation, 1974, N. C. State University, Raleigh, N. C., Department

of Physics; University Microfilms, Ann Arbor, Michigan).

Yang, C. N., "On the Angular Distribution in Nuclear Reactions and Coincidence Measurements," Phys. Rev., Vol. 74, (1948), p. 764.